Mechanistic Insight into Cationic Polymer Mediated Gene Delivery

A Dissertation
SUBMITTED TO THE FACULTY OF
UNIVERSITY OF MINNESOTA
BY

XIAO ZHONG

IN PARTIAL FULFILLMENT OF THE REQUIREMENTS
FOR THE DEGREE OF
DOCTOR OF PHILOSOPHY

Adviser: **Chun Wang, PhD.**

December 2014

Acknowledgements

I would like to express my deep gratitude towards my advisor Professor Chun Wang. Thank you very much for giving me the opportunity to join the Wang Lab. I sincerely appreciate all the guidance, support, help, patience and flexibility you extended along my journey to overcome various hurdles in achieving and completing all the work here, and more importantly, the degree I have dreamed of since I was in high school. I wish I could have more opportunities to learn from you, both professionally and personally.

I would also like to give special thanks to Professor Tranquillo for all his help during difficult times. Thanks to Dr. Wei Shen, Dr. Ronald Sigel, and Dr. Guisheng Song for their guidance and participation on my thesis committee.

I would also like to thank the past and present members of the Wang Lab: special thanks to Wenqing Han on helping me with animal experiments, immunostaining and washing all the glasswares; Weihang Ji, Dave Panus, Noelle Palumbo, Sunny Choh, Daisy Cross, Xiaoze Jiang, Wenshou Wang, and Dunwan Zhu for scientific discussions, help on experiments, and the support and encouragement when things were not going well.

I would like to thank the University Imaging Center (UIC), especially John Oja for assistance and training on various microscopes and live animal imaging; and Professor Justin Weinbaum for assistance on Western Blot.

Last but not least, a big and sincere thank you to my parents and the dear friends who are there for me during the ups and the downs of this journey!

Abstract

Gene therapy holds great potential to enhance human medicine since it could provide treatment to a vast variety of diseases. Viral gene delivery vectors have high transfection efficiency, but often they are associated with high risk of immunogenicity as well. Non-viral vectors, especially polycationic polymer based gene carriers provide the advantages of low immunogenicity and ease of synthesis, but they face two major challenges for a broader application in clinical trials: high toxicity and low transfection efficiency. In this study, we performed experiments to gain a better understanding of the mechanisms and pathways underlying the high toxicity and low transfection efficiency associated with polyplex-mediated gene delivery. In the first part of the thesis, we studied the toxicity resulted from polyplex-mediated gene delivery and found that polyplexes made from PEI/DNA plasmids were able to induce autophagy in fibroblasts, a third type of cytotoxicity besides apoptosis and necrosis. With the proper choice of treatment time and drug concentrations, we decoupled cell cytotoxicity due to apoptosis and necrosis from autophagy, and found that transfection efficiency is positively correlated with the regulation of autophagy. In the second part of the thesis, we performed in vitro physical characterization of polyplexes formed from six different polymers in order to understand their local in vivo performance. Homopolymer with a larger molecular weight (and polymer chain) was able to transfect cells in vitro, but not in vivo. On the other hand, a shorter polymer chain favored local in vivo transfection. PEGylation helped the polyplexes to be stable against serum protein, but PEGylation of long chain homopolymer did not improve its in vivo performance. Taken together, these findings

could help us to improve transfection efficiency through modulation of cytotoxicity (autophagy) and gain a better understanding of polyplex in vivo performance based on its in vitro behavior and therefore providing insight into the design of gene delivery vehicle.

Table of Contents

List of Figures

Chapter 1: Introduction

1.1 Non-viral vector for gene delivery

Gene therapy holds tremendous potential in treating a huge variety of genetic disorders such as haemophilia[1], muscular dystrophy[2], cystic fibrosis[3] and diabetes[4], and it has been developed rapidly for treatment of cardiovascular[5], neurological[6], and infectious diseases[7], as well as cancer[8]. To treat diseases caused by a missing or aberrant protein, DNA encoding the desired gene is introduced into the nucleus of a cell to replace the errant gene or to alter the expression of an existing gene. The delivered DNA is subsequently processed into a functional protein or prodrug-activating enzymes to kill tumor cells [9]or performing other desired functions in the affected cells. Historically, many deactivated viruses have been used as gene carriers and have been launched into clinical trials due to their high efficiency in gene transfection[10, 11]. Viral vectors, such as adenovirus, adeno-associated virus, retrovirus and lentivirus, have evolved ways to overcome cellular obstacles by fusing the viral envelope with the endosome membrane and releasing DNA into the cytoplasm, achieving high transfection efficiency[12]. However, the high transfection efficiency associated with viral vectors comes at a cost. Despite being rendered replication deficient, viral vectors still pose safety concerns since they can cause immunogenicity and toxicity, and severe immune response in the host often leads to fatalities[13]. Limitations to cell mitosis for retrovirus, contamination of adenovirus and packing constraints of adeno-associated virus also

lesson their appeal [14]. Fundamental problems associated with viral vectors have encouraged extensive research into non-viral carriers, which possess the potential advantages of low immunogenicity, unrestricted DNA cargo size, potential for repeated administrations and ease of synthesis[15]. They can also address many pharmaceutical considerations better than viral vectors, such as scale-up, storage stability and quality control. However, non-viral vectors have to overcome their major limitation before they can be widely applied in clinical trials, which is the low transfection efficiency compared to the viral vectors.

1.2 Design of cationic polymer for gene delivery

Non-viral vectors consist of synthetic cationic polymers, lipids, and peptides able form ionic complexes with plasmid DNA. Polycationic polymers have been extensively investigated as gene carriers because they offer a high level of flexibility in design. A basic characteristic of the nucleic acid backbone is its negative charge, which allows electrostatic interaction with cationic polymers for form polyplexes. Due to the neutralization of the negative charges, DNA molecules are able to collapse into nanostructures in the size range of 100 nm, which are much smaller in size than free DNA with a size in the micrometer range [16]. The great reduction in size is one of the major reasons made the complexed DNA amendable to endocytic pathways.

Physical properties such as polymer molecular weight or chain length and surface characteristics are important factors in the design of polycationic polymer based gene carriers, and they can be tuned to modulate gene delivery properties including DNA

binding, colloidal stability of the complex, endosomal escape, cytotoxicity and transfection efficiency. For different target cells and tissues, or different routes of administration, the optimal characteristics of the complexes would vary. In general, the rational design of polymer based gene carriers needs to address the key factors along the gene delivery pathways.

Molecular weight or chain length of the polymer chains is a critical factor influencing gene delivery efficiency, and the relationship between polymer molecular weight and transfection efficiency has been studied in various polymers. Hennink and colleagues reported that the molecular weight of poly(2-dimethylaminoethyl methacrylate) (PDMAEMA) significantly affected transfection efficiency, and with higher molecular weight favoring the high transfection efficiency[17]. Mikos and colleagues determined that the higher molecular weight polyethylenimine (PEI) transfected better than the lower molecular weight PEI [18]. On the other hand, Hashida and colleagues found that the lower molecular weight PEI yielded a better transfection result than the higher molecular weight polymer [19]. Ren and colleagues studied the effect of molecular weight of polyphosphoramidate (PPA) on gene transfection, and reported that a higher molecular weight of the polymer chain enhanced gene delivery efficiency [20]. Poly-L-lysine, another popular cationic polymer used as gene carrier besides PEI, has also been studied, and Kwoh and colleagues reported a result that the longer chain polymer favored transfection efficiency[21]. In general, a higher molecular weight favors higher gene expression, but some discrepancies exist[19]. A fundamental

understanding of the effect of linear polycation chain length on the gene delivery process, especially in the in vivo environment remains elusive.

1.3 Cytotoxicity associated with polyplex-mediated gene transfection

Besides the low transfection efficiency compared to the viral vector, another major hurdle stopping polymer mediated gene delivery going to clinical trials is the high cytotoxicity associated with polyplex-mediated gene transfer [22-24]. The understanding of mechanisms and pathways underling cellular cytotoxicity caused by exposure of target cells and tissues to polymeric non-viral delivery systems could greatly help to improve their safety profile drastically. Three types of cell death have been identified based on its morphological appearance, enzymological criteria, and functional aspects. They are apoptosis, necrosis and autophagy [25, 26].

Apoptotic cell death is morphologically defined by chromatin condensation, nuclear fragmentation, shrinkage of the cytoplasm and formation of apoptotic bodies [27]. It is often accompanied by rounding-up of the cell, retraction of pseudopods, little ultrastructural modifications of cytoplasmic organelles, plasma membrane blebbing and engulfment by phagocytes in vivo [28]. This form of cell death modality is usually, but not exclusively, associated with caspase activation [29] mitochondrial membrane permeabilization [30]. Hunter and colleagues have reported that mitochondrial-mediated apoptosis was significant in PEI/DNA polyplex induced cytotoxicity [24]. Palumbo and colleagues have also confirmed the observation in their study using PEI/DNA polyplexes [31], and further reported that the use of the broad spectrum caspase inhibitor N-

benzyloxycarbonyl-Val-Ala-Asp-fluoromethylketone (Z-VAD-fmk) could reduce apoptotic cell death. Besides PEI, poly(L-lysine) (PLL) is another intensively studied polymer for non-viral gene delivery. Symonds and colleagues examined the toxicity associated with PLL/DNA complex and reported it as apoptotic cell death [32]. They also discovered that apoptosis is more prominent in the high molecular weight PLL treated cells.

Necrosis is morphologically characterized by an increase in cell volume, leading to the early rupture of the plasma membrane[26]. This process is associated with dilation and final dismantling of cytoplasmic materials, including mitochondria [33]. This mode of cell death is often the unregulated consequence of non-physiological stress or massive cell injury. Fisher and colleagues detected predominantly necrotic cell death in cationic polymer mediated gene delivery [34]. Palumbo and colleagues reported necrosis in PEI/DNA complex treated cells as well [31].

Autophagy is a fundamental process of cells under stress that degrades cytoplasmic proteins and organelles to maintain cellular homeostasis [35]. Several pathways of autophagy have been identified including macroautophagy, microautophagy, chaperon-mediated autophagy (CMA), pxenophagy and mitophagy[36, 37]. During a short period of nutrient deprivation, the absence of amino acids prevents signaling through phosphatidylinositol-3-kinase (PI3K), deactivates the autophagy regulatory molecule target of rapamycin (mTor), and induces macroautophagy[38]. Portions of the cytoplasm are sequestered into a double-membrane structure known as autophagosome, and degraded in lysosomes when autophagosomes fuse with lysosomes. LC3 (autophagy-

related gene (Atg) 8) decorates the membrane of the autophagosome and it is considered as a distinctive autophagosome marker. Recently, it has been suggested that macroautophagy could be another possible mechanism involved in antigen presentation by MHC Class I molecules[39].

Most studies on autophagy were focused on starvation, essential amino acid deprivation or stressed condition such as heat treatment [35, 38, 40]. Only one reported talked about autophagy induction by cationic lipid gene carrier[41]. So far, no published documentation has been found on whether polymeric gene carriers can induce autophagy and how autophagy might affect transfection. Autophagy can be activated and regulated by many physiological and pathological conditions including starvation[42], intracellular viruses and bacteria[43], calcium phosphate precipitates[44], quantum dots[45] and gold nanoparticles[46]. Induced autophagy has also been observed in certain cell types exposed to various cationic molecules alone such as polyamidoamine (PAMAM) in human lung A549 cells[47], PEI in nephritic and hepatic cells[48] and cationic lipids in a HeLa cell line[41]. Because many cationic polymers are also gene transfection reagents, it is important to know whether polymer/DNA complexes can induce autophagy, and how induced autophagy influences gene transfection.

1.4 The gene delivery problem: extracellular challenges in vivo

The in vivo efficiency of a polyplex delivery system depends on its ability to overcome both the extracellular and intracellular hurdles. The extracellular barriers for gene delivery involve serum proteins and components of the extracellular matrix (ECM),

a large proportion of which are negatively charged [49] and present potential threats to the stability of polyplexes. When the negatively charged biomacromolecules encounter the positively charged polyplexes, the polyplexes are very likely to dissociate due to the polyelectrolyte exchange reaction [50]. Unpacking of polyplexes due to competitive binding interactions has been discovered in the nucleus when the polymer/DNA complexes were delivered to mammalian cells [51, 52]. Systematic injection of polyplexes may have been subject to similar premature unpacking due to the interactions with serum proteins or components of ECM, and the theory has been shown in vitro [53, 54].

To prevent the undesired interactions with serum proteins or ECM, shielding of polyplex surface charge is essential in the design of polymeric cationic gene carriers. One of the common approaches involves grafting of non-ionic, flexible hydrophilic polymers such as poly(ethylene glycol) (PEG) and poly[N-(2-hydoxypropyl)methacrylamide] (PHPMA) [55]. These polymers can effectively suppress the access and adsorption of biomacromolecules due to the excluded volume effect by the highly flexible and hydrated chains. The grafting of the PEG chain onto a polymer is termed PEGylation, and PEG has been shown to substantially prevent the aggregation or destabilization of polyplexes induced by serum proteins [56, 57]. Nomoto and colleagues used real-time confocal laser scanning microscope to observe the aggregate formation of polyplexes and confirmed that polyplexes formed aggregates quickly after intravenous injection [58].

Storm and colleagues have proposed a theory to explain the apparent protein shielding effect imparted to polymers when PEG chains are grafted [59]. Their theory

suggested that the surface PEG chains existed in a more extended conformation when free in solution due to their hydrophilic and flexible nature. When interacting with a serum protein, the van der Waals force is created due to the attraction between the protein and the PEG chain. The PEG chain is subsequently compressed, forcing the PEG chain into a more condensed configuration and generating an opposing force that tries to balance the attractive force between the negatively charged serum protein and the positively charged polymer chain. Therefore the PEG chain length and the grafting density are two key factors in the design of PEGylated polymer and they could influence the pharmacokinetic properties of the polyplexes [60]. However, in vivo studies reported in literature present controversial results. Some groups reported that a low graft density with a long PEG chain is more effective[61], and others found the grafting density is more dominant than PEG chain length[62]. A better understanding of the effect of PEGylation and PEG chain length on the in vivo physiological and biological properties of the nanocomplexes is essential to provide insight for the design of a more efficient gene carrier.

1.5 Thesis overview

In order to have a rational design for cationic polymer based gene carrier, it is critical to understand the rate limiting factors in the process. Two major challenges faced by polyplex-mediated gene delivery that prevent its wide application in clinical trials are its low transfection efficiency and its high cytotoxicity. Three pathways of cytotoxicity include apoptosis, necrosis and autophagy. Apoptosis and necrosis have been extensively

studied by researchers, but autophagy is only recently recognized as a pathway of cell death. In Chapter 2, we investigated autophagy induction by PEI/DNA polyplexes in murine fibroblasts using three different methods: transmission electron microscopy (TEM), immunofluorescence staining and Western blotting. We successfully decoupled polyplex-induced autophagy from apoptosis and necrosis and evaluated the influence of autophagy on polyplex-mediated transgene expression using small molecules known to inhibit or induce autophagy.

To improve transfection efficiency, many researchers have adjusted the structure of the polymer gene carriers to optimize the transgene expression in vitro. However, in vitro results often provide poor indication to in vivo conditions. To understand the in vivo performance of polymer based gene carrier in Chapter 3, we used 2 series of poly(2-aminoethyl methacrylate) (PAEM) polymers with well defined chain length and narrow molecular weight distribution to conduct a comprehensive investigation of colloidal properties of PAEM/DNA or PEG-PAEM/DNA polyplexes. Particle size, surface charge, polyplex stability in vitro and in vivo transfection, as well as local biodistribution were carefully examined to further elucidate the impact of polymer chain length, PEGylation and PEG chain length on gene carrier design.

Chapter 2: Modulating polyplex-mediated gene transfection by small molecule regulators of autophagy

2.1 Introduction

A major challenge in the development of polymeric gene delivery carrier is to achieve high transfection efficiency with minimal cytotoxicity. Unfortunately, many cationic polymer gene carriers are often cytotoxic, thereby limiting their gene transfection efficiency. For example, polyethylenimine (PEI) is one of the most widely investigated cationic gene carriers with generally good transfection efficiency in many cell types [15, 63-65]. However, PEI (especially the highly branched form) is also well-known for its substantial cytotoxicity that prohibits its application in humans [66]. Previous work, including ours, has shown that depending on the dose of the polyplex, PEI-mediated gene transfer induces apoptosis and necrosis in many cell types and that polyplex-induced cell death compromises transgene expression [3, 22, 24, 67, 68]. Various chemical modifications of PEI and a great variety of other cationic polymers have been evaluated that showed low cytotoxicity [22, 24, 69], but a thorough understanding of the relationship between cellular stress responses and polyplex-mediated transfection is still lacking.

There are three major modes of response by cells under stress: apoptosis, necrosis and autophagy [26]. Unlike apoptosis, autophagy (or "self-eating") is often considered a cell survival mechanism through removing damaged proteins and subcellular organelles, so as to cope with stressful conditions such as starvation and chemical or biological assaults [70-72]. The process starts with the formation of isolation membrane, a

subcellular single-membrane structure, enclosing the proteins and organelles that are targeted for degradation. When the isolation membrane completely surrounds the cytoplasmic materials, a double-membrane autophagosome is formed. During the formation of autophagosome, a cytoplasmic protein, LC3 I, becomes covalently linked to phosphatidylethanolamine (PE), giving rise to LC3 II, which then associates with both the inner and outer membranes of the autophagosome. Subsequently, autophagosome fuses with lysosome to degrade the sequestered content, releasing amino acids for recycle. Thus, autophagy can function as a mode of stress adaptation to avoid cell death. However, if the stress is too severe or prolonged, autophagy can lead to cell death. Autophagy can be activated and regulated by physiological and pathological stimuli including starvation [42], intracellular viruses and bacteria [43], and nanomaterials such as calcium phosphate precipitates[44], quantum dots[45] and gold nanoparticles[46]. Induced autophagy has also been observed in certain cell types exposed to various cationic molecules alone such as polyamidoamine (PAMAM) in human lung A549 cells[47], PEI in nephritic and hepatic cells[48] and cationic lipids in a HeLa cell line[41], and more recently, lipoplexes and polyplexes in several types of primary cells and cell lines [73, 74]. However, because there is much crosstalk between autophagy and apoptosis [75], it is not yet clear if polyplexes could activate autophagy directly without inducing apoptosis and *vice versa*. Furthermore, how autophagy activation might affect polyplex-mediated gene transfection is not well understood, although recent studies on polyplex intracellular trafficking[73] and transfection of genetically modified *atg5*$^{-/-}$ cells [74] imply that autophagy might hinder nonviral gene transfer.

In this study, we investigated autophagy induction by PEI/DNA polyplex in murine fibroblasts and attempted to (1) decouple polyplex-induced autophagy from apoptosis and necrosis, and (2) modulate polyplex-mediated gene transfection using small-molecule regulators of autophagy. We hope that this work could contribute to better mechanistic understanding of polyplex-induced cytotoxicity and to establish the feasibility of enhancing nonviral gene delivery through manipulating autophagy.

2.2 Experimental Methods

2.2.1 PEI/DNA polyplexes preparation

PEI (branched, 25 kDa, Sigma) and plasmid DNA stock solutions, both at concentration 1 mg/mL, were diluted to 0.1 mg/mL in 20 mM HEPES buffer (pH7.4). Polyplexes were prepared at an N/P ratio of 8 by vortex mixing equal concentrations of PEI and plasmid DNA in 20 mM HEPES buffer to a total volume of 100 μL, and allowed to incubate at room temperature for 30 min. To study autophagy induction by PEI/DNA polyplexes, a plasmid encoding the luciferase gene (pCMV-Luc, Elim Biopharmaceuticals) was used to prepare polyplexes. A plasmid encoding enhanced green fluorescence protein (GFP) (pEGFP-N1, Elim Biopharmaceuticals) was used to investigate the effect of autophagy on transfection efficiency.

2.2.2 Cell culture and transfection

NIH 3T3 murine fibroblasts (ATCC) were cultured in DMEM (1 g/L D-glucose, L-glutamine, 110 mg/L sodium pyruvate, Gibco) supplemented with 10% fetal bovine serum (heat inactivated, Gibco) and 100 units/mL penicillin/streptomycin (Gibco).

NIH 3T3 cells were plated at 5×10^4 per well in 12-well plates and allowed to adhere overnight. After washing with phosphate buffered saline (PBS, pH7.4), the cell media was replaced with serum free media and polyplexes were added to the cells, incubated for 4 h. The final concentrations of the plasmid, PEI, and polyplex were 2, 2.8, and 4.8 μg/mL, respectively. The cells were then washed three times with PBS before replacing the serum free media back to regular cell media with 10% serum. Twenty-four hours after

the initial addition of polyplexes, cells were washed with PBS, trypsinized, suspended in in FACS buffer (containing 1% bovine serum albumin, BSA, and 1 mM sodium azide in PBS) and analyzed by flow cytometry using LSR II flow cytometer (Becton Dickson) and FlowJo software. Cells transfected with luciferase encoding DNA were used as the control for any increased autofluorescence of cells caused by polyplexes nonspecifically. GFP-positive cells were gated against the luciferase transfected control cells.

To investigate the role of autophagy on transgene expression and apoptosis/necrosis, autophagy inhibitor 3-methyladenine (3-MA, Sigma) was incubated with the cells at a concentration of 10 mM during the 4 h transfection. Autophagy enhancer rapamycin (Rapa, Calbiochem) was given to the cells 2 h before transfection and again 4 h after the initial addition of polyplexes at a concentration of 100 nM and prepared as fresh solution again.

2.2.3 Transmission Electron Microscopy (TEM)

Twenty-four hours after the initial addition of polyplexes, cells were harvested by trypsinization, washed in 0.1 M sodium cacodylate buffer (pH 7.2), pelleted by centrifugation, fixed in 2.5% glutaraldehyde in 0.1 M sodium cacodylate buffer for 1 h, and post-fixed in 1% osmium tetroxide in 0.1 M sodium cacodylate buffer for another 1 h. After dehydration with graded ethanol and propylene oxide, cells were embedded in Epon resin (Polysciences). Ultra-thin sections of 65 nm were cut with a microtome, stained with 8% uranyl acetate and lead citrate and examined using JEOL 1200 EXII transmission electron microscope.

2.2.4 Immunofluorescence staining and microscopy

NIH 3T3 cells were plated on chamber slides, prepared and treated the same way as described above in Section 2.2. Twenty-four hours after the initial addition of polyplexes, cells were washed with PBS, fixed by Cytofix for 10 min and permeabilized in 0.2% Triton x-100 in PBS for 10 min. After blocking in 5% normal donkey serum (Jackson Immune) for 1 h at room temperature, the cells were incubated with 1:250 diluted rabbit anti-LC3 antibody (Novus Biologicals) for 1 h, followed with 1:500 diluted FITC-conjugated donkey anti-rabbit secondary antibody (Novus Biologicals) for 1 h. The cells were counter stained with Hoechst 33342 and visualized using an Olympus IX70 inverted microscope equipped with a standard FITC/TRITC/DAPI filter set, Olympus DP72 camera, and CellSens software. Five fields of view were taken for each sample. The total number of cells in each field of view was determined based on Hoechst nuclei staining. The number of cells with at least one autophagosome stained were counted in each field of view and used to calculate the percentage of cells with autophagosomes as a quantitative measure of autophagy.

2.2.5 Western Blot

Twenty-four hours after the initial addition of polyplexes, cells were harvested by trypsinization and lysed in 1% nonidet-P40 containing 1 mg/mL aprotinin (Sigma), 1 mg/mL leupeptin (Sigma) and 1mg/mL pepstatin A (Sigma). The cell lysates were separated by 8%-16% sodium dodecyl sulfate polyacrylamide gel electrophoresis (SDS-PAGE) and transferred to a nitrocellulose membrane at 200 mA, 4ºC for 45 min and β-actin was used as an internal loading control. The membrane was blotted with 5% non-fat

dry milk in PBS containing 0.1% Tween 20 for 1 h at room temperature. Following the application of the primary rabbit anti-LC3 (1:1000 diluted, Novus Biologicals) or mouse anti-β-actin (1:3000 diluted, Sigma) antibody for 1 h, the blot was incubated with horseradish peroxidase (HRP)-conjugated donkey anti-rabbit or goat anti-mouse secondary antibody (1:5000 diluted, Amersham) for 1 h and developed using chemiluminescent substrates. The relative intensity of each band was determined using the gel analyzer function in ImageJ software.

2.2.6 Apoptosis/necrosis assay

Twenty-four hours after the transfection, cells were harvested by trypsinization, washed with 300 μL of Annexin V staining buffer (BioLegend) and resuspended in 100 μL of Annexin V staining buffer before they were stained with Alexa Fluor 647-labelled Annexin V (BioLegend) and propidium iodide (PI, BioLegend). The cells were then analyzed by flow cytometry using LSR II flow cytometer (Becton Dickson) and FlowJo software.

2.2.7 Analysis of Reactive Oxygen Species (ROS)

NIH3T3 cells were plated at 5×10^4 per well in 96-well plates and treated the same way as described above in Section 2.2. Four or twenty-four hours after the initial transfection, 40 μM of 2',7'-dichlorodihydrogluorescein diacetate (DCFH-DA, Signam-Aldrich) was added to the cells and incubated for 20 min at 37 ℃. The fluorescent signal was detected using a plate reader (Bio-Tek) with excitation at 485 nm and emission at 528 nm.

2.2.8 Cellular uptake and subcellular trafficking

To understand how polyplexes interact with fibroblasts during autophagy, cellular uptake and subcellular trafficking were studied as described in a previously published paper from our group[76]. Briefly, NIH3T3 cells were plated on chamber slides and treated the same way as described in Section 2.2. Cy5 fluorophore labeled luciferase plasmid was used in transfection. Thirty minutes before imaging, Hoechst 33342 (Invitrogen) was added to each chamber at a final concentration of 30 μM followed by LysoTracker Green DND-26 at a final concentration of 100 nM. The cells were then washed with PBS and mounted with 5 μM of ascorbic acid to minimize photobleaching. Cell images were captured using an Olypus FC-1000 confocal microscope equipped with an Olympus 60x/1.42 NA oil-immersion lens (Center Valley) and analyzed using Image J software following the protocols described in the published paper.

2.2.9 Statistical analysis

Comparisons between groups were made using Student's *t*-test. A p-value of less than 0.05 was considered to be statistically significant. All results were presented as mean ± standard deviation (SD) except that of the nuclear localization studies, which was presented as mean ± standard error (SE).

2.3 Results

2.3.1 Physical characterization of PEI/DNA polyplexes

PEI/DNA complexes were prepared at an N/P ratio of 8. The average hydrodynamic diameter of the polyplexes measured by dynamic light scattering was 116.6 $\pm$ 0.964 nm and the average zeta potential was +36.06 $\pm$ 2.77 mV. The morphology of the complexes was captured by TEM and the images showed globular particles with a roughly uniform size distribution (Fig. 1).

A

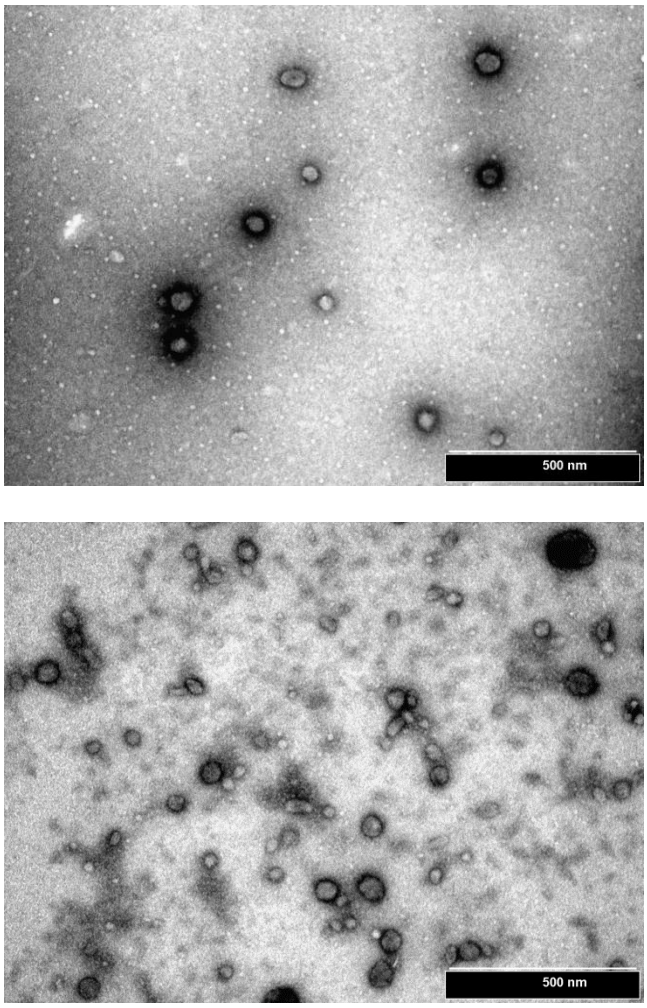

Fig. 1. Physical characterization of PEI/DNA polyplexes prepared at N/P ratio of 8. (A) A representative TEM image of PEI/DNA complexes at N/P ratio of 8.

2.3.2 Transfection by PEI/DNA polyplexes induced early autophagy in fibroblasts

The most traditional method for identifying autophagy is electron microscopy, and indeed, autophagy in mammalian cells was first discovered by this method[77, 78]. TEM reveals the presence of autophagosomes based on their unique morphology as double-membrane vesicles containing cytoplasmic materials or organelles such as the endoplasmic reticulum, mitochondria, and ribosomes. The diameter of autophagosomes in cultured cells usually averaged about 600 nm. Here TEM analysis showed that the majority of polyplexes transfected fibroblasts contained one or more double-membrane autophagosomes filled with cytoplasmic materials, whereas very few untreated cells had any autophagosomes (Fig. 2), indicating that exposure to PEI/DNA polyplexes induced early autophagy in fibroblasts.

The presence and subcellular distribution of the autophagy marker LC3 was validated and quantified by intracellular immunofluorescence staining with an anti-LC3 antibody followed by fluorescence microscopy. We observed that LC3 II was present in the untreated fibroblasts and localized to the autophagosomes as distinct puncta (Fig. 3A), which is typical for cells undergoing autophagy [25, 26]. The average fraction of polyplex-transfected cells containing at least one autophagosome was approximately 30%, significantly higher than untreated cells with basal autophagy (around 5%) (Fig. 3B). When transfected cells were treated the autophagy inhibitor 3-MA, the average fraction of autophagic cells was reduced to slightly below 20%, whereas treatment with the autophagy inducer rapamycin increased it to nearly 50% (Fig. 3). Treatment with PEI

alone also resulted in the formation of the characteristic LC3 puncta in fibroblasts, although at a slightly lower level than the fibroblasts treated with polyplexes (Fig. 4).

The two subtypes of LC3 proteins (I and II) were detected and quantified through analyzing the cell lysates by Western blot. Relative to the cytoplasmic LC3 I, the autophagosomal LC3 II was detected at low amounts in untreated cells but was at much higher levels in polyplex-transfected cells (Fig. 5A). The band intensity ratio of LC3 II over β-actin is known to highly correlate with the number of autophagosomes[79]. Therefore, LC3 II/β-actin ratio was much higher for polyplex-transfected cells than untreated cells (Fig. 5B), indicative of polyplex-induced autophagy. Treatment with 3-MA or rapamycin reduced or increased the relative expression of LC3 II in transfected cells (Fig. 5), suggesting less or more autophagy induction, which agrees well with the findings by LC3 immunofluorescence microscopy (Fig. 3).

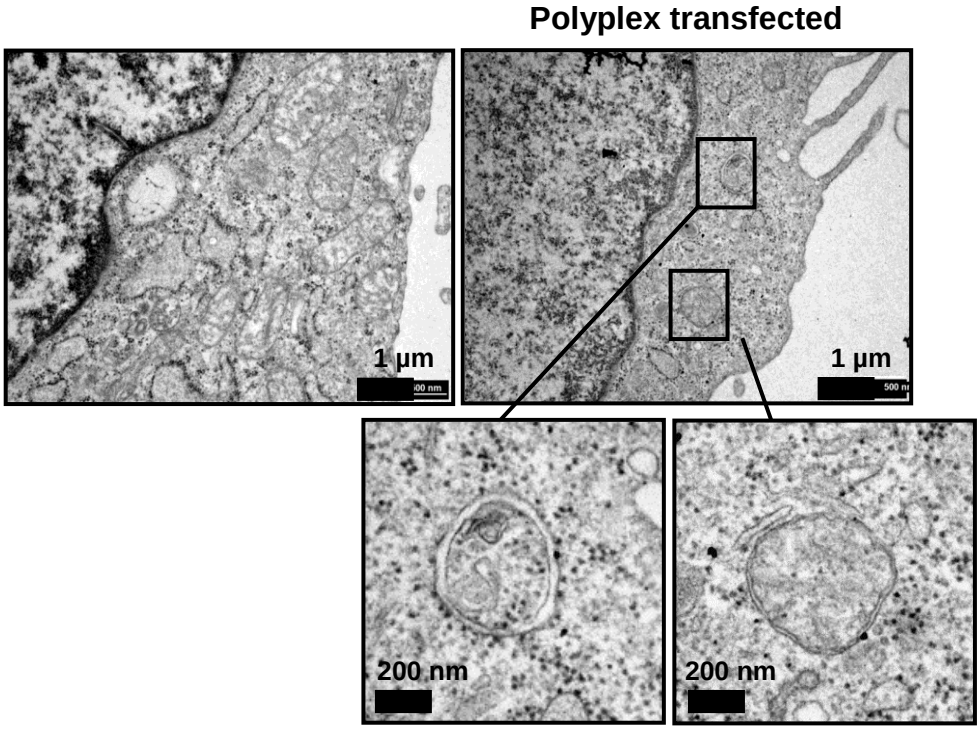

Fig. 2. Representative TEM images of the cytoplasm of untreated and PEI/DNA polyplex transfected fibroblasts, showing autophagosomes with distinct double-membrane structure inside transfected cells. Scale bar: 1 µm (top panels), 200 nm (enlarged panels).

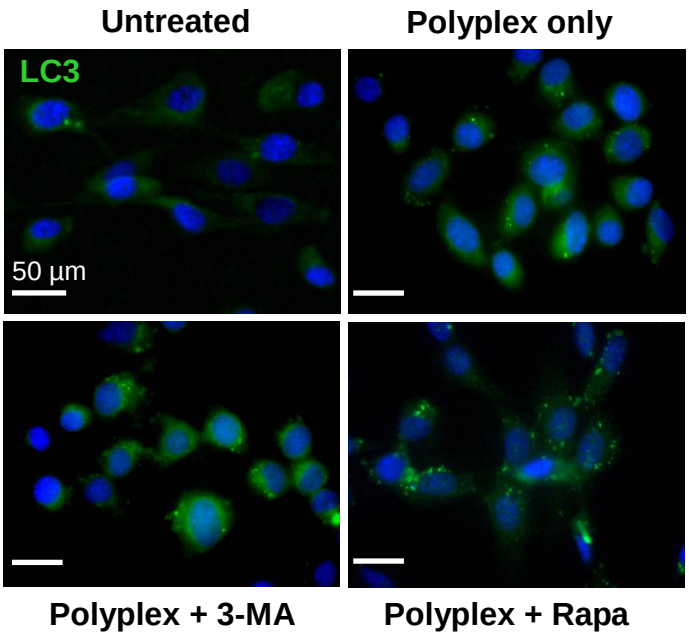
Untreated
Polyplex only
LC3
50 µm
Polyplex + 3-MA
Polyplex + Rapa

A

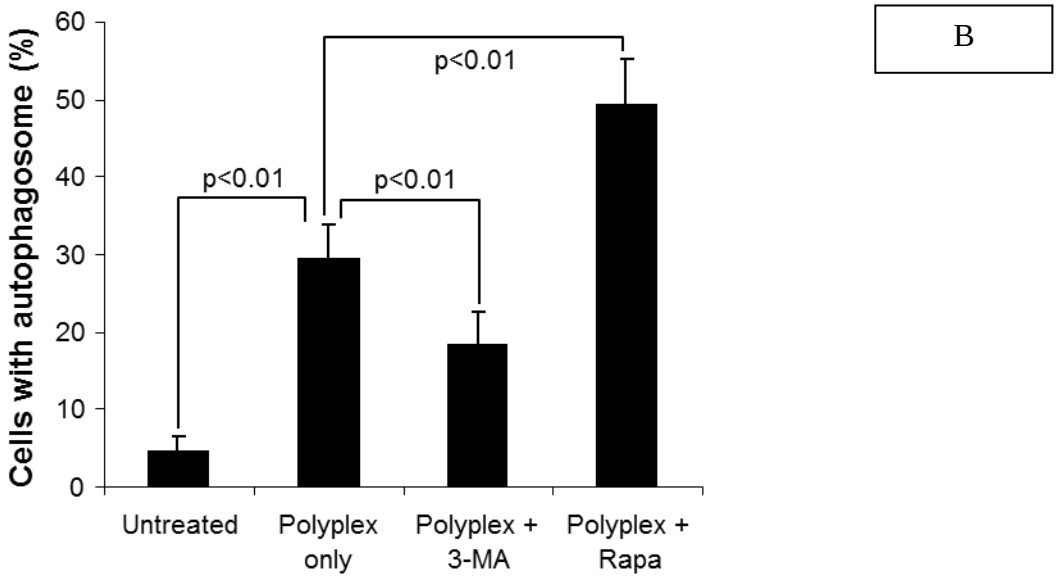

Fig. 3. PEI/DNA polyplex transfection resulted in LC3 puncta formation in fibroblasts. (A) A set of representative images of LC3 immunofluorescence staining in fibroblasts that were either untreated, transfected with polyplexes, or transfected in the presence of 10 mM 3-MA or 100 nM Rapa. Scale bar: 50 μm. (B) Quantification of LC3 puncta (representing autophagosomes) in fibroblasts. An average of 300 cells was counted for each sample.

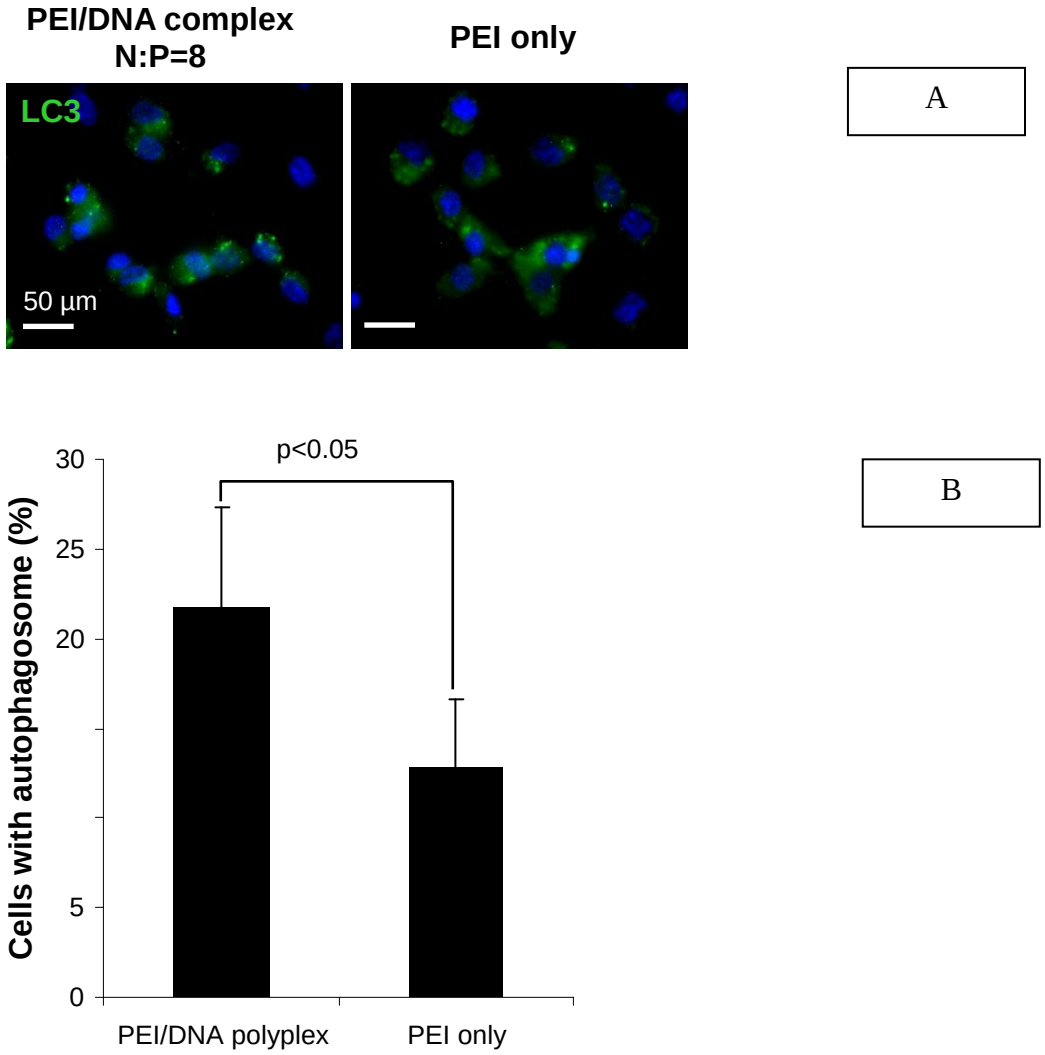

Fig. 4. PEI/DNA polyplex transfection resulted in LC3 puncta formation in fibroblasts. (A) A set of representative images of LC3 immunofluorescence staining in fibroblasts that was either untreated, transfected with polyplexes, or transfected in the presence of PEI only. Scale bar: 50 µm. (B) Quantification of LC3 puncta (representing autophagosomes) in fibroblasts. An average of 300 cells was counted for each sample.

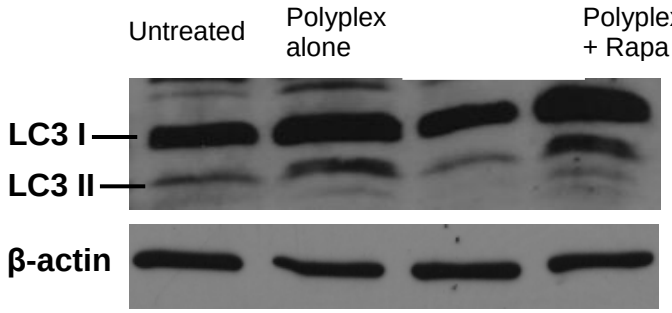

A

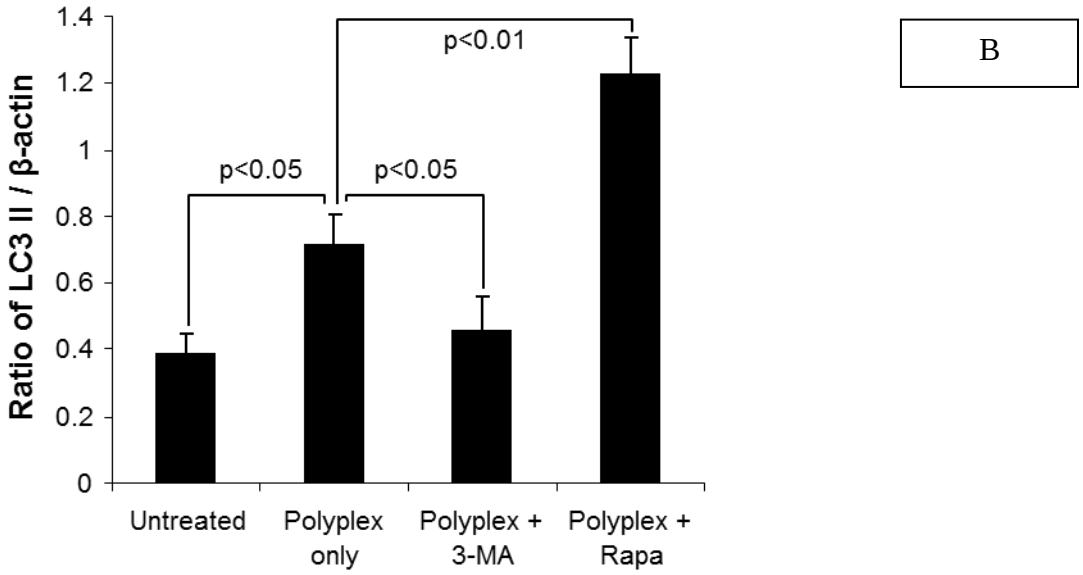

Fig. 5. Western blot of LC3 isoforms. (A) A representative blot of fibroblasts that were either untreated, transfected with polyplexes, transfected in the presence of 10 mM 3-MA or 100 nM Rapamycin. (B) Densitometry analysis of the ratio of band intensities between LC3 II and β-actin. The bar graph represented the average of three independent experiments with standard deviations.

2.3.3 Modulation of polyplex-induced autophagy in fibroblasts did not affect cytotoxicity due to apoptosis or necrosis

To decouple cytotoxicity due to autophagy from other pathways of cell death, we monitored the changes in apoptosis and necrosis by staining cells with Annexin V and PI after autophagy modulators were applied during transfection with polyplexes. Comparing to untreated cells, there was only minor cytotoxicity (~5.5%) due to apoptosis and necrosis in fibroblasts after transfection with PEI/DNA complexes at N:P ratio of 8 (Fig. 6), which is consistent with our previous findings [31]. Moreover, the addition of autophagy modulators, 3-MA (10 mM) or rapamycin (100 nM), did not change the percentage of apoptotic and necrotic cells significantly comparing to cells exposed to polyplexes without the autophagy modulators (Fig. 6).

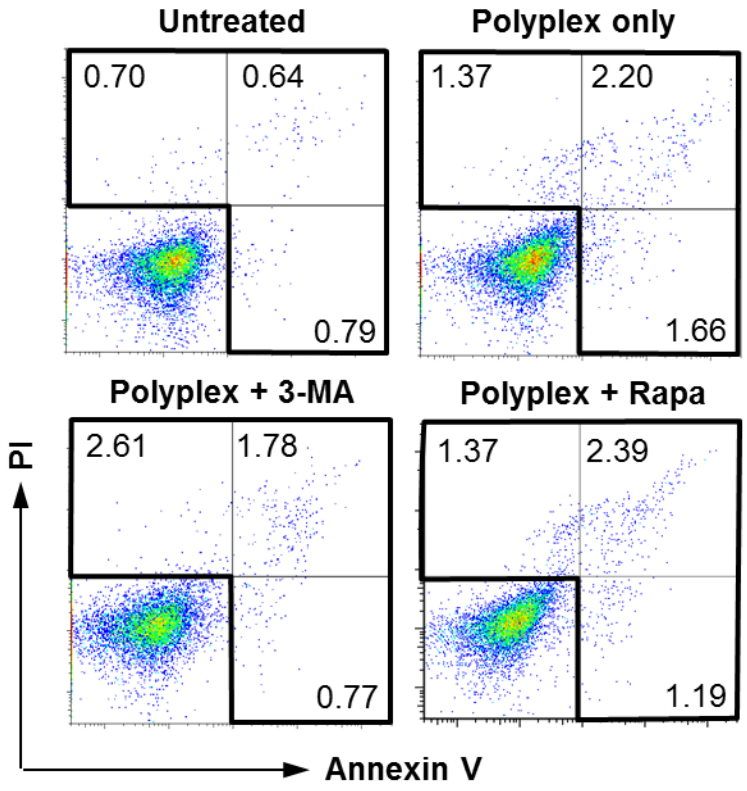
Untreated
Polyplex only
Polyplex + 3-MA
Polyplex + Rapa
0.70
0.64
0.79
1.37
2.20
1.66
2.61
1.78
0.77
1.37
2.39
1.19
PI
Annexin V

A

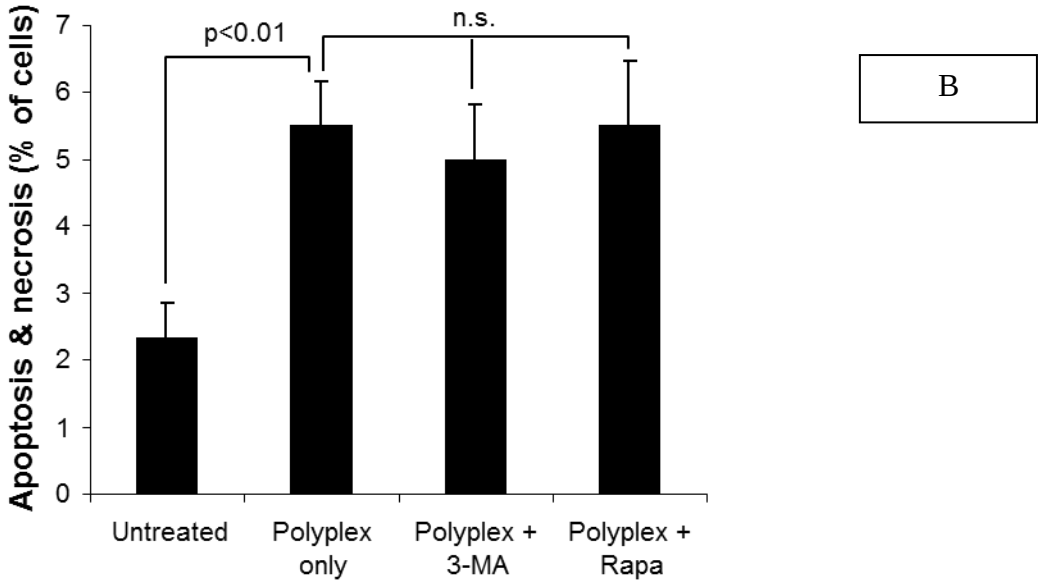

Fig. 6. Modulation of polyplex-induced autophagy in fibroblasts did not affect cytotoxicity due to apoptosis or necrosis. (A) A representative set of dot plots of apoptotic and necrotic cells by flow cytometry after staining with Annexin V and PI. (B) Quantification of apoptosis and necrosis. The bar graph represented the average of triplicates with standard deviations. n.s.: not significant statistically.

2.3.4. Transfection efficiency was positively correlated with polyplex-induced autophagy in fibroblasts

It has been shown in the previous section that the selected drug concentrations and treatment schemes did not aggravate apoptosis or necrosis. To examine the effect of modulating autophagy on transfection efficiency, we determined GFP transgene expression level in fibroblasts with treatment of 10 mM 3-MA or 100 nM rapamycin. After normalizing transfection efficiency against the polyplex only group (Fig.7), we found 3-MA reduced the fraction of GFP^+ cells by 80%, but the addition of rapamycin increased the percentage of GFP^+ cells by approximately 27% (Fig. 7). The corresponding reduction and increment in MFI of all cells was >90% and ~100%, respectively (Fig. 7). These results established a positive correlation between transfection efficiency and polyplex-induced autophagy. We further tested the effect of different doses of 3-MA and Rapa on gene transfection and the results are shown in Fig. 8. It is clear that with increasing dose of 3-MA, transfection efficiency decreased. Transfection was enhanced in the presence of 50 and 100 nM Rapa and no further enhancement was seen at 1000 nM. These results established a robust, positive correlation between transfection efficiency and autophagy modulation.

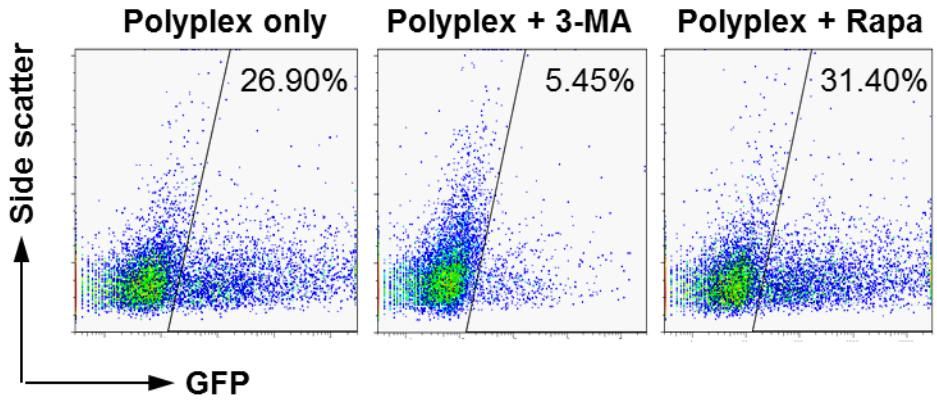
Polyplex only
Polyplex + 3-MA
Polyplex + Rapa
26.90%
5.45%
31.40%
Side scatter
GFP

A

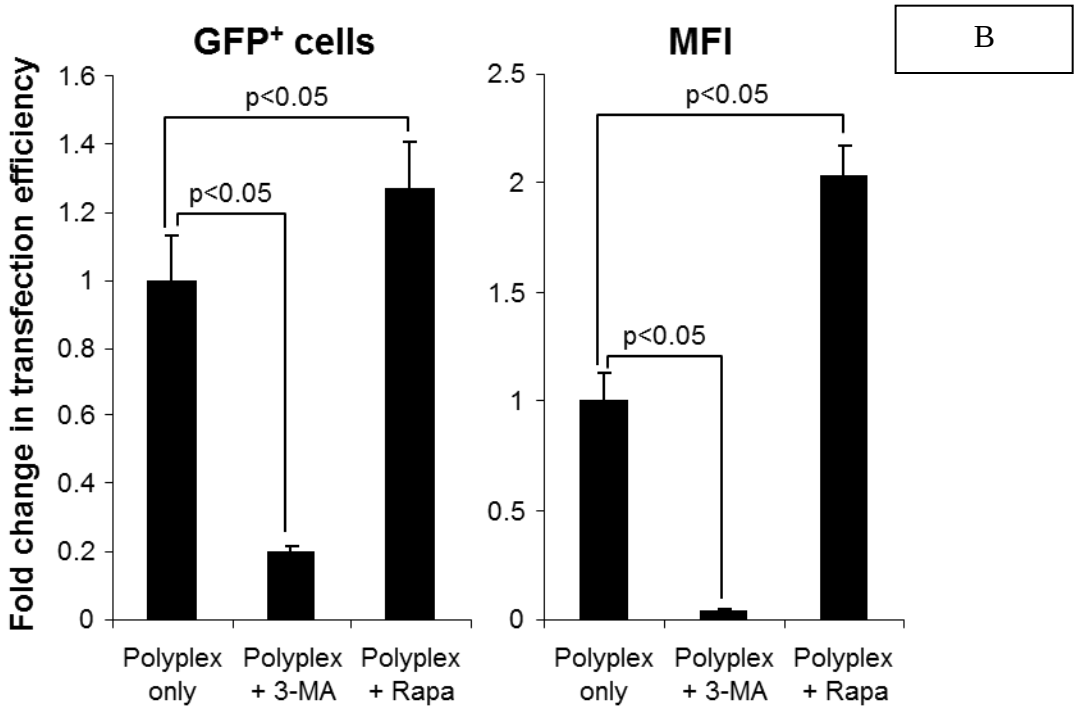

Fig. 7. Inhibition of polyplex-induced early autophagy decreased GFP transgene expression while promoting autophagy increased GFP transgene expression. (A) A representative set of dot plots of flow cytometry showing GFP^+ cells. (B) Quantification of transfection efficiency, either as percent of GFP+ cells or as mean fluorescence intensity (MFI), then normalized against that of the polyplex-transfected cells without any autophagy modulators. The bar graph represented the average of triplicates with standard deviations.

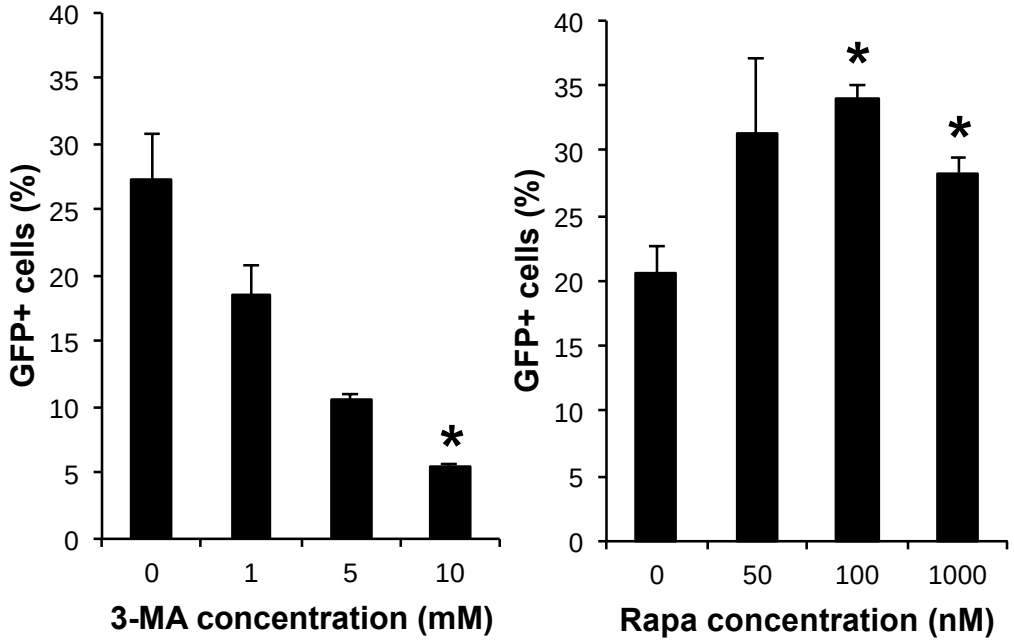

Fig. 8. Dose dependence of 3-MA/Rapa treatments on transfection efficiency. * $p<0.05$, compared to transfection without adding 3-MA or Rapa.

2.3.5 Transfection of PEI/DNA polyplexes elevated the level of intracellular ROS but modulating autophagy does not affect the ROS production

Intracellular ROS was probed with DCFH-DA 4 h and 24 h after the initial transfection with or without autophagy modulators. Early on during transfection (4 h), there was no significant difference in the intracellular ROS level between the untreated and polyplexes treated cells (Fig. 9). Although there is no statistically significant difference, the 3-MA treated cells had slightly higher ROS level than the polyplexes only group, and the rapamycin treated cells had slightly lower ROS level than the polyplexes only group. Twenty-four hours after the transfection, all three polyplexes treated groups showed a slight but significantly higher ROS production than the untreated group. However, the 3-MA or the rapamycin treated cells did not show any significant difference in ROS compared to the polyplexes only group (Fig. 9).

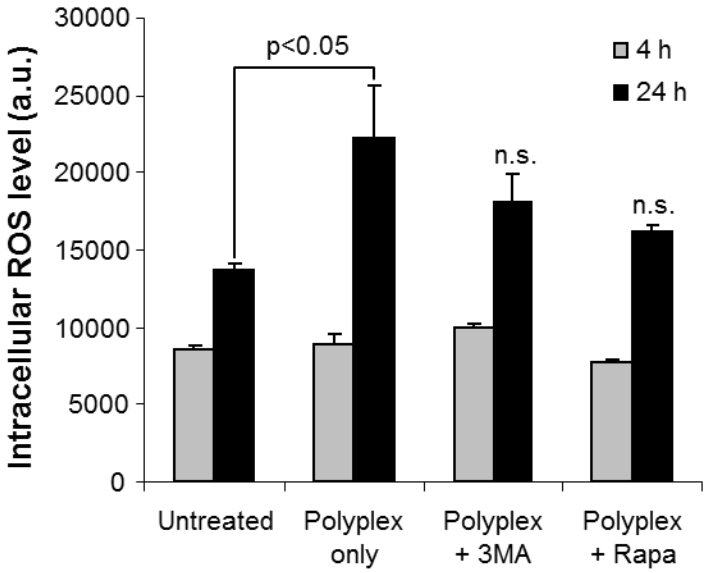

Fig. 9. ROS measurement of polyplexes with or without autophagy modulators.

2.3.6 Autophagy regulation affected cellular uptake and subcellular trafficking

Polyplex containing Cy5-labeld luciferase plasmid was used to visualize nuclear localization by confocal fluorescence microscopy 4 h and 24 h after transfection. The efficiency of nuclear entry by the plasmid was quantified by the total fluorescence intensity of Cy5 signal inside the nucleus (Fig. 10). There were expected increases in nuclear localization from 4 h to 24 h across all the groups. At 4 h there was less amount of plasmid localizing in the nuclei of cell treated with 3-MA and rapamycin than cells without these treatments. By 24 h, nuclear localization in 3-MA treated cells was still lower, but rapamycin treatment led to a significant higher nuclear uptake of plasmid (Fig. 10).

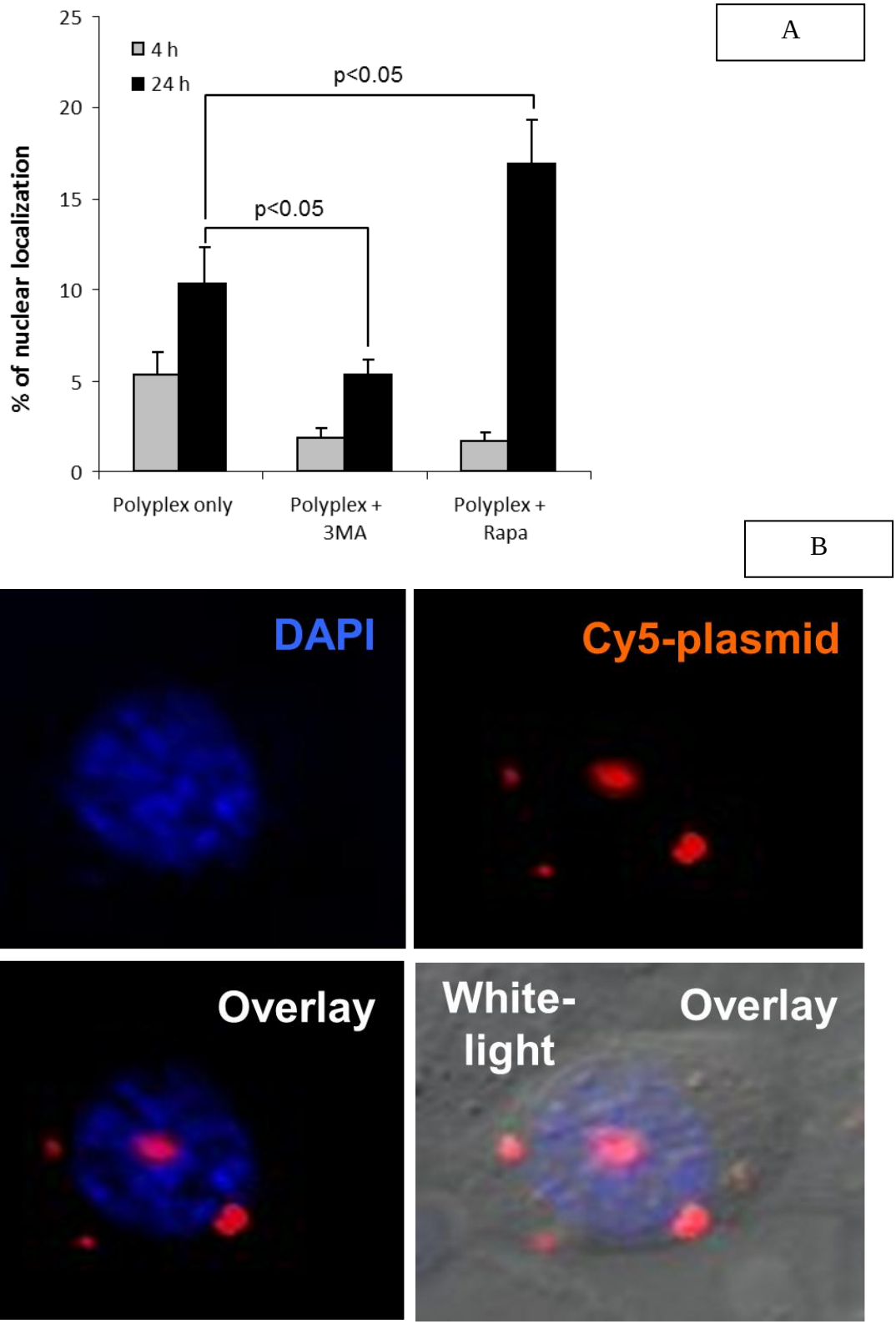
A
25
20
15
10
5
0
4 h
24 h
p<0.05
p<0.05
% of nuclear localization
Polyplex only
Polyplex + 3MA
Polyplex + Rapa
B
DAPI
Cy5-plasmid
Overlay
White-light
Overlay

Fig. 10. Nuclear uptake of plasmid DNA delivered as polyplexes with or without treatment of 3-MA (10 mM) or Rapa (100 nM). Quantification of (A) nuclear uptake was presented as the average of 30 cells with standard errors, and (B) a set of representative images.

2.4 Discussion

While autophagy, as an important form of cell stress response and cell death pathway, has long been established, it is only in recent years that nanomaterial-induced autophagy has been reported [41, 47, 48]. In this study, we demonstrated that transfecting fibroblasts with PEI/DNA polyplex led to the induction of autophagy using three different common techniques. By TEM analysis, autophagosomes are identified as characteristic double-membrane vacuoles containing cytoplasmic materials [77, 80]. Double-membrane autophagosomes were clearly observed in TEM images of fibroblasts treated with polyplex (Fig. 2). Further quantification using biochemical assays of LC3 confirmed our observation by TEM. Immunofluorescence staining of LC3 revealed the redistribution of LC3 from cytosolic soluble form (LC3 I) to the membrane-bound form (LC3 II), indicating the formation of autophagosomes (Fig. 3A). The conversion of LC3 I to LC3 II was also quantified by Western blot (Fig. 5). Taken together, these pieces of evidence strongly suggest that PEI/DNA polyplex transfection induced autophagy in fibroblasts, which is consistent with observations made by other groups different cell types and other cationic polymers [41, 47, 48, 73, 74, 81]. We also compared autophagy induction by PEI polymer alone with PEI/DNA polyplex at the same dose (Fig. 4), and the results suggest that the nanoparticulate form of the polyplex might be more potent in autophagy induction than the free polymer alone. This could be due to differences in positive charge density and particle size between the free polymer and the nanoparticulate polyplex.

The mechanism of autophagy induction by nanoparticles of diverse compositions is not clearly understood. An important mediator is likely to be reactive oxygen species (ROS).

First, ROS generation and oxidative stress are often found in different types of cells upon exposure to a variety of nanoparticles such as gold, silica, titanium oxide, iron oxide, lipoplexes, and polyplexes [46, 82, 83]. Intracellular ROS can oxidize genomic DNA, cellular proteins and lipids [84], resulting in breakage of DNA strands and accumulation of damaged proteins in the ER lumen that could eventually lead to cell death. Second, elevated ROS level is known to trigger autophagy to alleviate ROS-induced cytotoxicity through clearing damaged molecules and subcellular structures [85-88]. Therefore, we postulate that polyplex-induced autophagy in fibroblasts that we observed here may be related to the intracellular ROS production triggered by exposure to the PEI/DNA polyplex as well as free PEI chains. Compared to untreated cells, we have indeed detected a slightly higher level of ROS in polyplex treated cells that underwent autophagy (Fig. 8). Thus, our observation reinforces the possibility that the intracellular ROS production may play a role in polyplex-induced autophagy.

What is the impact of autophagy on polyplex-mediated gene delivery? To address this question, one must first decouple the potential effect due to autophagy from that due to apoptosis and necrosis. It is well established that autophagy and apoptosis share a complex functional relationship with each other, that is, inhibiting one often aggravates the other [75]. For example, when autophagy was inhibited in sulindac sulfide treated HT-29 colon carcinoma cells, apoptosis in these cells was enhanced [89]. On the other hand, suppressing apoptosis could activate autophagy in mouse fibroblasts or macrophages [90]. Previous work from our lab[7] and others [3, 24, 66, 68] has also shown that polyplex transfection induces apoptosis and necrosis. Here we took two measures to

ensure that the functional consequence of autophagy was examined and modulated without the interference from apoptosis. First, the dose and N:P ratio of PEI/DNA polyplex for transfection were chosen as such that apoptosis and necrosis due to polyplex treatment was minimized (Fig. 6). Second, the dosages of autophagy modulators (3-MA and rapamycin) and the time course of treatment were optimized so that they could effectively inhibit or activate autophagy (Fig. 3 & 4) without causing additional apoptotic or necrotic response (Fig. 6).

Interestingly, we found that inhibiting autophagy with 3-MA during polyplex-mediated gene delivery reduced transfection efficiency, whereas further activating autophagy using rapamycin increased transgene expression (Fig. 7). Attempting to explain our observation, we first consider the potential role of oxidative stress. Elevated level of intracellular ROS is known to correlate strongly with cytotoxicity of cationic polymers such as PEI in a number of cell types [91, 92]. It is also known that reducing oxidative damage through lowering intracellular ROS level could improve cell survival and enhance transfection efficiency [91, 92]. Thus, it might be possible that inhibiting or activating autophagy led to aggravation or relief of oxidative stress, thereby impairing or enhancing transfection. However, we found that treatment with 3-MA or rapamycin did not cause any significant change in intracellular ROS level (Fig. 8), suggesting that oxidative stress was not the reason for the observed changes in transfection efficiency. We then considered the possible scenario that autophagy modulation somehow altered the subcellular trafficking process of the polyplex. To achieve transgene expression, the polyplex must traverse several intracellular barriers to deliver the plasmid DNA into the

cell nucleus [93-95]. We found that nuclear localization of plasmid DNA was reduced in 3-MA-treated cells but was enhanced in rapamycin-treated cells (Fig. 10), which correlated well with the reduction and enhancement of transfection efficiency (Fig. 6). It was reported that some polyplex inside autophagosome was found in the perinuclear region[74]. In our case, the PEI/DNA polyplex escaping autophagosome in the vicinity of the nucleus would have a higher probability of entering the nucleus via a shorter path, which could be a plausible explanation for the observed increase in nuclear translocation of plasmid and transfection efficiency. Whatever the mechanism may be, it is certain that subcellular trafficking of polyplex must play a pivotal role in determining how autophagy modulation impacts gene delivery.

Two outstanding challenges require future investigation. The first challenge is to understand if selecting different molecular targets for autophagy modulation could impact gene delivery in different ways. Recently Roberts *et al* [74]reported that polyplex consisting of a proprietary polymer (JetPRIME, composition unknown) and plasmid DNA was endocytosed and localized in tubulovesicular autophagosomes (TVAs) of cells. They further showed that when TVA formation was disabled in *atg5* knockout cells, polyplex-mediated gene transfection was compromised, suggesting that autophagy could be a barrier for gene delivery. Numerous factors could account for the disparate conclusions of Roberts *et al* [74]and our study. There are major differences in the type of polyplex and cells used, time course/medium/dosage of transfection, and in particular, selection of molecular target for autophagy modulation. TVA, a special form of autophagosome, is formed through a noncanonical pathway of autophagy independent of

class III phosphatidylinositol 3-kinase (PIK3C3) but dependent on ATG5[74]. However, the small-molecule autophagy modulators used in this study target the canonical pathway of autophagy with 3-MA inhibiting phosphatidylinositol 3-kinase (PI3K) and rapamycin inhibiting mTOR [96]. Thus, targeting different molecules and pathways of autophagy does seem to produce different functional outcome in gene delivery. The second challenge is to gain comprehensive understanding of how autophagy modulation alters the subcellular trafficking pathways of polyplex. Autophagy activation and inhibition could potentially impact endocytic uptake, autophagosomal localization, and nuclear transport of polyplex. Previous studies suggest that entrapment inside autophagosome could be a hurdle for gene delivery [73, 74], but on the other hand, transportation of autophagosome-entrapped cargo to the perinuclear region[74] might actually increase the chance of delivery into the nucleus and enhance transgene expression. Our results here further indicate that small-molecule modulators of autophagy could either facilitate or hinder nuclear delivery of plasmid DNA. Visualization and quantitative assessment of subcellular trafficking of polyplex in autophagic cells will help identify rate-limiting steps of delivery and offer better strategies to overcome them. Amidst the growing interest in targeting autophagy for therapeutic purposes[97], this work advocate the possibility of enhancing the efficiency of nonviral gene delivery through autophagy modulation. It is envisioned that this approach could be carried out by co-delivery of small-molecule autophagy modulators [98] and therapeutic genes using appropriately designed dual functional polymeric carriers.

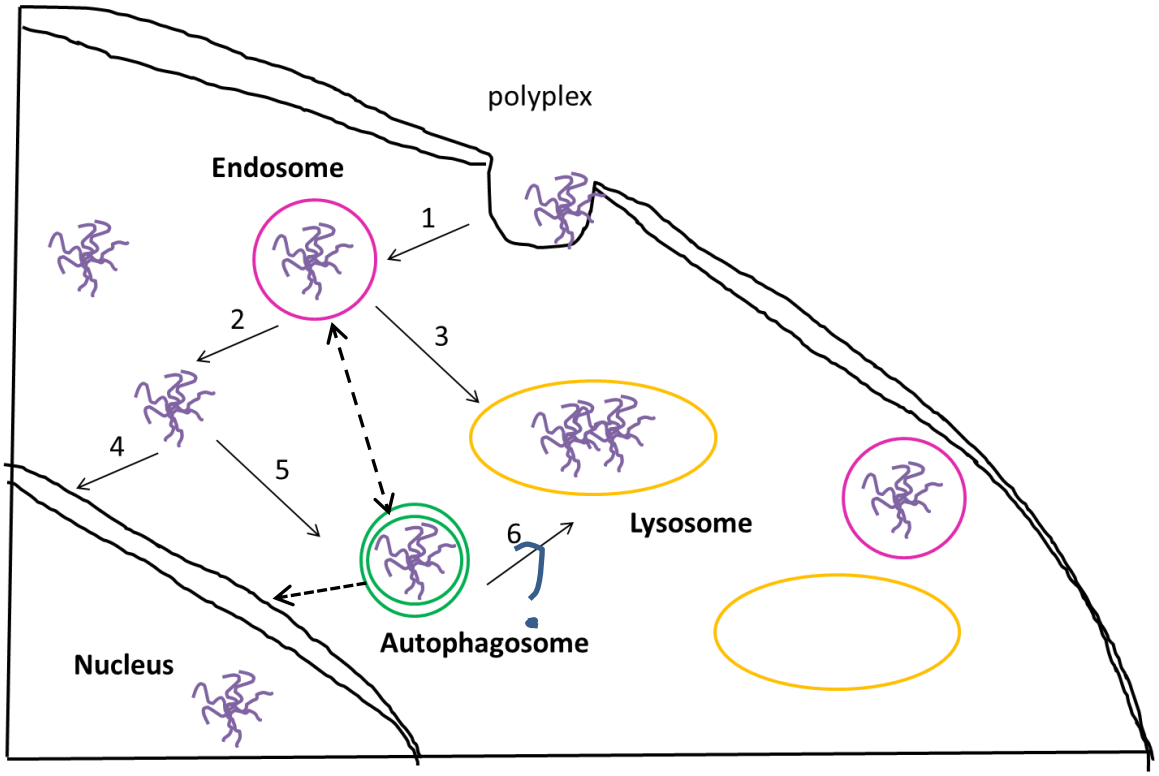

Fig. 11. A schematic summary of proposed intracellular trafficking pathway involving autophagy. Polyplex is taken up by cell through endocytosis (1). Some of the polyplexes can escape endosome (2) and enter cytoplasm. Other polyplexes remained in endosome and were delivered to lysosome for degradation when the endosome was fused with lysosome (3). Two possible fates could happen to the polyplexes free in the cytoplasm. They can swim towards the nucleus and enter the nucleus undisturbed (4), or some of them will be encapsulated by autophagosome on their way to the nucleus (5). Some of the autophagosomes may swim towards the nucleus, bring the polyplexes closer to the nucleus. Other autophagosomes may engulf endosomes that are loaded with polyplexes, preventing them from fusing with lysosome and therefore protecting polyplexes from lysosomal degradation.

To the best of our knowledge, this is the first study reporting that the induced autophagy plays an important role in regulating gene transfection efficiency. While an earlier work has reported that PEI-induced autophagy contributed to cell death [48], our study reveals that autophagy has a significantly positive impact on polyplex-mediated gene transfer. Our findings suggest that promoting autophagy may be a useful approach to augment polymer-mediated gene delivery. Conceivably, this could be accomplished through adjusting the dose of the polyplex and co-delivery of autophagy inducers or apoptosis inhibitors with the polyplex.

2.5 Conclusions

Transfection of mouse fibroblasts using appropriately formulated PEI/DNA polyplex activated early autophagy with only minimal apoptotic or necrotic cytotoxicity. Polyplex-induced autophagy was confirmed by visualization of double-membraned autophagosome, intracellular aggregation of LC3 indicative of autophagosome formation, and quantification of autophagosome-associated LC3 II protein. Treating polyplex-transfected cells with autophagy-inhibiting 3-MA reduced transfection efficiency, whereas cells treated with autophagy-activating rapamycin resulted in enhancement of transgene expression. Treatment by these small-molecule modulators of autophagy did not cause any additional apoptosis or necrosis in cells, thus allowing decoupling the functional consequence of autophagy from that of other modes of cellular stress response. Autophagy modulation had no impact on oxidative stress imposed by the polyplex but did alter significantly the amount of plasmid DNA localized to the cell nucleus, implicating subcellular trafficking as an important factor in determining how autophagy

affects gene delivery. These findings advocate a new strategy of enhancing polyplex-mediated gene transfection efficiency by small-molecule regulators of autophagy.

Chapter 3: Structure-function Relationship of Well-defined Polymeric Gene Carriers: Comparison of in vitro Properties with in vivo Performance

3.1 Introduction

Gene therapy holds great potential to enhance human medicine since it can potentially treat a variety of genetic disorders or cancers[12]. The goal is to deliver a sufficient amount of DNA to produce a therapeutic level of protein which in turn can alleviate the phenotypes of the disease. Many viral vectors have been used to deliver the genetic materials since they often provide a high delivery efficiency[10]. However, they pose safety concerns since they can provoke severe immune response in the host, leading to fatalities[99]. Non-viral vectors provides a synthetic alternative to the problem and possess the potential advantages of low immunogenicity and easy of synthesis[15]. The hurdle with non-viral vectors remains in the low delivery efficiency, and it is critical to develop safe and effective non-viral vector to bring the eventual success of gene therapy.

Polycationic polymers have been widely investigated as gene livery carrier because of their versatility. Physical properties such as polymer molecular weight or chain length and surface characteristics are important factors in the design of polycationic polymer based gene carriers, and they can be tuned to modulate gene delivery properties including DNA binding, colloidal stability of the complex, endosomal escape, cytotoxicity and transfection efficiency.

Molecular weight or polymer chain length plays a key role affecting transfection efficiency. Hennink and colleagues reported that the molecular weight of poly(2-dimethylaminoethyl methacrylate) (PDMAEMA) significantly affected transfection efficiency, and a higher molecular weight favored the high transfection efficiency[17]. Mikos and colleagues determined that the higher molecular weight PEI transfected better than the lower molecular weight PEI[18]. In general, a higher molecular weight is in favor of a high gene expression, but some discrepancies existed[19]. A fundamental understanding of the effect of linear polycation chain length on the gene delivery process, especially in the in vivo environment remains elusive.

The in vivo efficiency of the polyplex delivery system depends on its ability to overcome both the extracellular and intracellular hurdles. The extracellular barriers involve serum proteins and components of the extracellular matrix (ECM), a large proportion of which are negatively charged[49]. The negative charge interacts with the positive charge of the surface of the polyplexes, leading to complex dissociation or aggregation. To limit non-specific protein binding and mask the net positive charge, poly(ethylene glycol) (PEG) is often grafted to the surface of the complex, and PEGylation has been reported to be a very effective way to attenuate the positive surface charge and improve polyplex stability under physiological salt and serum condition[56, 57]. Both PEG chain length and grafting density could influence the pharmacokinetic properties of the polyplexes[100], however, in vivo studies reported in literature have controversial results. Some groups reported that a low graft density with a long PEG chain is more effective[61], and others found the grafting density is more dominant than

PEG chain length[62]. A better understanding of the effect of PEGylation and PEG chain length on the in vivo physiological and biological properties of the nanocomplexes is essential to provide insight for the design of a more efficient gene carrier.

In this study, we used 2 series of poly(2-aminoethyl methacrylate) (PAEM) polymers with well-defined chain length and narrow molecular weight distribution to conduct a comprehensive investigation of colloidal properties of PAEM/DNA or PEG-PAEM/DNA polyplexes. Particle size, surface charge, polyplex stability in vitro and in vivo transfection, as well as local biodistribution were carefully examined to further elucidate the impact of polymer chain length, PEGylation and PEG chain length on gene carrier design.

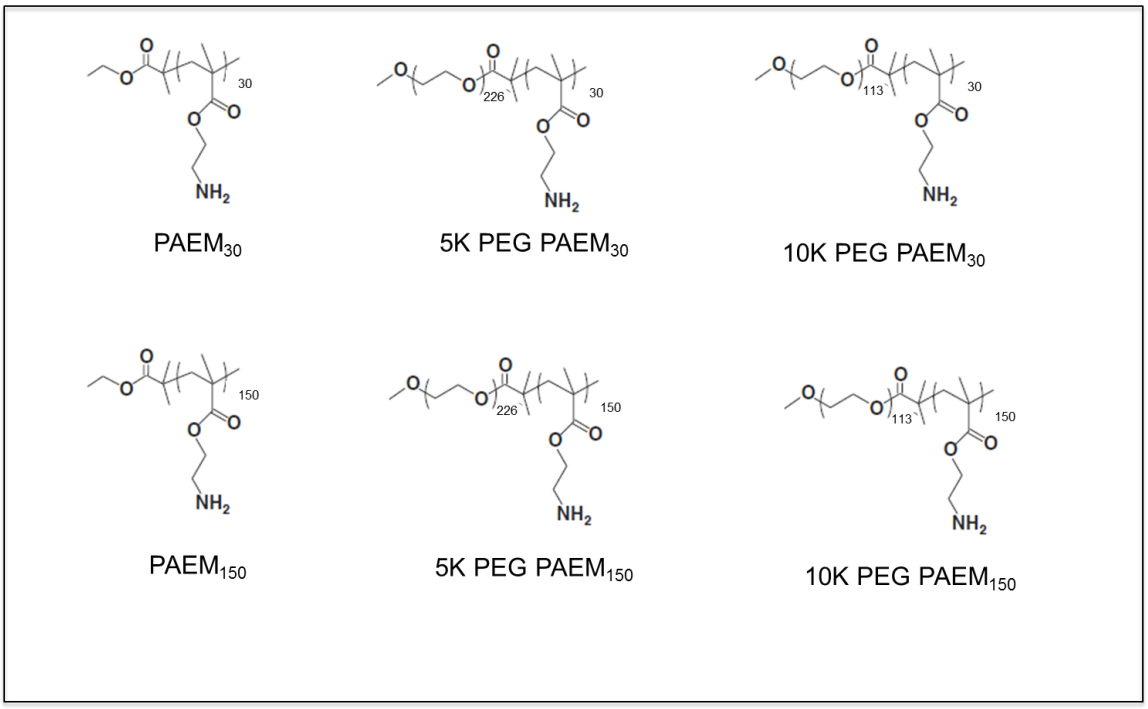

Fig. 12. Chemical structures of the 2 series of PAEM polymers tested.

3.2 Experimental Methods

3.2.1 Dynamic Light Scattering and Zeta Potential Measurement

The average hydrodynamic diameter and polydispersity index of polyplexes in HEPES buffer (20 mM) at 25 ℃ were determined using a ZetaPlus particle analyzer (Brookhaven Instruments Corp., Holtsville, NY; 27 mW laser; 658 nm incident beam, 90 °scattering angle). Polyplexes with N/P ratios ranging from ½ to 16 were prepared by adding 25 μL of polymer solution in 20 mM HEPES (pH 7.4) to 25 μL of DNA plasmid solution (0.2 μg/μL in 20 mM HEPES, pH 7.4), vortexed for 10 s, and incubated for 30 min at room temperature. The polyplex solutions were diluted 20 times to a final volume of 2 mL in HEPES buffer before measurement. Simultaneously, the zeta potential of the polyplexes was determined using the ZetaPal module of the particle analyzer.

3.2.2 Gel Retardation Assay

Polyplexes of N/P ratios ranging from 1/8 to 16 were prepared as described above and analyzed by electrophoresis on a 1.0% agarose gel containing 0.5 μg/mL ethidium bromide.

3.2.3 Heparin Competition Assay

To determine the strength of DNA binding by polymers with varying chain length, polyplexes at N/P ratio of 8 were incubated with increasing concentrations of heparin (0.1-0.9 IU per μg of DNA) for 20 min at room temperature and analyzed by agarose gel electrophoresis.

3.2.4 Ethidium Bromide (EB) Exclusion

Polymer solutions were added to premixed EB solution and plasmid solution with varying N/P ratios from 1/8 to 16 and incubated for 30 min. the intensity of EB fluorescence was recorded by a Bio-Tek Synergy HT plate reader with excitation wavelength of 530/25 nm and emission wavelength of 590/35 nm. DNA/EB solution without any polymer was used as a control.

3.2.5 Circular Dichroism

Polyplexes were prepared at an N/P ratio of 8 at a final volume of 200 μL by adding 100 μL of the polymer solution with the final concentration of 0.625 μg/μL to 100 μL pCMV-Luc plasmid DNA (Elim Biopharmaceuticals) solution (0.25 μg/μL) in 20mM HEPES. The complexes were then incubated at room temperature for 30 min prior to analysis. The secondary structure of the DNA plasmid was measured using a J-815 Spectropolarimeter (JASCO, Easton, MD). The polyplex samples were run using 200 μL of solution at a wavelength range of 220 to 320 nm at a scanning speed of 50 nm/min at 25 °C. A total of 5 accumulations were collected for each sample. Naked luciferase DNA plasmid and polymer only (for each polymer) were run as positive and negative controls.

3.2.6 Polyplexes Stability in Serum Containing Medium

Forty μL of polyplex solution containing 5 μg of Cy5-labeled plasmids DNA was added to another 40 μL of cell culture medium comprised of DMEM medium (1 g/L D-glucose, L-glutamine, 110 mg/L sodium pyruvate) supplemented with 10% heat-inactivated fetal bovine serum (FBS), 100 units/mL penicillin/streptomycin, and 10mM

HEPES (all cell medium components were from Gibco). Five μL of the polyplexes solution was removed immediately after dilution and after 1 h incubation at room temperature, placed onto a glass microscope slide, covered with a glass coverslip, and was observed under Nikon 100 motorized fluorescence microscope.

3.2.7 Gene Transfection In Vitro

NIH 3T3 murine fibroblasts (ATCC) were cultured in DMEM (1 g/L D-glucose, L-glutamine, 110 mg/L sodium pyruvate, Gibco) supplemented with 10% fetal bovine serum (heat inactivated, Gibco) and 100 units/mL penicillin/streptomycin (Gibco).

NIH 3T3 cells were plated at 5×10^4 per well in 12-well plates and allowed to adhere overnight. After washing with phosphate buffered saline (PBS, pH7.4), the cell media was replaced with serum free media and polyplexes were added to the cells, incubated for 4 h. The cells were then washed three times with PBS before replacing the serum free media back to regular cell media with 10% serum. Twenty-four hours after the initial addition of polyplexes, cells were washed with PBS, trypsinized, suspended in in FACS buffer (containing 1% bovine serum albumin, BSA, and 1 mM sodium azide in PBS) and analyzed by flow cytometry using LSR II flow cytometer (Becton Dickson) and FlowJo software. Cells transfected with luciferase encoding DNA were used as the control for any increased autofluorescence of cells caused by polyplexes nonspecifically. GFP-positive cells were gated against the luciferase transfected control cells.

3.2.8 Injection

Polyplex solutions were injected subcutaneously with a 29-gauge needle into the hind leg of 10 week old female Balb\c mice (Jackson Lab). Twenty-five μg of DNA complexed with polymers at an N/P ratio of 8 was prepared as described above and was injected into each mouse in a total volume of 200 μL. The same volume of naked DNA and buffer (5% glucose solution) only injections were also administered. Three mice per sample group were injected. Polyplexes containing all six cationic polymers ($PAEM_{30}$, 5K PEG-*b*-$PAEM_{30}$, 10K PEG-*b*-$PAEM_{30}$, $PAEM_{150}$, 5K PEG-*b*-$PAEM_{150}$, and 10 K PEG-*b*-$PAEM_{150}$) were tested for gene transfection in vivo. Only polyplexes containing the $PAEM_{30}$ series polymers ($PAEM_{30}$, 5K PEG-*b*-$PAEM_{30}$, and 10 K PEG-*b*-$PAEM_{30}$) were tested for biodistribution. All the mice were housed under specific pathogen-free conditions and cared for in accordance with the University of Minnesota and NIH guidelines.

3.2.9 Gene Transfection In Vivo

To assess gene transfection in vivo in live animals after subcutaneous injection, DNA plasmid encoding the luciferase gene (pCMV-Luc, Elim Biopharmaceuticals) was used to prepare the complexes. For luminescent signal measurement of luciferase expression, mice were given subcutaneous injection of D-luciferin (20 mg/mL), anesthetized using isofluorane at predetermined time points and imaged using IVIS Spectrum (Perkin Elmer). Three mice of the same experimental group were imaged together. The tails of the mice were marked to keep the order of mice (from left to right under the camera) the same for every time point. All images were taken at the stage

height and light position with a constant exposure time of 5 min. The bioluminescent data were processed using a constant region of interest (ROI) analysis with background subtraction using the Live Image software package (Perkin Elmer).

3.2.10 Biodistribution

To assess gene transfection in vivo in live animals after subcutaneous injection, Cy-5 labeled pCMV-Luc DNA plasmids were used to prepare the complexes. Mice were anesthetized using isofluorane at predetermined time points and imaged using IVIS Spectrum (Perkin Elmer). Three mice of the same experimental group were imaged together. The tails of the mice were marked to keep the order of mice (from left to right under the camera) the same for every time point. All images were taken at the stage height and light position with a constant exposure time of 1 ms. The fluorescence data were processed using a constant region of interest (ROI) analysis with background subtraction using the Live Image software package (Perkin Elmer).

3.2.11 Statistical Analysis

Comparisons between groups were made using Student's t-test. A p-value of less than 0.05 was considered to be statistically significant. All results were presented as mean $\pm$ standard deviation (SD).

3.3 Results

3.3.1 Average particle size and zeta potential

Particle size is a key parameter in the design of polymeric drug delivery system[101]. It can affect the efficiency and pathway of cellular uptake and in vivo biodistribution [101-103], and can be precisely controlled by adjusting the reaction parameters[104]. DLS revealed that the average particle size of polyplexes in aqueous buffer spanned a range of 70 to 200 nm with dependence on the N/P ratio and chain length (Fig. 13). The size distribution of each type of polyplexes was narrow with PDC ranging from 0.05 to 0.2. At neutral charge ratio, the shorter PAEM block group ($PAEM_{30}$, 5K PEG-*b*-$PAEM_{30}$, 10K PEG-*b*-$PAEM_{30}$) formed complexes with distinct larger particle sizes than the longer PAEM block group ($PAEM_{150}$, 5K PEG-*b*-$PAEM_{150}$, 10K PEG-*b*-$PAEM_{150}$), suggesting a chain length dependency of average particle size, which agreed with literature reported findings[105, 106]. Under this condition, polyplexes formed with PEGylated $PAEM_{150}$ were significantly larger than those formed with homopolymers, which is in good agreement with literature reported finding[21]. At N/P ratio of 8, average particle size stabilized for all six polyplexes. Complexes formed at N/P ratio of 8 were selected for further characterization of polyplex stability, DNA binding capacity, in vitro and in vivo transfection, as well as biodistribution.

At N/P ratio of 8, polyplexes of PAEM of different chain length shared similar zeta potential values around 35 mV (Fig. 14), suggesting a chain length independence of surface charge, which is in good agreement with our lab's previous finding[76].

Complexes formed with PEGylated polymers showed significantly lower zeta potential values than those formed with homopolymers, indicating an efficient shielding of the cationic charges by the PEG chains, which agreed well with literature reports[56, 60, 107]. There was no significantly difference in zeta potential values for polyplexes formed with different PEG chains.

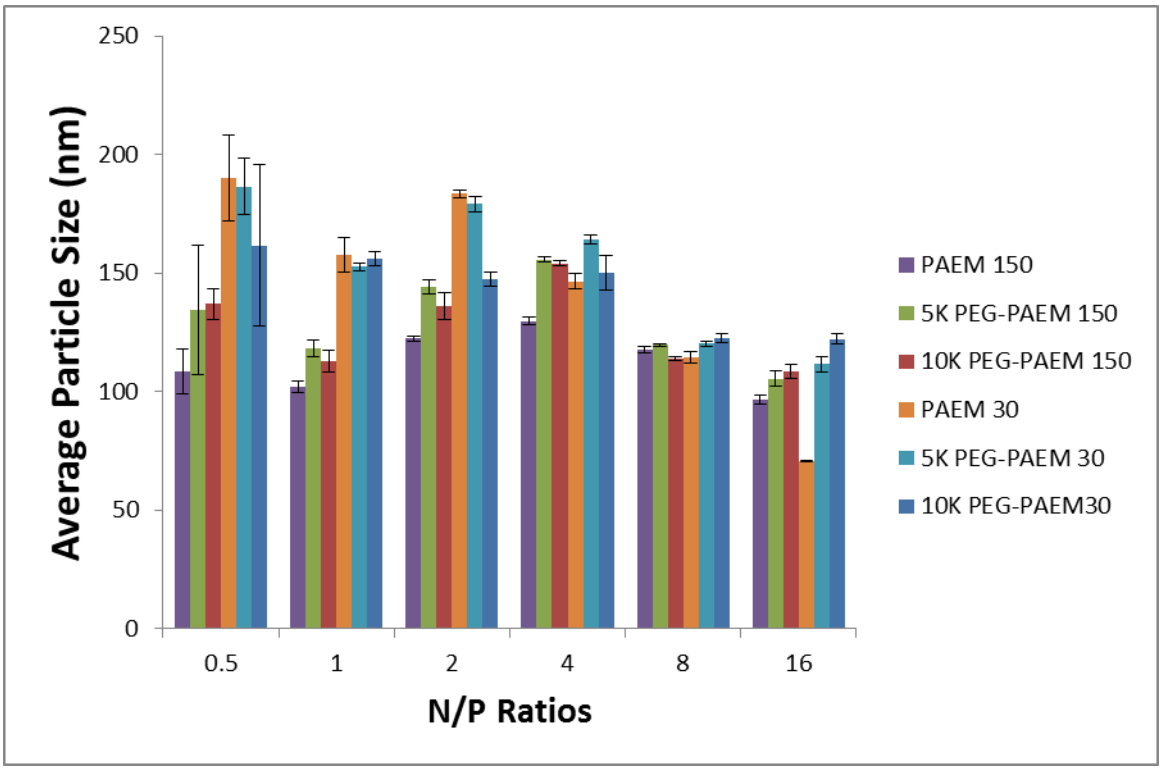

Fig. 13. Average particle size of polyplexes in aqueous buffer (20 mM HEPES, pH 7.4) as a function of N/P ratio determined by DLS.

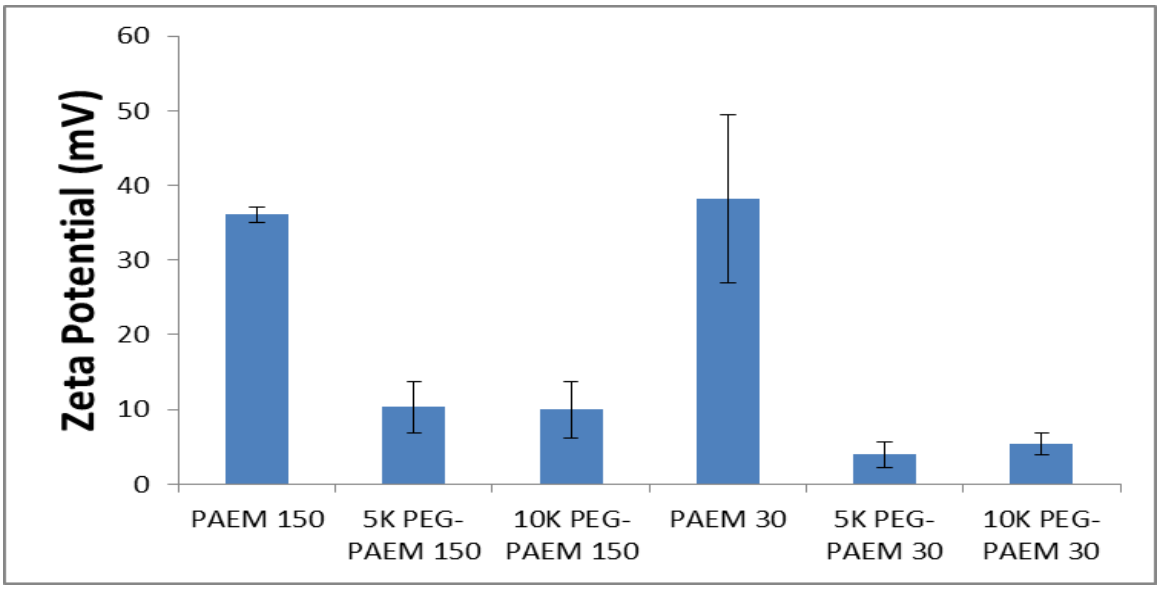

Fig. 14. Zeta potential of polyplexes at the N/P ratio of 8. The zeta potential is independent of polymer chain length, but is affected by polymer pegylation.

3.3.2 DNA binding and condensation

The gel retardation assay qualitatively revealed the difference in DNA binding ability among the six PAEM polymers. The $PAEM_{150}$ group polymers were able prevent completely the migration of plasmid DNA at the N/P ratio of 1 and beyond (Fig. 15 A). However, at this neutral charge ratio, the $PAEM_{30}$ group polymers were only be able to partially reduce the migration of plasmid DNA. Complete retardation of DNA migration happened at the N/P ratio of 2 and above.

DNA binding and condensation capacity of various PAEM polymers were further quantified by EB exclusion assays. Addition of increasing amounts of polymers to a solution of EB/DNA results in a rapid decrease in fluorescence. A relative binding affinity of the polymers can be inferred from the residual fluorescence of EB/DNA solutions[108]. The ability to condense DNA increased with the chain-length of PAEM block, showed by the lower N/P ratios at which half of the EB was displaced from intercalating with DNA, resulting in reduced fluorescence intensity (Fig. 15 B). Lower charge ratios were required for PEGylated polymers to quench fluorescence of EB/DNA to the same extent as the equivalent homopolymers.

A

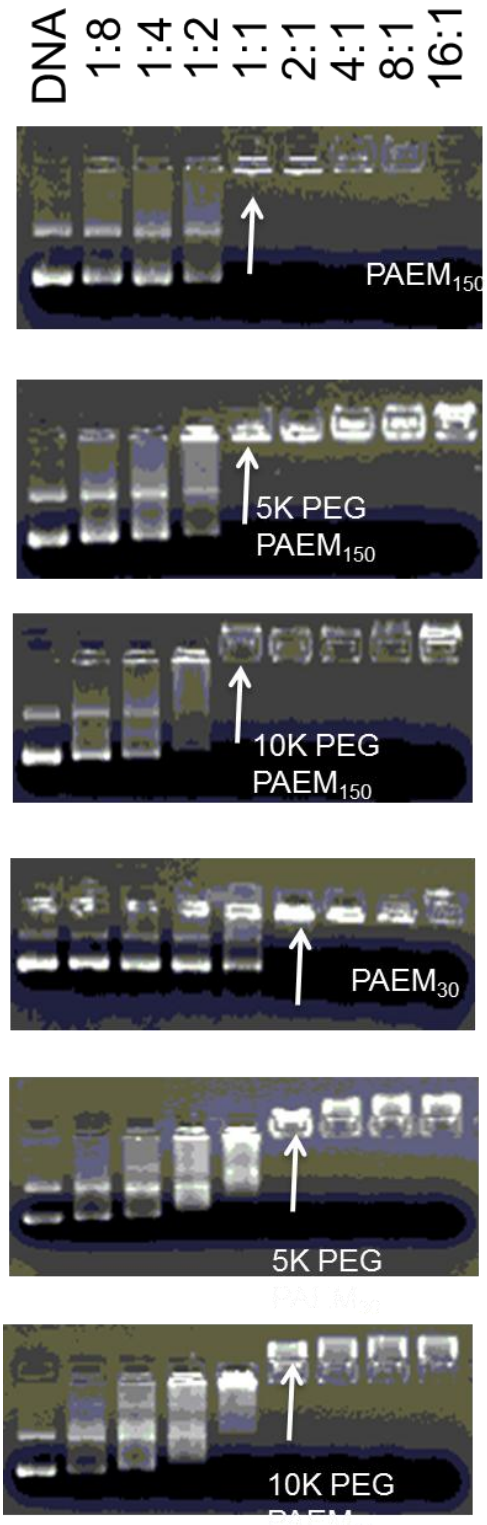
N:P Ratio
DNA
1:8
1:4
1:2
1:1
2:1
4:1
8:1
16:1
PAEM150
5K PEG
PAEM150
10K PEG
PAEM150
PAEM30
5K PEG
10K PEG

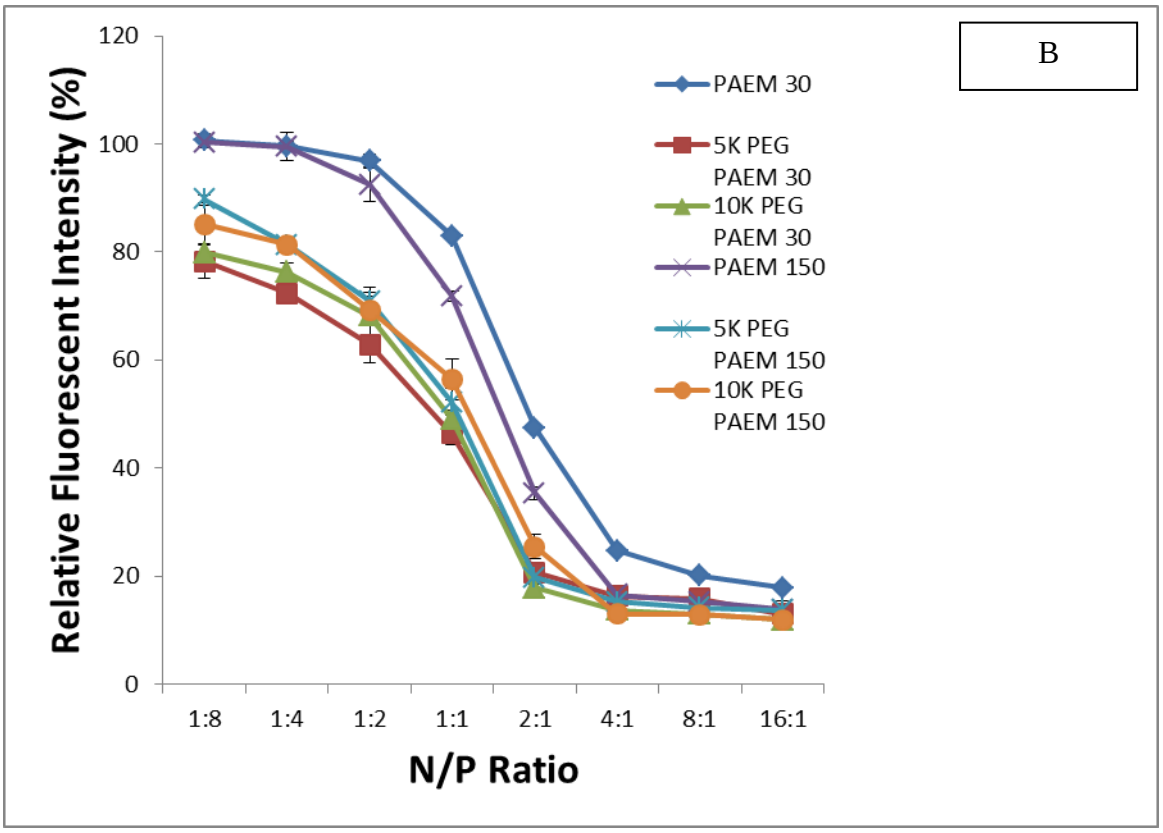

Fig.15. Capacity of DNA binding and condensation by the PAEM polymers with different chain length and PEGylation. (A) Gel retardation assay of polyplexes prepared at various N/P ratios. Arrows point to the threshold N/P ratio where retardation of DNA migration through the gel occurred. (B) Ethidium bromide (EB) exclusion due to polyplex formation. Fluorescence intensity of EB mixed with plasmid without addition of polymer was taken at 100%.

3.3.3 Polyplexes stability

The stability of polyplexes at N/P ratio of 8 was studied in the presence of increasing amount of heparin, a polyanion that can compete with DNA for the binding to the polycation, followed by agarose gel electrophoresis. The greater amount of heparin needed to dissociate the polymer from the plasmid DNA, the greater the binding affinity. The threshold concentration of heparin at which polyplex disruption occurred was 0.3 and 0.4 IU/μg of DNA for polyplexes formed with $PAEM_{30}$ and $PAEM_{150}$ respectively (Fig. 16), suggesting that the longer chain-length of homopolymer can protect complex dissociation better than the shorter chain-length. PEGylation of PAEM did not alter the threshold value of the heparin concentration needed for complex dissociation. However, the threshold amount of heparin required to disrupt the polyplexes was 0.5 IU/μg of DNA for PEGylated $PAEM_{30}$ polymers, indicating a decrease in polyplex stability by adding the PEG chain to the homopolymer.

The interaction of the polycationic polymer with DNA plasmid can also be studied by evaluating the changes of the DNA structure by Circular Dichroism (Fig. 17). The naked Luc DNA control showed a characteristic β-form profile with a negative peak at 244 nm and a maximum peak at 274 nm. With the addition of polymer to the Luc plasmid, the maximum positive peak experienced a red shift and a decrease in magnitude of the positive peak. This suggested that the DNA plasmid underwent a conformational change form β-form structure into a c-form secondary structure[109]. The negative peak also underwent a change in magnitude while undergoing a red shift affecting the helicity of the DNA plasmid[110]. With the addition of the PEG chain to the homopolymers, a

smaller red shift in the positive and negative peaks accompanied by an increase in magnitude were observed, suggesting a weaker DNA binding capacity of PEGylation, which agreed with the heparin assay result. Though there was no significant difference in the spectra shift between homopolymers of different chain-lengths, PEGylated $PAEM_{150}$ polymers showed a greater spectra shift than the PEGylated $PAEM_{30}$ polymers, suggesting a stronger DNA binding capacity of the PEGylated $PAEM_{150}$ polymers.

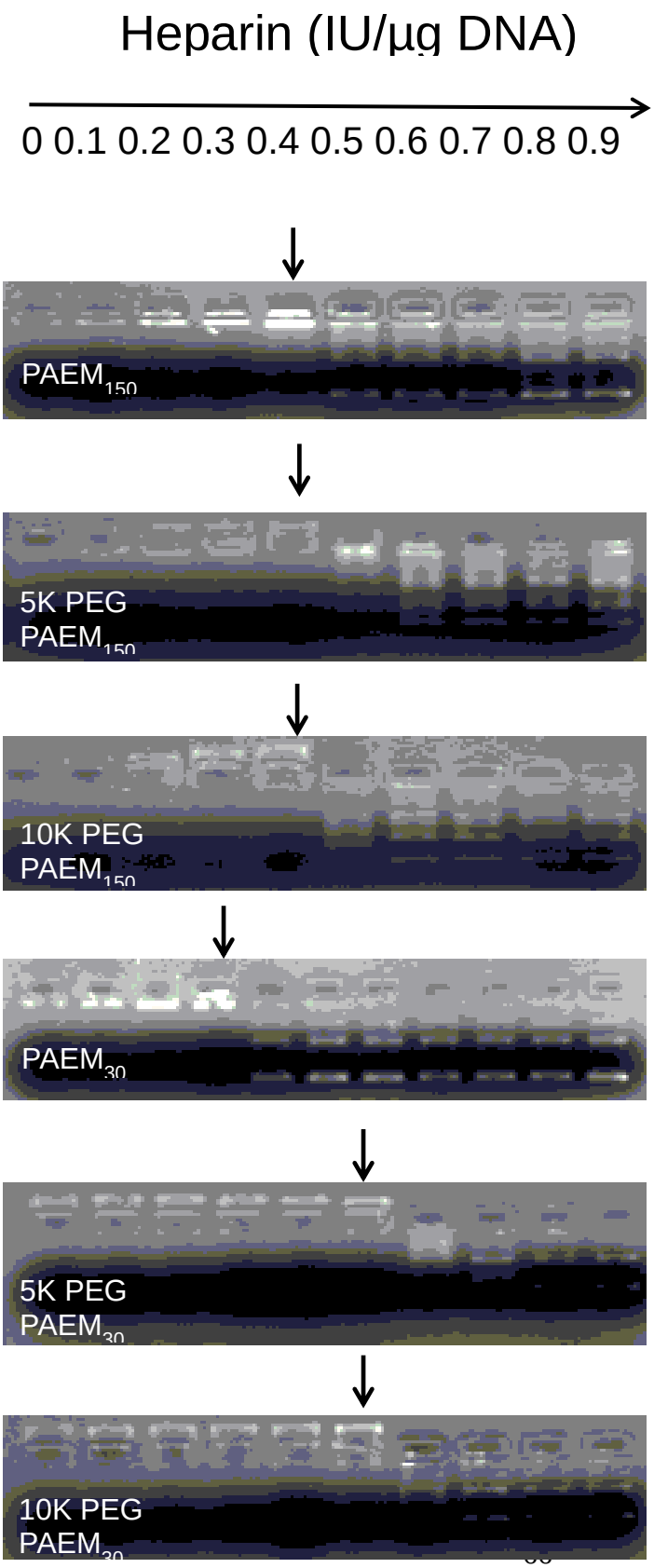

Fig. 16. Destabilization of polyplexes with increasing concentration of heparin. Arrows point to the threshold concentration of heparin beyond which unpackaging of DNA occurred.

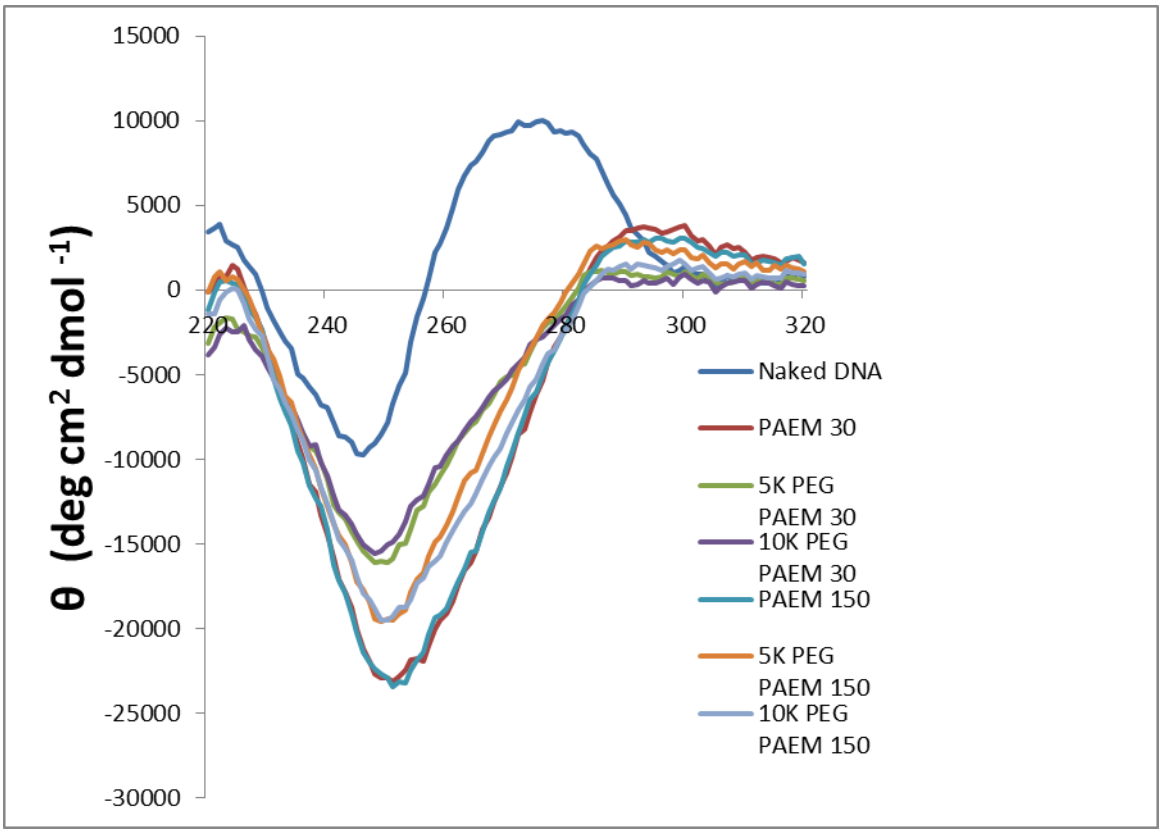

Fig.17. Configuration of DNA packing by complexation with cationic polymers measured by Circular Dichroism. With the addition of the polymers to the DNA plasmid, the maximum positive peak experienced a red shift and a decrease in magnitude of the positive peak. This suggested that the DNA-plasmid underwent a conformational change from the B-form structure into a C-form secondary structure. PEGylated $PAEM_{150}$ polymers experienced a red shift and decrease in magnitude of the negative peaks compared to PEGylated $PAEM_{30}$ polymers, suggesting chain length affecting DNA secondary structure in PEGylated polymers.

3.3.4 Visual assessment of polyplex stability in simulated in vivo media

Polyplexes containing Cy5-labeld plasmid DNA were dissolved in full cell culture medium supplemented with 10% serum and buffer salts to mimic the in vivo fluid environment, and visualized by fluorescence microscopy (Fig. 18). The fluorescence microscopy method we employed here provided a direct visualization of the aggregation process. Shortly after mixing, aggregates of $PAEM_{30}$ and $PAEM_{150}$ polyplexes were seen in the serum containing medium, and the aggregates become more serve after 1 h (Fig. 18). Qualitatively, aggregates of $PAEM_{150}$ polyplexes were bigger than the $PAEM_{30}$ polyplexes. No visible aggregation was seen in the PEGylated polyplexes after 1 h in complete cell culture medium PEGylation enhanced polyplexes stability against aggregation, and the longer PEG chain performed slightly better than the shorter PEG chain.

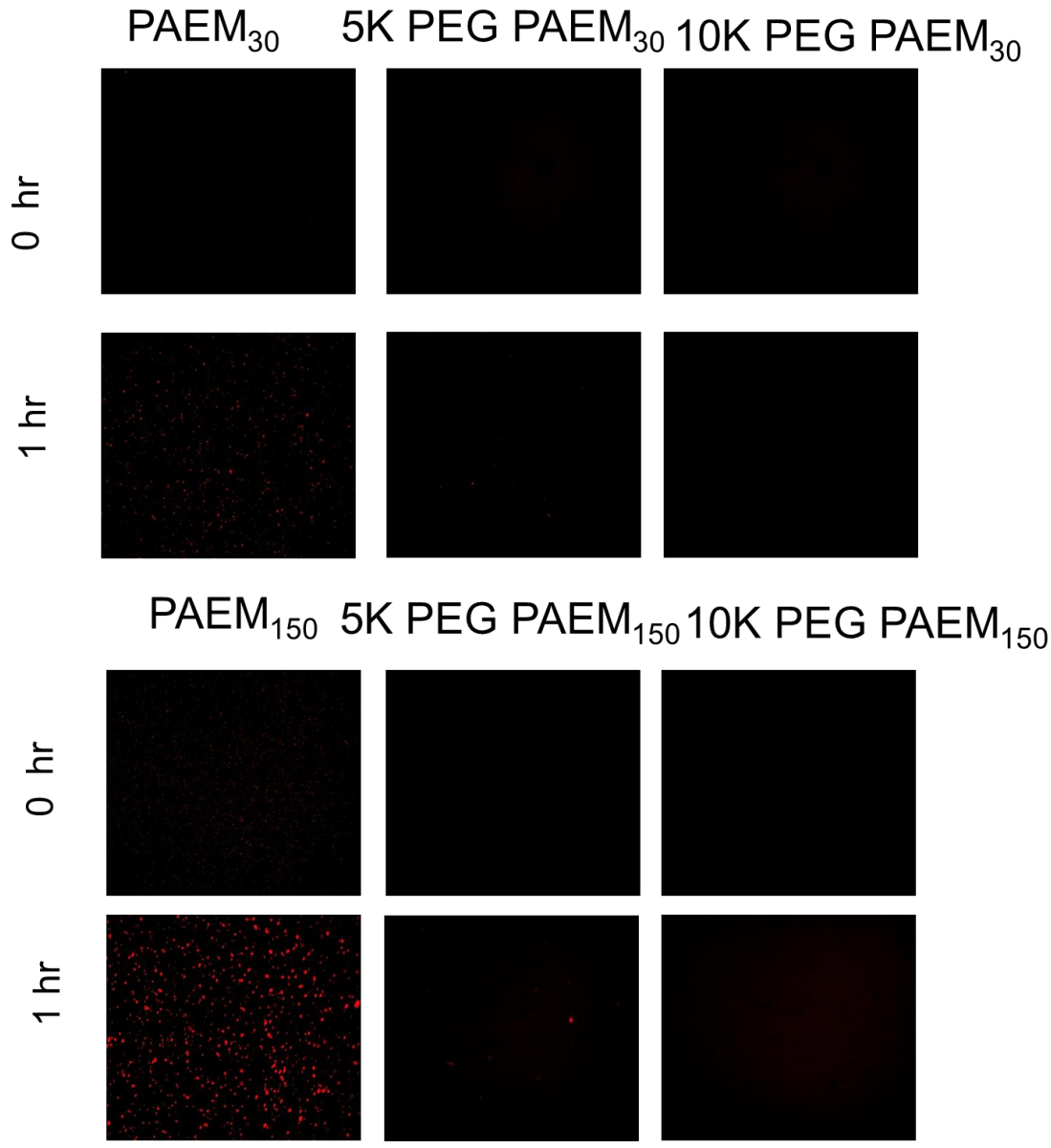

Fig.18. Visual assessment of polyplex stability in cell medium containing 10% serum, condition that mimics the in vivo fluid environment.

3.3.5 Transfection of murine fibroblasts in vitro

Polyplex-mediated transfection of murine fibroblasts NIH 3T3 with a GFP plasmid was conducted and the expression level of GFP was determined by flow cytometry (Fig. 19). Cell autofluorescence was subtracted by transfecting the 3T3 cells under the identical conditions with a luciferase plasmid serving as a negative control to set the GFP positive gate. Polyplexes made from PEI and GFP plasmid were given to the fibroblast under the same transfection condition to provide a positive control and a standard for comparison. For both two rounds, PEI/DNA polyplex resulted in a transfection efficiency around 42%, which agreed well with our previous finding reported in literature[31]. The fibroblasts received $PAEM_{30}$/DNA complexes had only 5% GFP^+ cells, and those received the PEGylated complexes showed less than 1% GFP^+ cells. On the other hand, $PAEM_{150}$/DNA polyplexes led to an almost 40% GFP^+ cells observed, which was statistically the same as PEI/DNA polyplex treated group. The PEGylated $PAEM_{150}$ complexes generated much less GFP^+ cells (about 5%), and there was no statistical difference seen between groups with different PEG chains.

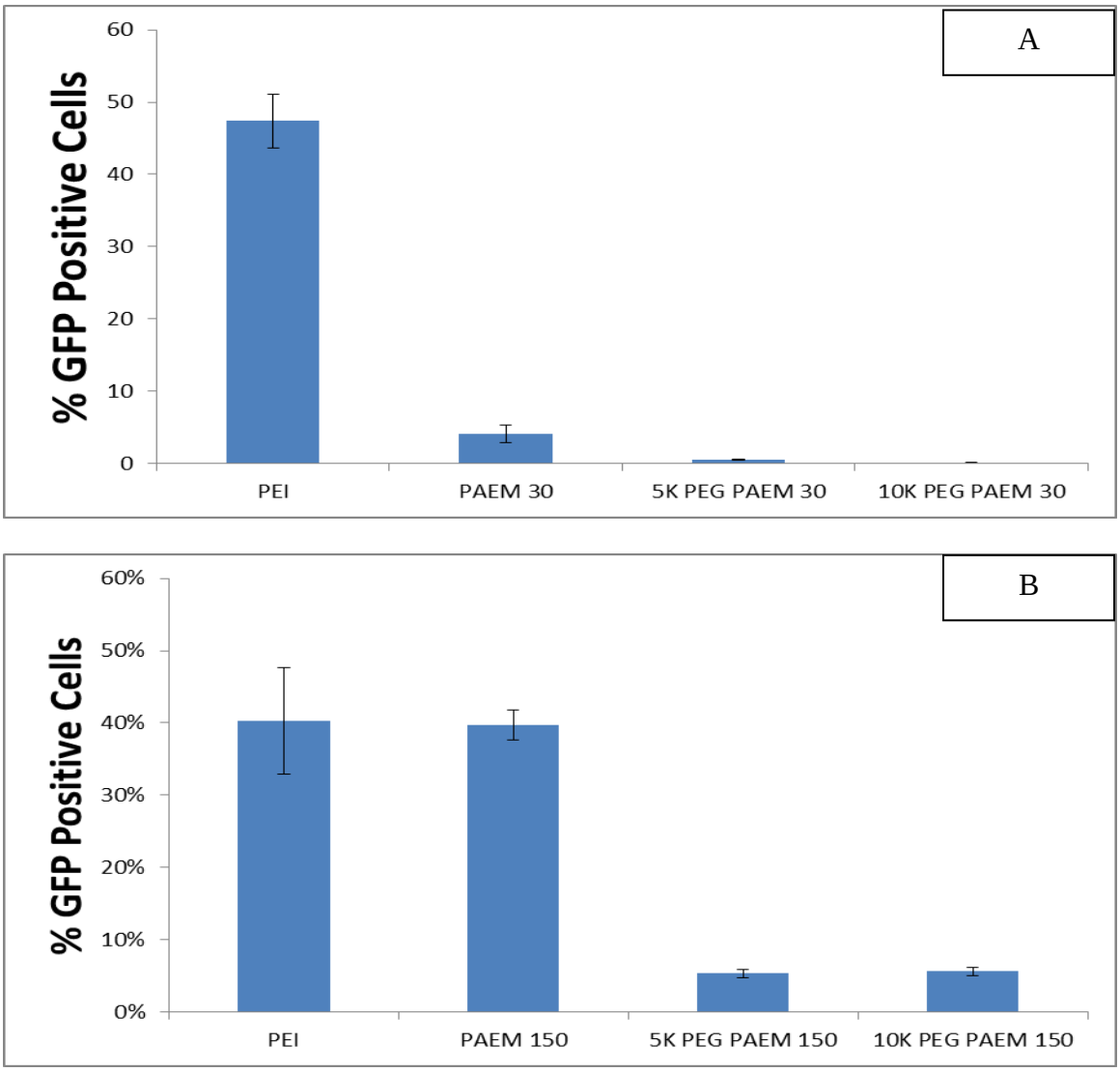

Fig.19. Transfection efficiency of NIH 3T3 fibroblasts by polyplexes (A), $PAEM_{30}$ series and (B), $PAEM_{150}$ series, determined by flow cytometry. Longer polymer chains facilitated transfection and PEG chains were not in favor of high transfection efficiency.

3.3.6 Transfection in vivo

Polyplexes containing all 6 polymers were injected subcutaneously into the hind quadriceps region of mice and the mice were imaged live using IVIS Spectrum starting one day after injection and monitored every day or every other day after that (Fig. 20). Five percent glucose solution at the same total final volume was administered to a mouse to serve as a negative control and to provide the measurement of any luminescent signal coming from the tissue itself. After subtracting the background luminescence, mice injected with $PAEM_{30}$ series polyplexes showed positively transfected cells, but none of the $PAEM_{150}$ series polyplexes generated detectable luminescent signals. One day after the initial injection, mice received complexes made of 10K PEG $PAEM_{30}$ showed significantly higher transgene expression, about 4 times higher than other polyplexes. On the other hand, mice received the polyplexes of homopolymers $PAEM_{30}$ did not generate any luminescent signal on day 1, but showed a peak of luminescent intensity on day 7 after the initial injection, which was significantly higher than other two polyplexes. Interestingly, mice received 5K PEG $PAEM_{30}$ polyplexes showed a stable transgene expression throughout the time course of study.

The data reported in Fig. 20 B and C were after background subtraction and normalized against the average of background luminescent signals collected from 3 mice received buffer injection. They were expressed as a percentage of the background luminescent signal.

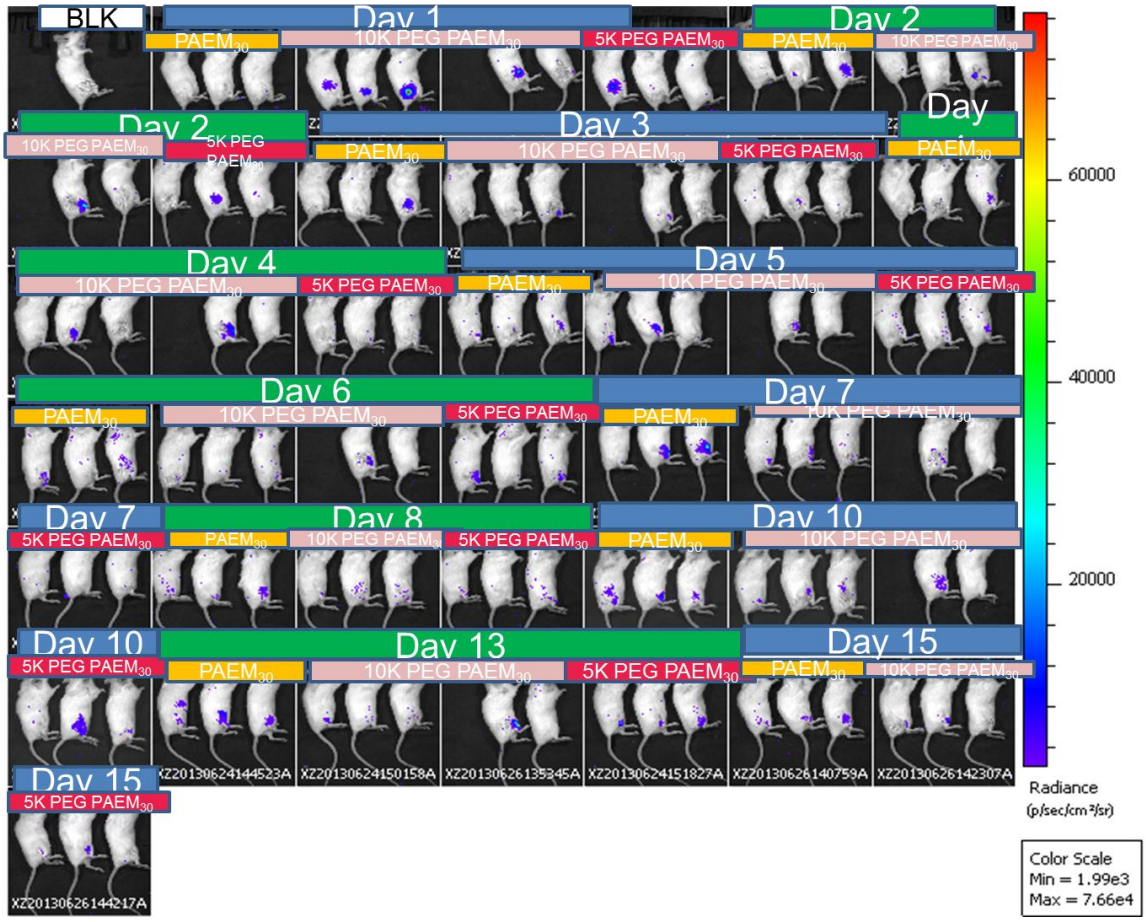
BLK
Day 1
PAEM30
10K PEG PAEM30
5K PEG PAEM30
Day 2
PAEM30
10K PEG PAEM30
Day 2
10K PEG PAEM30
5K PEG PAEM30
Day 3
PAEM30
10K PEG PAEM30
5K PEG PAEM30
Day
PAEM30
Day 4
10K PEG PAEM30
5K PEG PAEM30
Day 5
PAEM30
10K PEG PAEM30
5K PEG PAEM30
Day 6
PAEM30
10K PEG PAEM30
5K PEG PAEM30
Day 7
PAEM30
Day 7
5K PEG PAEM30
Day 8
PAEM30
10K PEG PAEM30
5K PEG PAEM30
Day 10
PAEM30
10K PEG PAEM30
Day 10
5K PEG PAEM30
Day 13
PAEM30
10K PEG PAEM30
5K PEG PAEM30
Day 15
PAEM30
10K PEG PAEM30
Day 15
5K PEG PAEM30
XZ20130624144523A
XZ20130624150158A
XZ20130626135345A
XZ20130624151827A
XZ20130626140759A
XZ20130626142307A
XZ20130626144217A
60000
40000
20000
Radiance
(p/sec/cm²/sr)
Color Scale
Min = 1.99e3
Max = 7.66e4

A

B

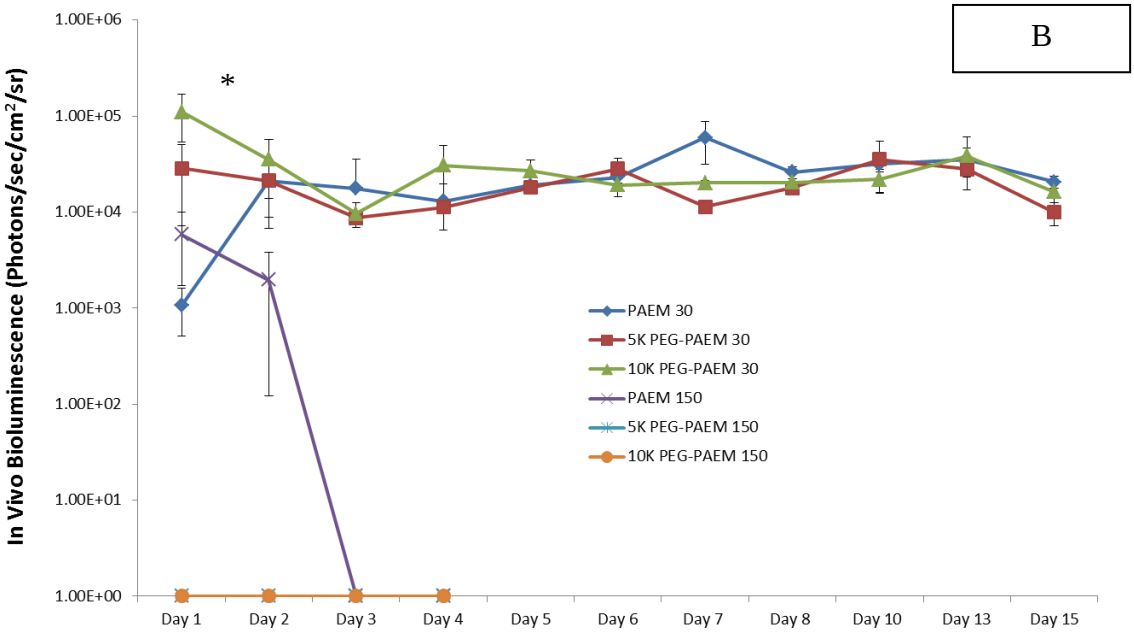
In Vivo Bioluminescence (Photons/sec/cm²/sr)
1.00E+06
1.00E+05
1.00E+04
1.00E+03
1.00E+02
1.00E+01
1.00E+00
*
Day 1
Day 2
Day 3
Day 4
Day 5
Day 6
Day 7
Day 8
Day 10
Day 13
Day 15
PAEM 30
5K PEG-PAEM 30
10K PEG-PAEM 30
PAEM 150
5K PEG-PAEM 150
10K PEG-PAEM 150

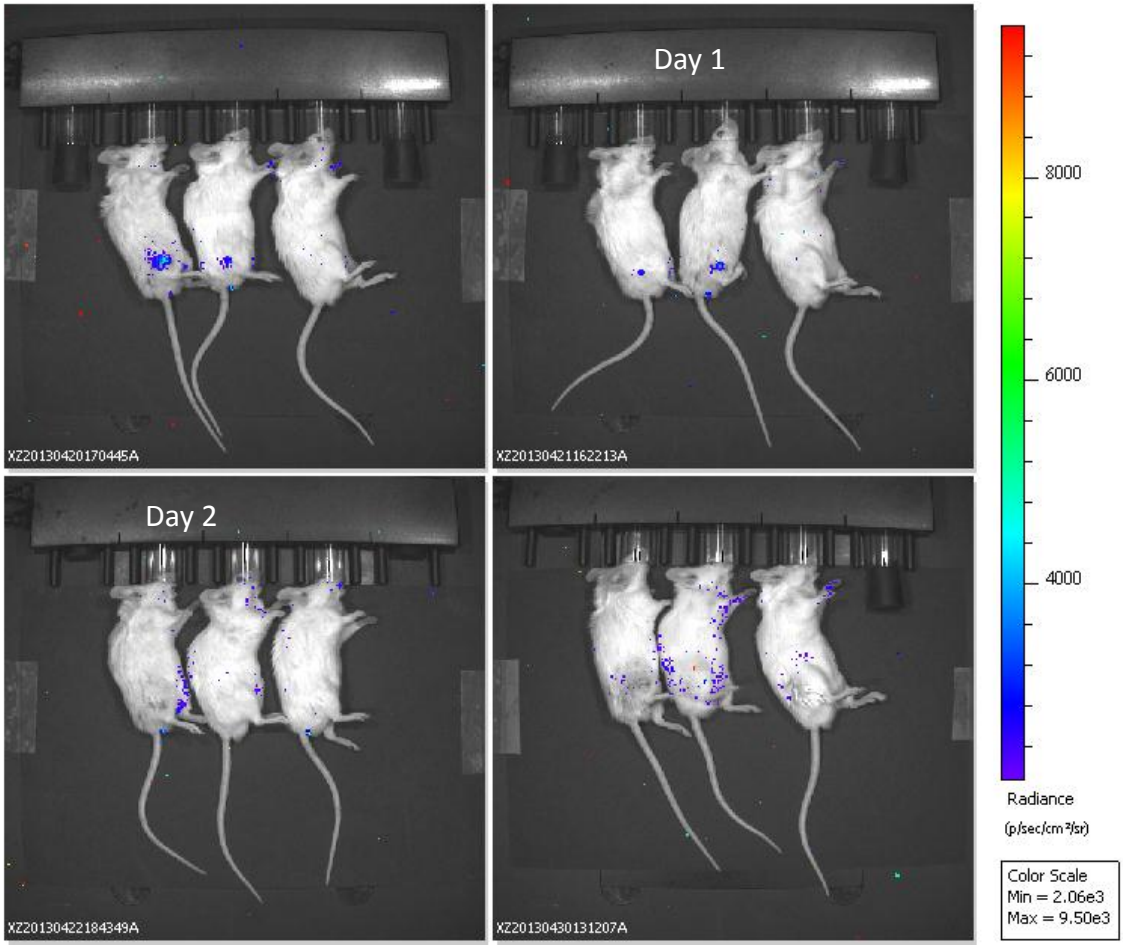
Day 1
Day 2
XZ20130420170445A
XZ20130421162213A
XZ20130422184349A
XZ20130430131207A
8000
6000
4000
Radiance
(p/sec/cm²/sr)
Color Scale
Min = 2.06e3
Max = 9.50e3

C

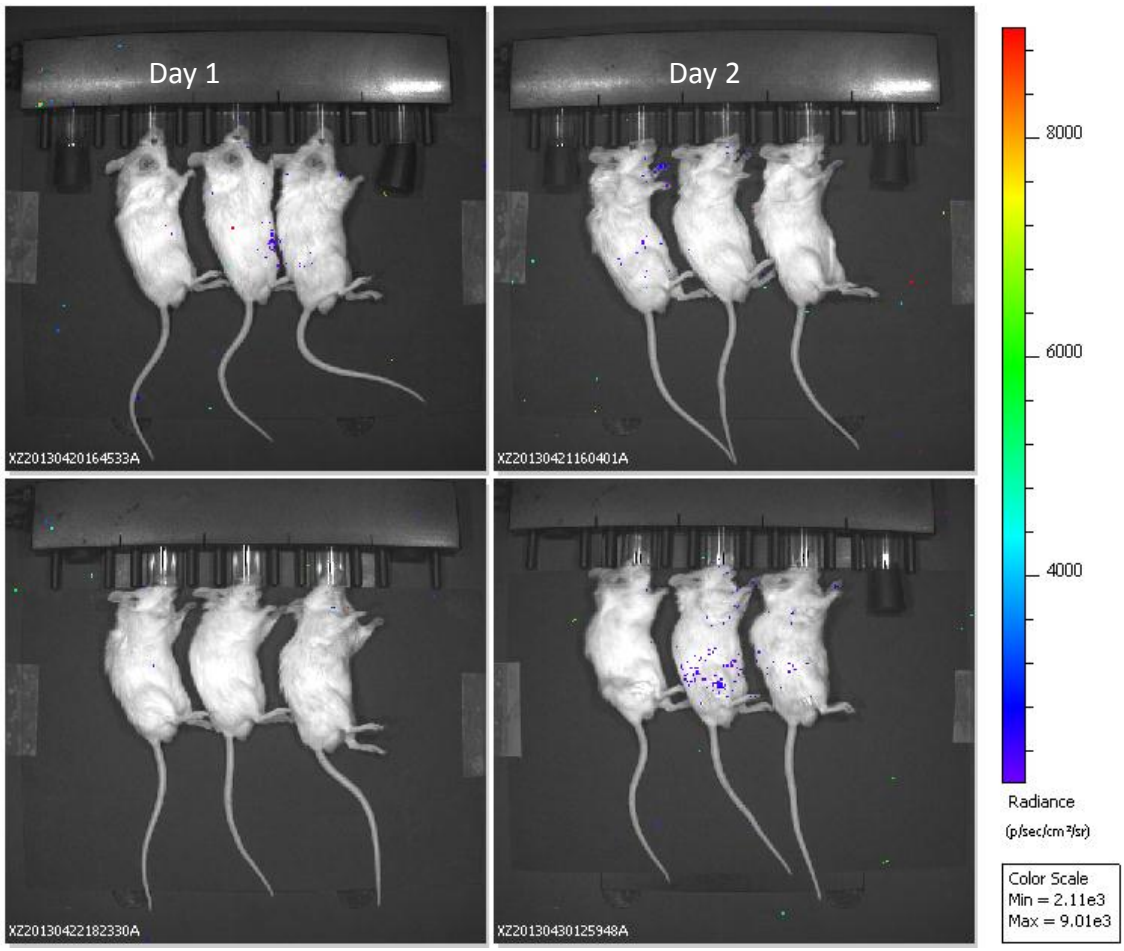
Day 1
Day 2
XZ20130420164533A
XZ20130421160401A
XZ20130422182330A
XZ20130430125948A
8000
6000
4000
Radiance
(p/sec/cm²/sr)
Color Scale
Min = 2.11e3
Max = 9.01e3

D

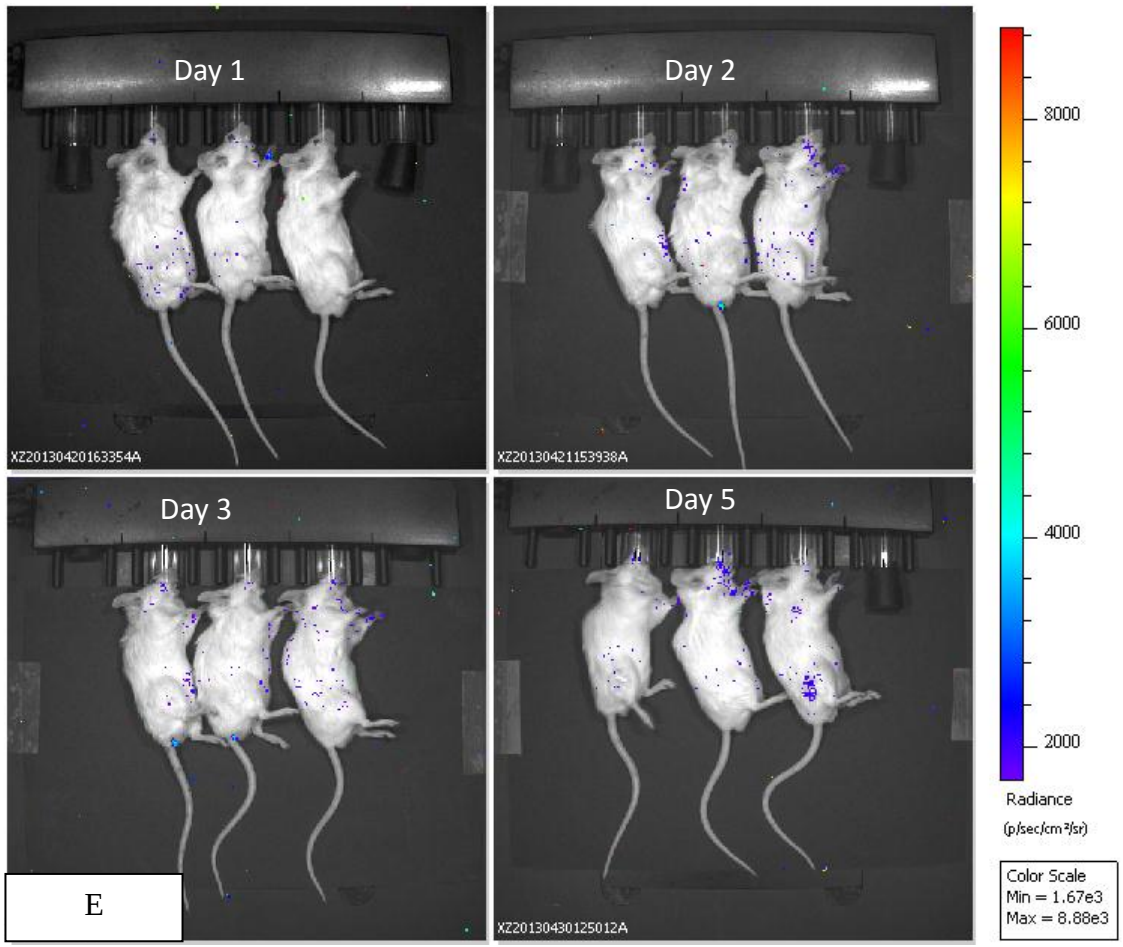

Fig. 20. Transfection of poplyplexes in live animals. Three or five mice were injected with polyplexes containing 25 μg of luciferase plasmid DNA in the right hind quadriceps region with subcutaneous injection. (A) Visualization of $PAEM_{30}$ series polyplexes transfection. (B) Quantification of $PAEM_{30}$ and $PAEM_{150}$ series polyplexes transfection normalized against background luminescent signals. * $p<0.05$. (C) Visualization of $PAEM_{150}$ polyplexes transfection. (D) Visualization of 5K PEG $PAEM_{150}$ polyplexes transfection. (E) Visualization of 10K PEG $PAEM_{150}$ polyplexes transfection.

3.3.7 Biodistribution of $PAEM_{30}$ series polymers

To determine the persistence and clearance kinetics of the naked DNA plasmid and polyplexes, we monitored the fluorescence signals of Cy5-labeled plasmid DNA either by itself or in complexes after subcutaneous injection into the hind quadriceps region of mice using whole-animal live imaging with IVIS Spectrum (Fig. 21). After subtracting background and tissue autofluorescence, the measured fluorescence intensity was normalized against the measured fluorescence signal on day 0 right after the injection. Two days after the initial injection, 85% of the naked plasmid DNA was cleared from the injection region. However, only 65% of the fluorescence signal was cleared in $PAEM_{30}$ polyplex injected mice. Throughout the time course of study, a larger amount of labeled DNA plasmid was present in mice received in $PAEM_{30}$ polyplexes than naked plasmid DNA. PEGylation helped to reduce DNA clearance 2 days after injection and was able to reserve a larger amount of DNA in the injection region than naked DNA, but not as much as the homopolymer.

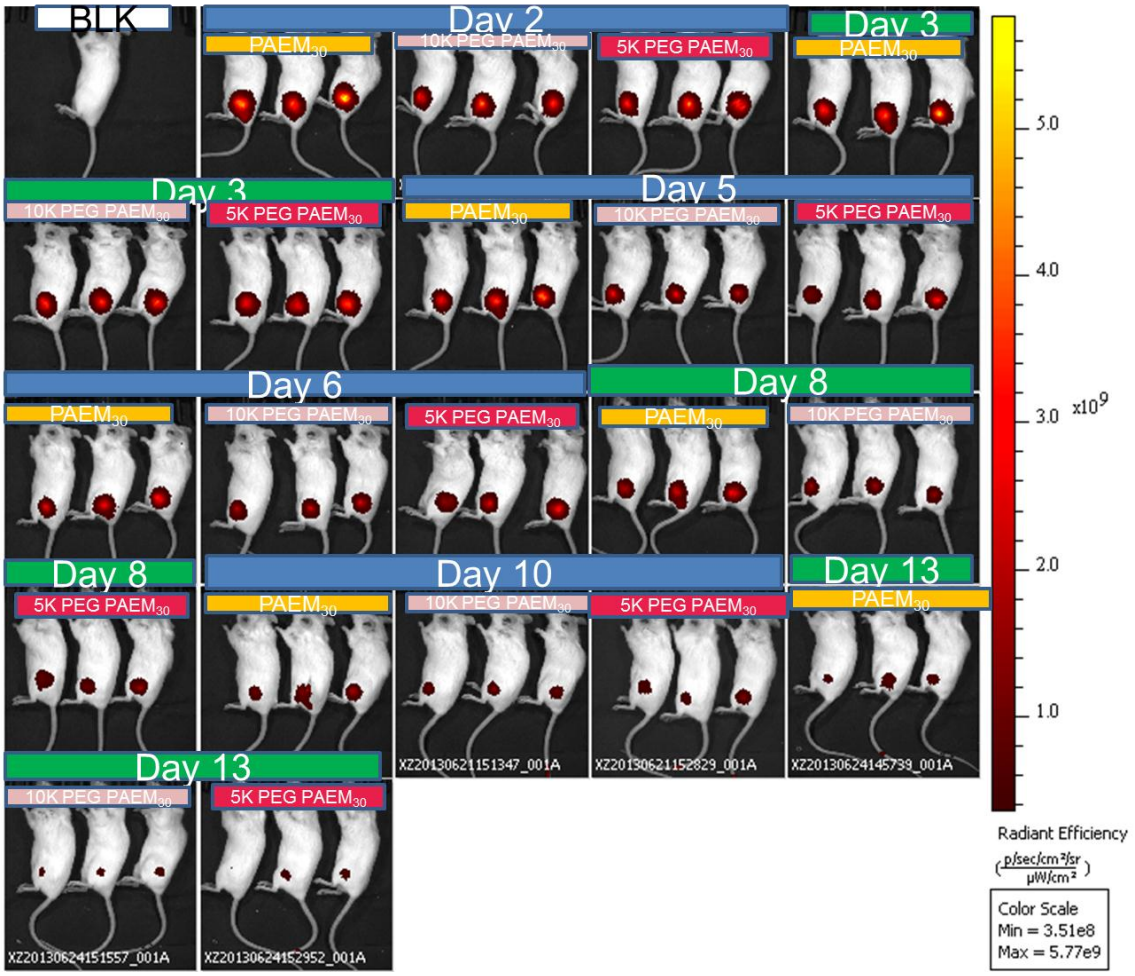
BLK
Day 2
PAEM30
10K PEG PAEM30
5K PEG PAEM30
Day 3
PAEM30
Day 3
10K PEG PAEM30
5K PEG PAEM30
Day 5
PAEM30
10K PEG PAEM30
5K PEG PAEM30
Day 6
PAEM30
10K PEG PAEM30
5K PEG PAEM30
Day 8
PAEM30
10K PEG PAEM30
Day 8
5K PEG PAEM30
Day 10
PAEM30
10K PEG PAEM30
5K PEG PAEM30
Day 13
PAEM30
Day 13
10K PEG PAEM30
5K PEG PAEM30
XZ20130624151557_001A
XZ20130624152952_001A
XZ20130621151347_001A
XZ20130621152829_001A
XZ20130624145739_001A
5.0
4.0
3.0
2.0
1.0
x10^9
Radiant Efficiency
(p/sec/cm²/sr / µW/cm²)
Color Scale
Min = 3.51e8
Max = 5.77e9

A

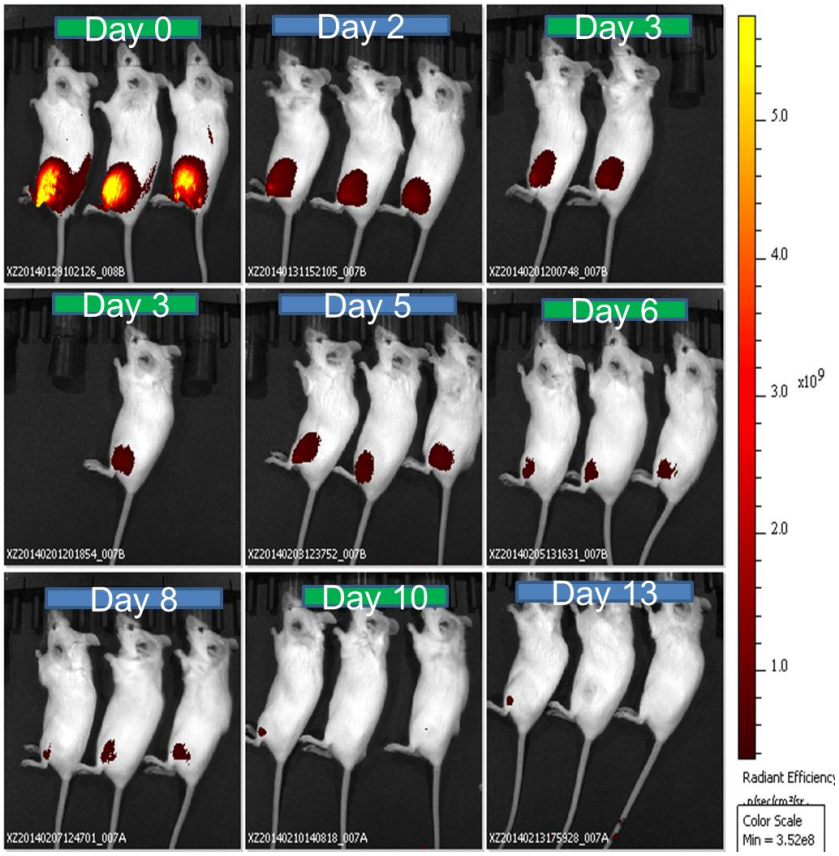
Day 0
Day 2
Day 3
Day 3
Day 5
Day 6
Day 8
Day 10
Day 13
5.0
4.0
3.0
x10^9
2.0
1.0
Radiant Efficiency
Color Scale
Min = 3.52e8

B

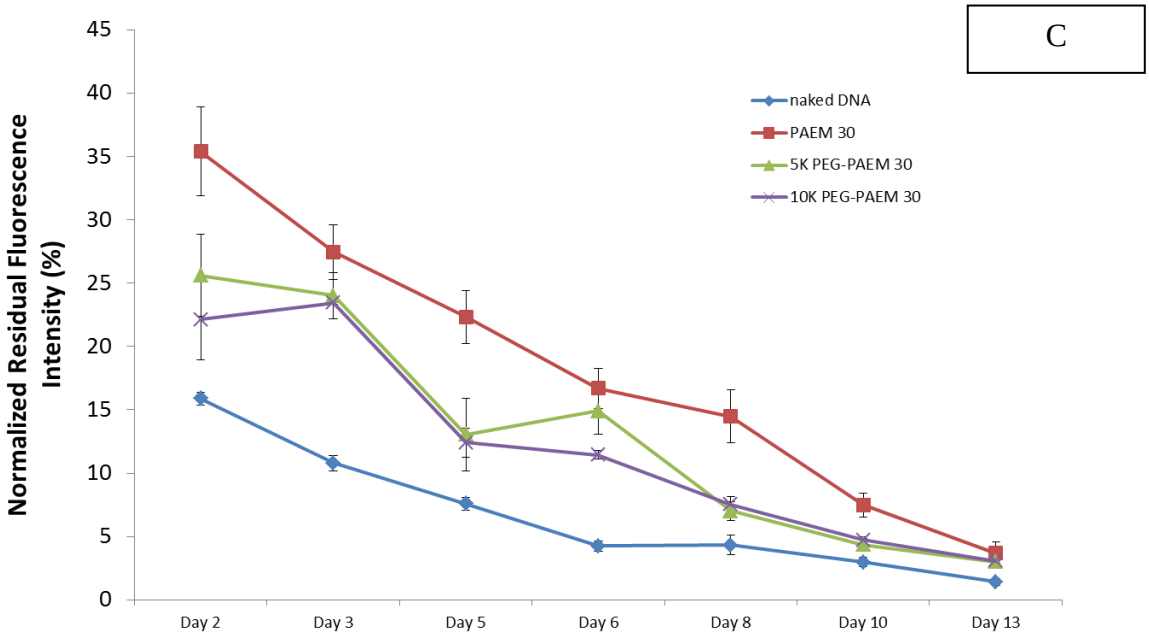

Fig. 21. In vivo performance of the $PAEM_{30}$ series polyplexes. (A) Tissue distribution of polyplexes in live animals after subcutaneous injection. Three mice were each injected with polyplexes containing 25 μg of Cy5-labeld DNA in the left hind quadriceps region. (B) Tissue distribution of naked DNA in live animals after subcutaneous injection of 25 μg Cy5-labeld DNA in the left hind quadriceps region. (C) Quantification of total fluorescent signal intensity reduction.

3.4 Discussion

Designing an efficient non-viral gene delivery vehicle needs the understanding of specific structural features and stability requirements in order for the vehicle to remain intact when it maneuvers through the extracellular space or vasculature to reach its targeted cell types before releasing its cargo. Molecular weight or length of the polymer chain is a critical factor influencing polyplex-mediated transfection efficiency in vitro. Many studies have shown the positive correlation between chain length and transfection efficiency for a variety of polymers [18, 76, 105, 111] though discrepancies existed. In the work here, we observed that the homopolymer with a longer polymer chain ($PAEM_{150}$) generated a higher transgene expression when complexed with plasmid DNA and delivered to murine fibroblasts in vitro. This is because $PAEM_{150}$ was able to form more stable complexes than $PAEM_{30}$ (as shown in the gel retardation and EB assay results (Fig. 15)), which facilitated a higher cellular uptake and a higher nuclear uptake of the polyplexes by the fibroblasts[76].

However, the trend we observed for in vivo transfection was the opposite of the result of the in vitro transfection. Polyplexes made of $PAEM_{150}$ generated much lower transgene expression in mice than those of $PAEM_{30}$ (Fig. 20). This is not surprising because studies done by various researchers have shown that in vitro transfection could be a poor indicator of in vivo success[112-114]. The big discrepancy between in vitro and in vivo results lies in the fact the nanocomplexes need to overcome the extracellular barrier while remain as stable complexes before they present themselves for efficient

cellular uptake. Biomacromolecules, such as serum albumin[115, 116], present in skin tissue and they could non-specifically interact with polyplexes, inducing their dissociation or aggregation [55]. To understand the effect of serum protein on polyplexes aggregation, we conducted the in vitro experiment in simulated body fluid environment by incubating polyplexes made of fluorescently labeled DNA plasmid in complete cell culture medium containing serum. With direct visualization through fluorescence microscopy, we observed that $PAEM_{150}$ formed considerable aggregates after 1 h incubation. Consistent with our in vitro finding, a previously published study by our group has shown that $PAEM_{150}$ polyplexes formed aggregates at the injection site through immunofluorescence staining of skin specimen of polyplexes treated mice[117]. The polyplexes remained as aggregates throughout the 4 day of investigation and the large aggregates had limited diffusivity in the skin tissue. There could be very little $PAEM_{150}$ polyplexes left to interact with cells, resulting in a low transfection in the skin tissue.

Interestingly, $PAEM_{30}$ polyplexes had similar particle size and zeta potential as $PAEM_{150}$ polyplexes at N/P ratio of 8 when measured in vitro in buffer solution (Fig. 13, Fig. 14), but $PAEM_{30}$ polyplexes generated detectable transgene expression after subcutaneous injection in mice (Fig. 20). This agrees with the literature reported molecular-weight-dependency of polyplexes transfection in vivo. Turunen and colleagues, as well as Abdallah and colleagues have found a higher transfection efficiency with lower molecular weight PEI in vivo[112, 118]. Hoggard and colleagues reported a superior transgene level with lower molecular weight chitosan oligomers[119]. This could be due to the difference in polyplex stability between them. From the physical

characterization assays, $PAEM_{30}$ homopolymer needed a higher N/P ratio to completely prevent DNA migration and quench EB fluorescence than $PAEM_{150}$. At the same time, a smaller amount of heparin was necessary to disrupt complex association for $PAEM_{30}$ polyplexes than $PAEM_{150}$ polyplexes. The lower DNA binding capacity combined with the reduced chain entanglement effect resulted in a less stable complex formed with $PAEM_{30}$ than $PAEM_{150}$. The $PAEM_{30}$ complexes are more easily dissociated to release the DNA cargo, which could be the possible explanation for the high level of transgene expression as reported by Hoggard and colleagues[120]. In addition to the polyplex stability, our in vitro data with the simulated body fluid, $PAEM_{30}$ polyplexes formed much smaller and fewer aggregates than $PAEM_{150}$ polyplexes. It is also possible that $PAEM_{30}$ polyplexes had better diffusivity than $PAEM_{150}$ polyplexes in a large aggregate, and therefore they could have a better chance to interact with cells.

The net positive charges on the surface of polyplexes induce non-specific interactions with anionic components in the body such as serum albumin or negatively charged molecules in the ECM [49]. This leads to the formation of distinct large aggregates with size in the micrometer range and persisting for a long time[58]. To minimize the undesired interactions of anionic components with polyplexes, surface shielding is essential in the design of gene delivery vehicles. One of the most extensively developed approaches involves the integration of the flexible hydrophilic PEG chain into polyplexes[121, 122]. Nomoto and colleagues observed directly the stabilization against aggregation by PEGylated polyplexes after intravenous injection in vivo[58]. In our in vitro experiment with the simulated body fluid incubation, we did not see any

aggregation of PEGylated polyplexes (Fig. 20). Consistent with the in vitro finding here, our previous study in live animal showed a broader dispersion of PEGylated polyplexes after intradermal injection in mouse skin and many smaller aggregates spread out in the skin tissue.

However, PEGylated $PAEM_{150}$ polyplexes did not show any detectable transgene expression in vivo either. This could be caused by the "PEG dilemma" that transfection efficiency is compromised due to the reduced cellular internalization and endosomal escape of PEGylated polyplexes.

PEGylated $PAEM_{30}$ has a shorter polymer chain than PEGylated $PAEM_{150}$, and therefore the amount of positive charge per molecule is smaller for PEGylated $PAEM_{30}$. To achieve the same N/P ratio as the PEGylated $PAEM_{150}$ polyplex, we would need more PEGylated $PAEM_{30}$ molecules per complex. Looking from the outside of the complex, there would be a higher density of the PEG chain on the surface of the complex. PEG density affects the stabilization of polyplexes and Storm and colleagues have proposed that a high surface density of PEG chain would decrease the steric hindrance protection of the PEG layer because the lateral movement of the PEG chain is more limited, resulting in weaker DNA binding capacity of the polyplexes[59]. PEGylated $PAEM_{30}$ polyplex may behave similarly to $PAEM_{30}$ polyplexes in vivo. They could become relatively easily dissociated and release the DNA cargo for gene transfection.

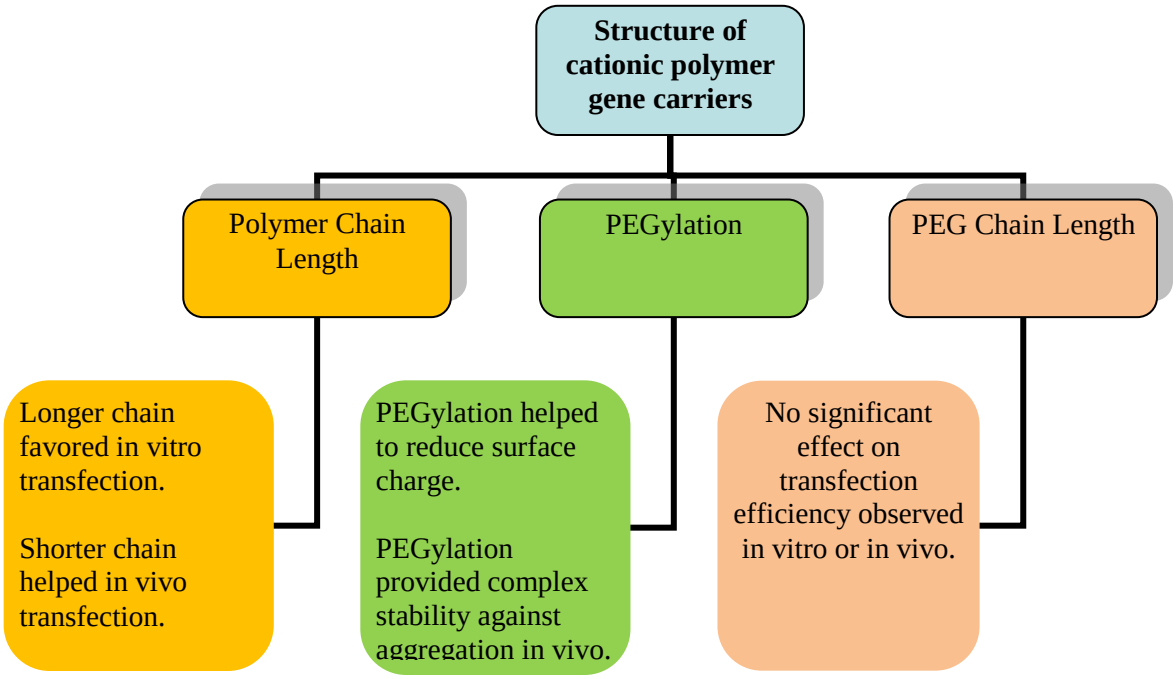

Fig. 22. A schematic summary of the finding. We studied the characteristics and properties of polyplexes in vitro to provide understanding of their behavior for local in vivo gene delivery efficiency through subcutaneous injection.

3.5 Conclusions

We performed in vitro physical characterization of polyplexes formed from six different polymers in order to understand their in vivo performance. Homopolymer with a larger molecular weight (and polymer chain) was able to transfect cells in vitro, but not in vivo. On the other hand, a shorter polymer chain favored in vivo transfection. PEGylation helped the polyplexes to be stable against serum protein, but PEGylation of long chain homopolymer did not improve its in vivo performance. Taken together, these findings could help us gain a better understanding of polyplex in vivo performance based on its in vitro behavior and therefore providing insight into the design of gene delivery vehicle.

Chapter 4: Overall Conclusions and Future Prospects

Much effort has been given to developing cationic polymeric gene delivery system that will achieve high transfection efficiency and low cytotoxicity. This thesis studies the in vitro properties and characteristics of polymer/DNA complex in order to understand their in vivo performance. Understanding the mechanisms and pathways underlying toxicity associated with polyplex-mediated gene delivery could provide insight in designing new polymers with a safer profile. In Chapter 2, we used the widely studied polymer PEI as a model polymer to explore the existence of the newly recognized form of cellular cytotoxicity. We have successfully confirmed the presence of autophagy associated with polyplex-mediated gene delivery using 3 different methods in vitro. The 3 modalities of cell death often have a cross talk and apply a compound effect on cellular cytotoxicity. To better understand the effect of autophagy alone on gene transfection efficiency, we decoupled autophagy from apoptotic and necrotic cell death and reported a positive correlation between gene delivery efficiency and autophagy regulation. This provided another option to regulate transgene expression.

The above mentioned work was done with cell culture in vitro. Artificial manipulation of autophagy in vivo involves ischemia, exposure to cadmium or pathogens and 3-MA [123-126], but polymer-based gene carriers have not been tested. In vivo studies of apoptosis were based on pathogen invasions or treating tumor cells with chemotherapeutic drugs [127-129], but not involving polymeric gene carriers either. It is important to confirm the induction of different programmed cell death (PCD) pathways

by polymer gene carriers in vivo before we implement new polymer design or drug treatment to alter PCDs in vivo.

Due to the limited number of biomarkers for autophagy detection, the standard method to date for monitor autophagy in vivo has been transmission electron microscopy (TEM) [42, 80, 123, 130]. Autophagy detection through TEM involves the recognition of changes in cell morphology such as extensive vacuolization, formation of membranous whorls and depletion of organelles. However, it is often difficult to distinguish autophagic vacuoles from other cellular structures. Autophagy detection using fluorescence microscopy on tissue sections for LC3 staining is an alternative solution to the conventional approach since LC3 is a distinct biomarker for autophagy.

TUNEL assay is a common method for visualizing and quantifying apoptosis in vivo that requires processing tissue post-mortem [131, 132]. Non-invasive detection of apoptosis in live animals has been reported recently [127, 128]. Z-VED-aminoluciferin is a modified firefly luciferase substrate that can be cleaved by caspase-3 in apoptotic cells. It will liberate aminoluciferin, a substrate for luciferase to generate luminescence signals that can be detected and quantified using a live imaging instrument such as the Xenogen IVIS system. The new technique will allow us to track the kinetics of apoptosis induction by polymer gene carrier continuously and non-invasively in live animals after polyplex administration.

In Chapter 3, we tackled the other hurdle in polymeric based gene delivery, which is the general low transfection efficiency in vivo compared to the viral vectors. Literature has reported a variety of factors potentially influencing gene transfection efficiency in

vitro. However, the understanding for polyplex performance in vivo remains much unclear. In this study, we synthesized a PAEM diblock copolymer in our lab which has a nearly uniform distribution of chain length and well-defined chemical structure [67]. We performed a comprehensive analysis of polyplex characteristics in vitro in order to compare their in vitro properties with in vivo performance. We identified molecular weight or polymer chain length is the dominant factor influencing both in vitro and in vivo transgene efficiency though with opposing trend. We attributed this difference to their varied stabilities under different environment. Further experiment could be conducted to confirm this speculation, especially the polyplex stability, DNA binding and condensation capacity under the influence of serum protein and ECM components. Burke and Pun have examined the extracellular barriers for PEI and PEGylated PEI in vivo delivery to the liver [49], but a more detailed examination on the effect of chain length on polyplex stability due to the interaction with ECM components and serum proteins is much needed.

PEGylated polyplexes have been shown to be more stable in serum containing cell culture media in this study. They have a better chance to diffuse through a larger area in the skin tissue and remain intact in order to interact with cells. PEGylation has often come with compromised transfection efficiency and this could very likely contribute to the non-significant difference between homopolymer and PEGylated $PAEM_{30}$ in vivo transfection efficiency. It would be of great interest and benefit for a better design of gene carrier to manipulate the PEG chain in the hope to further improve the in vivo transfection efficiency.

Researchers have tried to lose the PEG chain after the polyplexes being internalized by cells. Wagner and colleagues have developed hydrazine derivative as the linking structure between PEG and PLL, demonstrating a pH-responsive chemistry to un-shield the PEG protection on polyplexes [133]. While still being able to retain polyplex stability, their pH-responsive PEGylated polymer was able to improve the gene transfection 2 logs order of magnitude in vitro, and 1 order of magnitude in vivo. It would be very interesting to investigate a detachable PEG chain with our $PAEM_{30}$ series polymer in the hope to further improve in vivo gene delivery efficiency.

Instead of dropping the PEG chain, another approach to solve the problem associated with PEGylation, which is the low cellular internalization, is to introduce a target specific ligand to the distal end of the PEG chain. Kursa and colleagues have added transferrin to PEGylated PEI, and found the transfection efficiency was greatly improved in tumor cells in vivo [134]. Kim and colleagues explained that the targeted PEGylated polyplexes showed selectively enhanced gene expression only in cells expressing the receptors [135]. Oba and colleagues further explored and discovered that this enhanced transfection is highly correlated with the facilitated cellular internalization of polyplexes via receptor-mediated endocytosis [136]. The ligand introduction techniques can also be utilized for enhanced endosomal escape of PEGylated polyplexes [133]. In this design, the target specific ligand is grafted on the longer PEG chain. When the longer PEG chain is detached, the endosomal disrupting component will be exposed, mediating endosomal escape. The combination of detachable PEG and ligand targeting could be an interesting topic to explore with our polymer system.

References

[1] C.E. Walsh, Gene therapy Progress and Prospects: Gene therapy for the hemophilias, Gene Ther., 10 (2003) 999-1003.
[2] J.C.T. van Deutekom, G.J.B. van Ommen, Advances in Duchenne muscular dystrophy gene therapy, Nature Reviews Genetics, 4 (2003) 774-783.
[3] B.I. Florea, C. Meaney, H.E. Junginger, G. Borchard, Transfection efficiency and toxicity of polyethylenimine in differentiated Calu-3 and nondifferentiated COS-1 cell cultures, AAPS Pharmsci, 4 (2002).
[4] A. Rivard, M. Silver, D. Chen, M. Kearney, M. Magner, B. Annex, K. Peters, J.M. Isner, Rescue of diabetes-related impairment of angiogenesis by intramuscular gene therapy with adeno-VEGF, The American journal of pathology, 154 (1999) 355-363.
[5] V.J. Dzau, K. Beatt, G. Pompilio, K. Smith, Current perceptions of cardiovascular gene therapy, The American Journal of Cardiology, 92 (2003) 18-23.
[6] M.G. Kaplitt, A. Feigin, C. Tang, H.L. Fitzsimons, P. Mattis, P.A. Lawlor, R.J. Bland, D. Young, K. Strybing, D. Eidelberg, Safety and tolerability of gene therapy with an adeno-associated virus (AAV) borne< i> GAD</i> gene for Parkinson's disease: an open label, phase I trial, The Lancet, 369 (2007) 2097-2105.
[7] F. Pereyra, M.M. Addo, D.E. Kaufmann, Y. Liu, T. Miura, A. Rathod, B. Baker, A. Trocha, R. Rosenberg, E. Mackey, Genetic and immunologic heterogeneity among persons who control HIV infection in the absence of therapy, Journal of Infectious Diseases, 197 (2008) 563-571.
[8] R.R. Sawant, S.K. Sriraman, G. Navarro, S. Biswas, R.A. Dalvi, V.P. Torchilin, Polyethyleneimine-lipid conjugate-based pH-sensitive micellar carrier for gene delivery, Biomaterials, 33 (2012) 3942-3951.
[9] R.G. Vile, S.J. Russell, N.R. Lemoine, Cancer gene therapy: hard lessons and new courses, Gene Ther., 7 (2000) 2-8.
[10] M.A. Kay, J.C. Glorioso, L. Naldini, Viral vectors for gene therapy: the art of turning infectious agents into vehicles of therapeutics, Nature medicine, 7 (2001) 33-40.
[11] D.H. Palmer, L.S. Young, V. Mautner, Cancer gene-therapy: clinical trials, Trends in biotechnology, 24 (2006) 76-82.
[12] D.W. Emery, Gene therapy for genetic diseases: On the horizon, Clinical and Applied Immunology Reviews, 4 (2004) 411-422.
[13] J. Kaiser, Death prompts a review of gene therapy vector, (2007).
[14] H. Atkinson, R. Chalmers, Delivering the goods: viral and non-viral gene therapy systems and the inherent limits on cargo DNA and internal sequences, Genetica, 138 (2010) 485-498.
[15] M.A. Mintzer, E.E. Simanek, Nonviral Vectors for Gene Delivery, Chemical Reviews, 109 (2009) 259-302.
[16] S.Y. Wu, N.A. McMillan, Lipidic systems for in vivo siRNA delivery, AAPS J, 11 (2009) 639-652.

[17] P. van de Wetering, J.Y. Cherng, H. Talsma, D.J.A. Crommelin, W.E. Hennink, 2-(dimethylamino)ethyl methacrylate based (co)polymers as gene transfer agents, Journal of Controlled Release, 53 (1998) 145-153.
[18] W.T. Godbey, K.K. Wu, A.G. Mikos, Size matters: Molecular weight affects the efficiency of poly(ethylenimine) as a gene delivery vehicle, Journal of Biomedical Materials Research, 45 (1999) 268-275.
[19] K. Morimoto, M. Nishikawa, S. Kawakami, T. Nakano, Y. Hattori, S. Fumoto, F. Yamashita, M. Hashida, Molecular weight-dependent gene transfection activity of unmodified and galactosylated polyethyleneimine on hepatoma cells and mouse liver, Molecular Therapy, 7 (2003) 254-261.
[20] Y. Ren, X. Jiang, D. Pan, H.-Q. Mao, Charge Density and Molecular Weight of Polyphosphoramidate Gene Carrier Are Key Parameters Influencing Its DNA Compaction Ability and Transfection Efficiency, Biomacromolecules, 11 (2010) 3432-3439.
[21] D.Y. Kwoh, C.C. Coffin, C.P. Lollo, J. Jovenal, M.G. Banaszczyk, P. Mullen, A. Phillips, A. Amini, J. Fabrycki, R.M. Bartholomew, S.W. Brostoff, D.J. Carlo, Stabilization of poly-l-lysine/DNA polyplexes for in vivo gene delivery to the liver, Biochimica et Biophysica Acta (BBA) - Gene Structure and Expression, 1444 (1999) 171-190.
[22] A.C. Hunter, Molecular hurdles in polyfectin design and mechanistic background to polycation induced cytotoxicity, Adv. Drug Deliv. Rev., 58 (2006) 1523-1531.
[23] T.G. Park, J.H. Jeong, S.W. Kim, Current status of polymeric gene delivery systems, Adv. Drug Deliv. Rev., 58 (2006) 467-486.
[24] S.M. Moghimi, P. Symonds, J.C. Murray, A.C. Hunter, G. Debska, A. Szewczyk, A two-stage poly(ethylenimine)-mediated cytotoxicity: implications for gene transfer/therapy, Mol Ther, 11 (2005) 990-995.
[25] L. Galluzzi, M.C. Maiuri, I. Vitale, H. Zischka, M. Castedo, L. Zitvogel, G. Kroemer, Cell death modalities: classification and pathophysiological implications, Cell Death Differ, 14 (2007) 1237-1243.
[26] G. Kroemer, L. Galluzzi, P. Vandenabeele, J. Abrams, E.S. Alnemri, E.H. Baehrecke, M.V. Blagosklonny, W.S. El-Deiry, P. Golstein, D.R. Green, M. Hengartner, R.A. Knight, S. Kumar, S.A. Lipton, W. Malorni, G. Nunez, M.E. Peter, J. Tschopp, J. Yuan, M. Piacentini, B. Zhivotovsky, G. Melino, Classification of cell death: recommendations of the Nomenclature Committee on Cell Death 2009, Cell Death and Differentiation, 16 (2009) 3-11.
[27] J.F. Kerr, A.H. Wyllie, A.R. Currie, Apoptosis: a basic biological phenomenon with wide-ranging implications in tissue kinetics, British journal of cancer, 26 (1972) 239.
[28] E.H. Baehrecke, How death shapes life during development, Nature Reviews Molecular Cell Biology, 3 (2002) 779-787.
[29] G. Kroemer, S.J. Martin, Caspase-independent cell death, Nature medicine, 11 (2005) 725-730.
[30] G. Kroemer, L. Galluzzi, C. Brenner, Mitochondrial membrane permeabilization in cell death, Physiological reviews, 87 (2007) 99-163.

[31] R.N. Palumbo, X. Zhong, C. Wang, Polymer-mediated DNA vaccine delivery via bystander cells requires a proper balance between transfection efficiency and cytotoxicity, Journal of Controlled Release, 157 (2012) 86-93.
[32] P. Symonds, J.C. Murray, A.C. Hunter, G. Debska, A. Szewczyk, S.M. Moghimi, Low and high molecular weight poly(l-lysine)s/poly(l-lysine)–DNA complexes initiate mitochondrial-mediated apoptosis differently, FEBS Letters, 579 (2005) 6191-6198.
[33] A.L. Edinger, C.B. Thompson, Death by design: apoptosis, necrosis and autophagy, Current Opinion in Cell Biology, 16 (2004) 663-669.
[34] D. Fischer, Y. Li, B. Ahlemeyer, J. Krieglstein, T. Kissel, In vitro cytotoxicity testing of polycations: influence of polymer structure on cell viability and hemolysis, Biomaterials, 24 (2003) 1121-1131.
[35] N. Mizushima, Autophagy: process and function, Genes & Development, 21 (2007) 2861-2873.
[36] T. Yorimitsu, D.J. Klionsky, Autophagy: molecular machinery for self-eating, Cell Death & Differentiation, 12 (2005) 1542-1552.
[37] L. Yu, L. Strandberg, M.J. Lenardo, The selectivity of autophagy and its role in cell death and survival, Autophagy, 4 (2008) 567-573.
[38] Y.-T. Wu, H.-L. Tan, G. Shui, C. Bauvy, Q. Huang, M.R. Wenk, C.-N. Ong, P. Codogno, H.-M. Shen, Dual Role of 3-Methyladenine in Modulation of Autophagy via Different Temporal Patterns of Inhibition on Class I and III Phosphoinositide 3-Kinase, Journal of Biological Chemistry, 285 (2010) 10850-10861.
[39] V.L. Crotzer, J.S. Blum, Autophagy and Its Role in MHC-Mediated Antigen Presentation, The Journal of Immunology, 182 (2009) 3335-3341.
[40] L. English, M. Chemali, J. Duron, C. Rondeau, A. Laplante, D. Gingras, D. Alexander, D. Leib, C. Norbury, R. Lippe, M. Desjardins, Autophagy enhances the presentation of endogenous viral antigens on MHC class I molecules during HSV-1 infection, Nature Immunology, 10 (2009) 480-487.
[41] N. Man, Y. Chen, F. Zheng, W. Zhou, L.P. Wen, Induction of genuine autophagy by cationic lipids in mammalian cells, Autophagy, 6 (2010) 449-454.
[42] W. Martinet, G.R.Y. De Meyer, L. Andries, A.G. Herman, M.M. Kockx, In Situ Detection of Starvation-induced Autophagy, Journal of Histochemistry & Cytochemistry, 54 (2006) 85-96.
[43] K. Kirkegaard, M.P. Taylor, W.T. Jackson, Cellular autophagy: Surrender, avoidance and subversion by microorganisms, Nature Reviews Microbiology, 2 (2004) 301-314.
[44] W. Gao, W.-X. Ding, D.B. Stolz, X.-M. Yin, Induction of macroautophagy by exogenously introduced calcium, Autophagy, 4 (2008) 754-761.
[45] O. Seleverstov, O. Zabirnyk, M. Zscharnack, L. Bulavina, M. Nowicki, J.-M. Heinrich, M. Yezhelyev, F. Emmrich, R. O'Regan, A. Bader, Quantum Dots for Human Mesenchymal Stem Cells Labeling. A Size-Dependent Autophagy Activation, Nano Letters, 6 (2006) 2826-2832.
[46] J.J. Li, D. Hartono, C.-N. Ong, B.-H. Bay, L.-Y.L. Yung, Autophagy and oxidative stress associated with gold nanoparticles, Biomaterials, 31 (2010) 5996-6003.

[47] C. Li, H. Liu, Y. Sun, H. Wang, F. Guo, S. Rao, J. Deng, Y. Zhang, Y. Miao, C. Guo, J. Meng, X. Chen, L. Li, D. Li, H. Xu, H. Wang, B. Li, C. Jiang, PAMAM Nanoparticles Promote Acute Lung Injury by Inducing Autophagic Cell Death through the Akt-TSC2-mTOR Signaling Pathway, Journal of Molecular Cell Biology, 1 (2009) 37-45.
[48] X. Gao, L. Yao, Q. Song, L. Zhu, Z. Xia, H. Xia, X. Jiang, J. Chen, H. Chen, The association of autophagy with polyethylenimine-induced cytotoxity in nephritic and hepatic cell lines, Biomaterials, 32 (2012) 8613-8625.
[49] R.S. Burke, S.H. Pun, Extracellular Barriers to in Vivo PEI and PEGylated PEI Polyplex-Mediated Gene Delivery to the Liver, Bioconjugate Chemistry, 19 (2008) 693-704.
[50] K. Bakeev, V. Izumrudov, S. Kuchanov, A. Zezin, V. Kabanov, Kinetics and mechanism of interpolyelectrolyte exchange and addition reactions, Macromolecules, 25 (1992) 4249-4254.
[51] D.V. Schaffer, N.A. Fidelman, N. Dan, D.A. Lauffenburger, Vector unpacking as a potential barrier for receptor-mediated polyplex gene delivery, Biotechnology and bioengineering, 67 (2000) 598-606.
[52] M. Bertschinger, G. Backliwal, A. Schertenleib, M. Jordan, D.L. Hacker, F.M. Wurm, Disassembly of polyethylenimine-DNA particles in vitro: implications for polyethylenimine-mediated DNA delivery, Journal of controlled release, 116 (2006) 96-104.
[53] M. Ruponen, S. Rönkkö, P. Honkakoski, J. Pelkonen, M. Tammi, A. Urtti, Extracellular glycosaminoglycans modify cellular trafficking of lipoplexes and polyplexes, Journal of Biological Chemistry, 276 (2001) 33875-33880.
[54] H. Eliyahu, A. Joseph, J. Schillemans, T. Azzam, A. Domb, Y. Barenholz, Characterization and in vivo performance of dextran–spermine polyplexes and DOTAP/cholesterol lipoplexes administered locally and systemically, Biomaterials, 28 (2007) 2339-2349.
[55] K. Miyata, N. Nishiyama, K. Kataoka, Rational design of smart supramolecular assemblies for gene delivery: chemical challenges in the creation of artificial viruses, Chemical Society Reviews, 41 (2012) 2562-2574.
[56] K. Itaka, K. Yamauchi, A. Harada, K. Nakamura, H. Kawaguchi, K. Kataoka, Polyion complex micelles from plasmid DNA and poly(ethylene glycol)–poly(l-lysine) block copolymer as serum-tolerable polyplex system: physicochemical properties of micelles relevant to gene transfection efficiency, Biomaterials, 24 (2003) 4495-4506.
[57] K. Itaka, A. Harada, K. Nakamura, H. Kawaguchi, K. Kataoka, Evaluation by Fluorescence Resonance Energy Transfer of the Stability of Nonviral Gene Delivery Vectors under Physiological Conditions, Biomacromolecules, 3 (2002) 841-845.
[58] T. Nomoto, Y. Matsumoto, K. Miyata, M. Oba, S. Fukushima, N. Nishiyama, T. Yamasoba, K. Kataoka, In situ quantitative monitoring of polyplexes and polyplex micelles in the blood circulation using intravital real-time confocal laser scanning microscopy, Journal of Controlled Release, 151 (2011) 104-109.

[59] G. Storm, S.O. Belliot, T. Daemen, D.D. Lasic, Surface modification of nanoparticles to oppose uptake by the mononuclear phagocyte system, Adv. Drug Deliv. Rev., 17 (1995) 31-48.
[60] T. Merdan, K. Kunath, H. Petersen, U. Bakowsky, K.H. Voigt, J. Kopecek, T. Kissel, PEGylation of Poly(ethylene imine) Affects Stability of Complexes with Plasmid DNA under in Vivo Conditions in a Dose-Dependent Manner after Intravenous Injection into Mice, Bioconjugate Chemistry, 16 (2005) 785-792.
[61] S. Mao, M. Neu, O. Germershaus, O. Merkel, J. Sitterberg, U. Bakowsky, T. Kissel, Influence of Polyethylene Glycol Chain Length on the Physicochemical and Biological Properties of Poly(ethylene imine)-graft-Poly(ethylene glycol) Block Copolymer/SiRNA Polyplexes, Bioconjugate Chemistry, 17 (2006) 1209-1218.
[62] S. Jeon, J. Lee, J. Andrade, P. De Gennes, Protein—surface interactions in the presence of polyethylene oxide: I. Simplified theory, Journal of Colloid and Interface Science, 142 (1991) 149-158.
[63] D.W. Pack, A.S. Hoffman, S. Pun, P.S. Stayton, Design and development of polymers for gene delivery, Nat Rev Drug Discov, 4 (2005) 581-593.
[64] W.T. Godbey, K.K. Wu, A.G. Mikos, Tracking the intracellular path of poly(ethylenimine)/DNA complexes for gene delivery, Proceedings of the National Academy of Sciences, 96 (1999) 5177-5181.
[65] O. Boussif, F. Lezoualch, M.A. Zanta, M.D. Mergny, D. Scherman, B. Demeneix, J.P. Behr, A Versatile Vector for Gene and Oligonucleotide Transfer into Cells in Culture and in-Vivo - Polyethylenimine, Proc. Natl. Acad. Sci. U. S. A., 92 (1995) 7297-7301.
[66] D. Fischer, T. Bieber, Y. Li, H.-P. Elsasser, T. Kissel, A Novel Non-Viral Vector for DNA Delivery Based on Low Molecular Weight, Branched Polyethylenimine: Effect of Molecular Weight on Transfection Efficiency and Cytotoxicity, Pharmaceutical Research, 16 (1999) 1273-1279.
[67] R. Tang, R.N. Palumbo, L. Nagarajan, E. Krogstad, C. Wang, Well-defined block copolymers for gene delivery to dendritic cells: Probing the effect of polycation chain-length, Journal of Controlled Release, 142 (2009) 229-237.
[68] Y.J. Choi, S.J. Kang, Y.J. Kim, Y.B. Lim, H.W. Chung, Comparative studies on the genotoxicity and cytotoxicity of polymeric gene carriers polyethylenimine (PEI) and polyamidoamine (PAMAM) dendrimer in Jurkat T-cells, Drug Chem. Toxicol., 33 (2010) 357-366.
[69] M.P. Xiong, M.L. Forrest, G. Ton, A. Zhao, N.M. Davies, G.S. Kwon, Poly(aspartate-g-PEI800), a polyethylenimine analogue of low toxicity and high transfection efficiency for gene delivery, Biomaterials, 28 (2007) 4889-4900.
[70] D.J. Klionsky, The molecular machinery of autophagy: unanswered questions, Journal of Cell Science, 118 (2005) 7-18.
[71] Z. Xie, D.J. Klionsky, Autophagosome formation: core machinery and adaptations, Nat Cell Biol, 9 (2007) 1102-1109.
[72] T. Yoshimori, Autophagy: a regulated bulk degradation process inside cells, Biochemical and Biophysical Research Communications, 313 (2004) 453-458.

[73] D. Vercauteren, H. Deschout, K. Remaut, J.F. Engbersen, A.T. Jones, J. Demeester, S.C. De Smedt, K. Braeckmans, Dynamic colocalization microscopy to characterize intracellular trafficking of nanomedicines, Acs Nano, 5 (2011) 7874-7884.
[74] R. Roberts, W.T. Al-Jamal, M. Whelband, P. Thomas, M. Jefferson, J. van den Bossche, P.P. Powell, K. Kostarelos, T. Wileman, Autophagy and formation of tubulovesicular autophagosomes provide a barrier against nonviral gene delivery, Autophagy, 9 (2013) 667-682.
[75] M.C. Maiuri, E. Zalckvar, A. Kimchi, G. Kroemer, Self-eating and self-killing: crosstalk between autophagy and apoptosis, Nat Rev Mol Cell Biol, 8 (2007) 741-752.
[76] W. Ji, D. Panus, R.N. Palumbo, R. Tang, C. Wang, Poly(2-aminoethyl methacrylate) with Well-Defined Chain Length for DNA Vaccine Delivery to Dendritic Cells, Biomacromolecules, 12 (2011) 4373-4385.
[77] E.-L. Eskelinen, Fine Structure of the Autophagosome, Methods in Molecular Biology 445 (2008) 11-28.
[78] P.i. Yla ¨-Anttila, H. Vihinen, E. Jokitalo, E.-L. Eskelinen, Chapter 10 Monitoring Autophagy by Electron Microscopy in Mammalian Cells, in: Methods in Enzymology, Academic Press, 2009, pp. 143-164.
[79] Y. Kabeya, N. Mizushima, T. Ueno, A. Yamamoto, T. Kirisako, T. Noda, E. Kominami, Y. Ohsumi, T. Yoshimori, LC3, a mammalian homologue of yeast Apg8p, is localized in autophagosome membranes after processing, EMBO J, 19 (2000) 5720-5728.
[80] N. Mizushima, Methods for monitoring autophagy, International Journal of Biochemistry & Cell Biology, 36 (2004) 2491-2502.
[81] S.J. You, Y. Xie, Y.L. Zhang, Q. Han, Y.J. Cao, X.S. Xu, Y.P. Yang, J. Li, C.F. Liu, PROTECTIVE ROLE OF AUTOPHAGY IN AGE-INDUCED EARLY INJURY OF HUMAN VASCULAR ENDOTHELIAL CELLS, European Journal of Neurology, 18 (2011) 397-397.
[82] A. Nel, T. Xia, L. Madler, N. Li, Toxic potential of materials at the nanolevel, Science, 311 (2006) 622-627.
[83] W. Yan, W. Chen, L. Huang, Reactive oxygen species play a central role in the activity of cationic liposome based cancer vaccine, Journal of Controlled Release, 130 (2008) 22-28.
[84] Y. Chen, M.B. Azad, S.B. Gibson, Superoxide is the major reactive oxygen species regulating autophagy, Cell Death Differ, 16 (2009) 1040-1052.
[85] R. Scherz-Shouval, E. Shvets, E. Fass, H. Shorer, L. Gil, Z. Elazar, Reactive oxygen species are essential for autophagy and specifically regulate the activity of Atg4, EMBO J, 26 (2007) 1749-1760.
[86] J. Yang, L.-J. Wu, S.-I. Tashino, S. Onodera, T. Ikejima, Reactive oxygen species and nitric oxide regulate mitochondria-dependent apoptosis and autophagy in evodiamine-treated human cervix carcinoma HeLa cells, Free Radical Research, 42 (2008) 492-504.
[87] Y. Xiong, A.L. Contento, P.Q. Nguyen, D.C. Bassham, Degradation of Oxidized Proteins by Autophagy during Oxidative Stress in Arabidopsis, Plant Physiology, 143 (2007) 291-299.

[88] M.N. Moore, Autophagy as a second level protective process in conferring resistance to environmentally-induced oxidative stress, Autophagy, 4 (2008) 254-256.
[89] C. Bauvy, P. Gane, S. Arico, P. Codogno, E. Ogier-Denis, Autophagy Delays Sulindac Sulfide-Induced Apoptosis in the Human Intestinal Colon Cancer Cell Line HT-29, Experimental Cell Research, 268 (2001) 139-149.
[90] L. Yu, A. Alva, H. Su, P. Dutt, E. Freundt, S. Welsh, E.H. Baehrecke, M.J. Lenardo, Regulation of an ATG7-beclin 1 Program of Autophagic Cell Death by Caspase-8, Science, 304 (2004) 1500-1502.
[91] D. Dey, M. Inayathullah, A.S. Lee, M.C. LeMieux, X. Zhang, Y. Wu, D. Nag, P.E. De Almeida, L. Han, J. Rajadas, J.C. Wu, Efficient gene delivery of primary human cells using peptide linked polyethylenimine polymer hybrid, Biomaterials, 32 (2011) 4647-4658.
[92] K. Toh, T. Yoshitomi, Y. Ikeda, Y. Nagasaki, Novel redox nanomedicine improves gene expression of polyion complex vector, Sci. Technol. Adv. Mater., 12 (2011).
[93] I.A. Khalil, K. Kogure, H. Akita, H. Harashima, Uptake Pathways and Subsequent Intracellular Trafficking in Nonviral Gene Delivery, Pharmacological Reviews, 58 (2006) 32-45.
[94] C.H. Jones, C.-K. Chen, A. Ravikrishnan, S. Rane, B.A. Pfeifer, Overcoming nonviral gene delivery barriers: perspective and future, Molecular pharmaceutics, 10 (2013) 4082-4098.
[95] Y.K. Oh, D. Duh, J.M. Kim, H.G. Choi, K. Shin, J.J. Ko, Polyethylenimine-mediated cellular uptake, nucleus trafficking and expression of cytokine plasmid DNA, Gene Ther., 9 (2002) 1627-1632.
[96] H. Cheong, C. Lu, T. Lindsten, C.B. Thompson, Therapeutic targets in cancer cell metabolism and autophagy, Nature biotechnology, 30 (2012) 671-678.
[97] D.C. Rubinsztein, J.E. Gestwicki, L.O. Murphy, D.J. Klionsky, Potential therapeutic applications of autophagy, Nat Rev Drug Discov, 6 (2007) 304-312.
[98] M. Zhou, R. Wang, Small-Molecule Regulators of Autophagy and Their Potential Therapeutic Applications, ChemMedChem, 8 (2013) 694-707.
[99] M. Cavazzana-Calvo, A. Thrasher, F. Mavilio, The future of gene therapy, Nature, 427 (2004) 779-781.
[100] X. Zhang, S.-R. Pan, H.-M. Hu, G.-F. Wu, M. Feng, W. Zhang, X. Luo, Poly(ethylene glycol)-block-polyethylenimine copolymers as carriers for gene delivery: Effects of PEG molecular weight and PEGylation degree, Journal of Biomedical Materials Research Part A, 84A (2008) 795-804.
[101] M. Gaumet, A. Vargas, R. Gurny, F. Delie, Nanoparticles for drug delivery: The need for precision in reporting particle size parameters, European Journal of Pharmaceutics and Biopharmaceutics, 69 (2008) 1-9.
[102] C. He, Y. Hu, L. Yin, C. Tang, C. Yin, Effects of particle size and surface charge on cellular uptake and biodistribution of polymeric nanoparticles, Biomaterials, 31 (2010) 3657-3666.
[103] C. Foged, B. Brodin, S. Frokjaer, A. Sundblad, Particle size and surface charge affect particle uptake by human dendritic cells in an in vitro model, International journal of pharmaceutics, 298 (2005) 315-322.

[104] F. Cui, F. Qian, C. Yin, Preparation and characterization of mucoadhesive polymer-coated nanoparticles, International Journal of Pharmaceutics, 316 (2006) 154-161.
[105] J.M. Layman, S.M. Ramirez, M.D. Green, T.E. Long, Influence of Polycation Molecular Weight on Poly(2-dimethylaminoethyl methacrylate)-Mediated DNA Delivery In Vitro, Biomacromolecules, 10 (2009) 1244-1252.
[106] R. Tang, R.N. Palumbo, L. Nagarajan, E. Krogstad, C. Wang, Well-defined block copolymers for gene delivery to dendritic cells: Probing the effect of polycation chain-length, Journal of Controlled Release, 142 (2010) 229-237.
[107] G. Maurstad, B.T. Stokke, K.M. Vårum, S.P. Strand, PEGylated chitosan complexes DNA while improving polyplex colloidal stability and gene transfection efficiency, Carbohydrate Polymers, 94 (2013) 436-443.
[108] M. Tang, F. Szoka, The influence of polymer structure on the interactions of cationic polymers with DNA and morphology of the resulting complexes, Gene Ther., 4 (1997).
[109] C. Wang, M. Feng, J. Deng, Y. Zhao, X. Zeng, L. Han, S. Pan, C. Wu, Poly(α-glutamic acid) combined with polycation as serum-resistant carriers for gene delivery, International Journal of Pharmaceutics, 398 (2010) 237-245.
[110] H. Jaganathan, J.M. Kinsella, A. Ivanisevic, Circular dichroism study of the mechanism of formation of DNA templated nanowires, ChemPhysChem, 9 (2008) 2203-2206.
[111] K. Kunath, A. von Harpe, D. Fischer, H. Petersen, U. Bickel, K. Voigt, T. Kissel, Low-molecular-weight polyethylenimine as a non-viral vector for DNA delivery: comparison of physicochemical properties, transfection efficiency and in vivo distribution with high-molecular-weight polyethylenimine, Journal of Controlled Release, 89 (2003) 113-125.
[112] M. Turunen, M. Hiltunen, M. Ruponen, L. Virkamäki, F. Szoka Jr, A. Urtti, S. Ylä-Herttuala, Efficient adventitial gene delivery to rabbit carotid artery with cationic polymer–plasmid complexes, Gene Ther., 6 (1999).
[113] H. Gharwan, L. Wightman, R. Kircheis, E. Wagner, K. Zatloukal, Nonviral gene transfer into fetal mouse livers (a comparison between the cationic polymer PEI and naked DNA), Gene Ther., 10 (2003) 810-817.
[114] N.K. Egilmez, Y. Iwanuma, R.B. Bankert, Evaluation and Optimization of Different Cationic Liposome Formulations for< i> in Vivo</i> Gene Transfer, Biochemical and biophysical research communications, 221 (1996) 169-173.
[115] J. Katz, G. Bonorris, S. Golden, A.J. Sellers, Extravascular Albumin Mass and Exchange in Rat Tissues, Clinical Science, 39 (1970) 705-724.
[116] C.C. Gyenge, O. Tenstad, H. Wiig, In vivo determination of steric and electrostatic exclusion of albumin in rat skin and skeletal muscle, The Journal of Physiology, 552 (2003) 907-916.
[117] R.N. Palumbo, X. Zhong, D. Panus, W. Han, W. Ji, C. Wang, Transgene expression and local tissue distribution of naked and polymer-condensed plasmid DNA after intradermal administration in mice, Journal of Controlled Release, 159 (2012) 232-239.

[118] B. Abdallah, A. Hassan, C. Benoist, D. Goula, J.P. Behr, B.A. Demeneix, A powerful nonviral vector for in vivo gene transfer into the adult mammalian brain: polyethylenimine, Human gene therapy, 7 (1996) 1947-1954.
[119] M. Koping-Hoggard, K.M. Varum, M. Issa, S. Danielsen, B.E. Christensen, B.T. Stokke, P. Artursson, Improved chitosan-mediated gene delivery based on easily dissociated chitosan polyplexes of highly defined chitosan oligomers, Gene Ther, 11 (2004) 1441-1452.
[120] A. Vila, A. Sánchez, M. Tobío, P. Calvo, M.J. Alonso, Design of biodegradable particles for protein delivery, Journal of Controlled Release, 78 (2002) 15-24.
[121] K. Park, To PEGylate or not to PEGylate, that is not the question, Journal of Controlled Release, 142 (2010) 147-148.
[122] M. Lee, S.W. Kim, Polyethylene glycol-conjugated copolymers for plasmid DNA delivery, Pharmaceutical research, 22 (2005) 1-10.
[123] A. Chargui, S. Zekri, G. Jacquillet, I. Rubera, M. Ilie, A. Belaid, C. Duranton, M. Tauc, P. Hofman, P. Poujeol, M.V. El May, B. Mograbi, Cadmium-Induced Autophagy in Rat Kidney: An Early Biomarker of Subtoxic Exposure, Toxicological Sciences, 121 (2011) 31-42.
[124] F. Tian, K. Deguchi, T. Yamashita, Y. Ohta, N. Morimoto, J. Shang, X. Zhang, N. Liu, Y. Ikeda, T. Matsuura, K. Abe, In vivo imaging of autophagy in a mouse stroke model, Autophagy, 6 (2010) 1107-1114.
[125] S. Romao, C. Munz, Autophagy of pathogens alarms the immune system and participates in its effector functions, Swiss Medical Weekly, 141 (2011) w13198.
[126] C.L. Luo, B.X. Li, Q.Q. Li, X.P. Chen, Y.X. Sun, H.J. Bao, D.K. Dai, Y.W. Shen, H.F. Xu, H. Ni, L. Wan, Z.H. Qin, L.Y. Tao, Z.Q. Zhao, Autophagy is involved in traumatic brain injury-induced cell death and contributes to functional outcome deficits in mice, Neuroscience, 184 (2011) 54-63.
[127] J. Hickson, S. Ackler, D. Klaubert, J. Bouska, P. Ellis, K. Foster, A. Oleksijew, L. Rodriguez, S. Schlessinger, B. Wang, D. Frost, Noninvasive molecular imaging of apoptosis in vivo using a modified firefly luciferase substrate, Z-DEVD-aminoluciferin, Cell Death and Differentiation, 17 (2010) 1003-1010.
[128] M. Scabini, F. Stellari, P. Cappella, S. Rizzitano, G. Texido, E. Pesenti, In vivo imaging of early stage apoptosis by measuring real-time caspase-3/7 activation, Apoptosis, 16 (2011) 198-207.
[129] A.D. Garg, D. Nowis, J. Golab, P. Vandenabeele, D.V. Krysko, P. Agostinis, Immunogenic cell death, DAMPs and anticancer therapeutics: An emerging amalgamation, Biochimica et Biophysica Acta (BBA) - Reviews on Cancer, 1805 (2010) 53-71.
[130] W. Martinet, G.R.Y.D. Meyer, L. Andries, A.G. Herman, M.M. Kockx, Detection of Autophagy in Tissue by Standard Immunohistochemistry: Possibilities and Limitations, Autophagy, 2 (2006) 55-57.
[131] J.F. Ma, Y. Huang, S.D. Chen, G. Halliday, Immunohistochemical evidence for macroautophagy in neurones and endothelial cells in Alzheimer's disease, Neuropathology and Applied Neurobiology, 36 (2010) 312-319.

[132] W.S. Chen, K.A. Masterman, S. Basta, S.M.M. Haeryfar, N. Dimopoulos, B. Knowles, J.R. Bennink, J.W. Yewdell, Cross-priming of CD8(+) T cells by viral and tumor antigens is a robust phenomenon, European Journal of Immunology, 34 (2004) 194-199.
[133] G.F. Walker, C. Fella, J. Pelisek, J. Fahrmeir, S. Boeckle, M. Ogris, E. Wagner, Toward synthetic viruses: Endosomal pH-triggered deshielding of targeted polyplexes greatly enhances gene transfer in vitro and in vivo, Molecular Therapy, 11 (2005) 418-425.
[134] M. Kursa, G.F. Walker, V. Roessler, M. Ogris, W. Roedl, R. Kircheis, E. Wagner, Novel Shielded Transferrin−Polyethylene Glycol−Polyethylenimine/DNA Complexes for Systemic Tumor-Targeted Gene Transfer, Bioconjugate Chemistry, 14 (2002) 222-231.
[135] S. Hwa Kim, J. Hoon Jeong, K. Chul Cho, S. Wan Kim, T. Gwan Park, Target-specific gene silencing by siRNA plasmid DNA complexed with folate-modified poly(ethylenimine), Journal of Controlled Release, 104 (2005) 223-232.
[136] M. Oba, S. Fukushima, N. Kanayama, K. Aoyagi, N. Nishiyama, H. Koyama, K. Kataoka, Cyclic RGD Peptide-Conjugated Polyplex Micelles as a Targetable Gene Delivery System Directed to Cells Possessing αvβ3 and αvβ5 Integrins, Bioconjugate Chemistry, 18 (2007) 1415-1423.

Appendix 1: Visualization of PEI-mediated transfection efficiency and associated cytotoxicity in NIH 3T3 murine fibroblast by fluorescence microscopy

A 1.1 Method

A 1.1.1 Visualization of PEI-mediated transfection efficiency in NIH 3T3 murine fibroblast by fluorescence microscopy

PEI (branched, 25 kDa, Sigma) and plasmid DNA stock solutions, both at the concentration of 1 mg/mL, were diluted to 0.1 mg/mL in 20 mM HEPES buffer (pH7.4). Polyplexes were prepared at N/P ratios from 4 to 20 by vortex mixing equal concentrations of PEI and plasmid DNA in 20 mM HEPES buffer to a total volume of 100 μL, and allowed to incubate at room temperature for 30 min. A plasmid encoding enhanced green fluorescence protein (GFP) (pEGFP-N1, Elim Biopharmaceuticals) was used to investigate the transfection efficiency. A plasmid encoding the luciferase gene (pCMV-Luc, Elim Biopharmaceuticals) was used to serve as a negative control and gate for cell autofluorescence.

NIH 3T3 murine fibroblasts (ATCC) were cultured in DMEM (1 g/L D-glucose, L-glutamine, 110 mg/L sodium pyruvate, Gibco) supplemented with 10% fetal bovine serum (heat inactivated, Gibco) and 100 units/mL penicillin/streptomycin (Gibco). NIH 3T3 cells were plated at 5×10^4 per well chamber slides and allowed to adhere overnight. After washing with phosphate buffered saline (PBS, pH7.4), the cell media was replaced with serum free media and polyplexes were added to the cells, incubated for 4 h. The cells were then washed three times with PBS before replacing the serum free

media back to regular cell media with 10% serum. Twenty-four hours after the initial addition of polyplexes, cells were washed with PBS, counterstained with 1:200 diluted Hoechst 33342 (Invitrogen) and mounted with Vectashield. The cells were visualized using an Olympus IX70 inverted microscope equipped with a standard FITC/TRITC/DAPI filter set and Olympus DP72 camera, and analyzed using CellSens software.

A 1.1.2 Toxicity study in PEI-mediated gene delivery by TUNEL staining

We determined apoptosis of PEI-mediated gene transfection in fibroblasts through TUNEL staining. At the end of the 24 h transfection, cells undergoing apoptosis and DNA fragmentation were examined using DeadEndTM Colorimetric TUNEL system (Promega). Cells were washed twice with PBS and fixed by immersing in 4% paraformaldehyde (Sigma) for 25 min at room temperature. After two 5-min washes with PBS, cells were permeabilized with 0.2% Triton X-100, washed twice with PBS and equilibrated in 100 μL of Equilibrium Buffer for 10 min. Recombinant terminal deoxynucleotidyl transferase (rTdT) of 100 μL was added to each sample, and slides were covered with plastic coverslips to ensure even distribution of the reagent. After a 60 min incubation at 37 ℃ in a humidity chamber, the reaction was stopped by immersing cells in 2-times SSC buffer in a Coplin jar for 15 min at room temperature, followed by 3 washes with PBS. Cells were then incubated with 0.3% hydrogen peroxide for 5 min, washed three times with PBS, and treated with 100 μL of horseradish peroxidase-labeled streptavidin for 30 min at room temperature. After three more washes in PBS, cells were stained with 100 μL of diaminobezidine (DAB) for 8 min at room temperature and

washed three times with de-ionized water. Slides were mounted using Bectashield and visualized using an Olympus IX70 inverted microscope equipped with Olympus DP72 camera, and analyzed using CellSens software.

A 1.2 Results

NIH 3T3 cells were transfected with PEI/DNA complexes of different N/P ratios for 4 h in serum free media and analyzed using fluorescence microscopy (Fig. 23). The GFP positive cells are green and the nuclei are stained blue. Qualitatively, the polyplexes were able to transfect fibroblasts efficiently, especially at lower N/P ratios like 4 and 8. The fraction of GFP positive cells seemed decreasing at higher N/P ratios (12, 16 and 20). This agreed well with our previously published paper where transfection efficiency was quantified through flow cytometry [31].

Apoptosis was also visualized through TUNEL assays (Fig. 24). Brown staining is indicative of apoptotic cells. At lower N/P ratios (4 and 8) there were little brown staining, suggesting minor cytotoxicity. At higher N/P ratios (12, 16 and 20), the fraction of apoptotic cells increased. This agreed well with our previously published paper where transfection efficiency was quantified through flow cytometry [31].

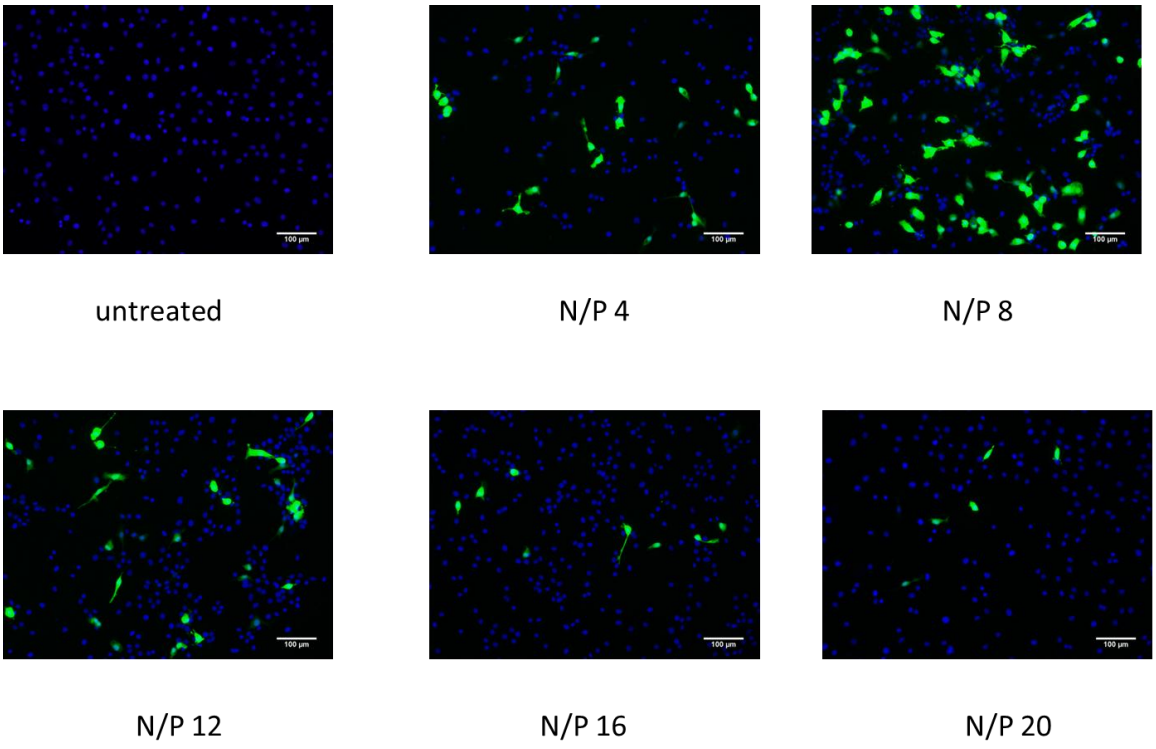

Fig. 23. Visualization of PEI-mediated gene delivery. A representative set of images of 24 h transfected and untreated NIH 3T3 fibroblasts. GFP positive cells are green and the nuclei of all cells are blue. Scale bar: 100 µm.

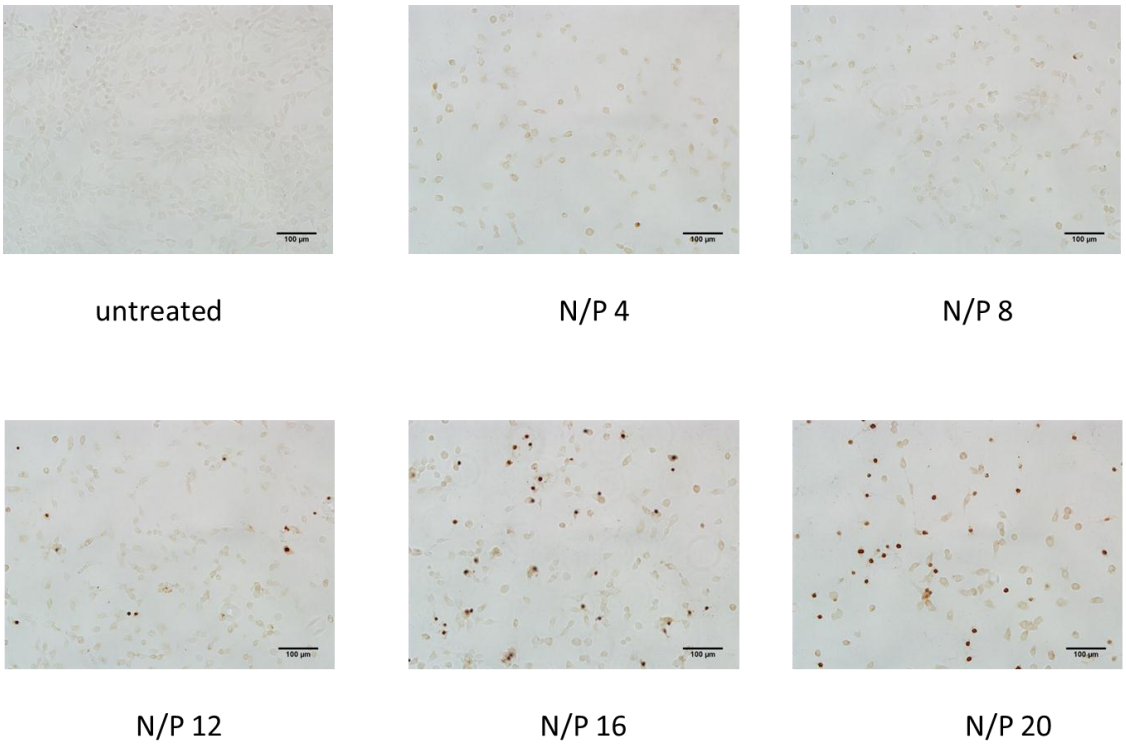

Fig. 24. Visualization of cytotoxicity (apoptosis) associated with PEI-mediated gene delivery. A representative set of images of transfected cells with brown staining indicative apoptotic cells. Scale bar: 100 μm.

Appendix 2: In Vivo transgene expression by immunohistochemical fluorescence staining for PAEM polymers

A 2.1 Method

A 2.1.1 Intradermal gene delivery

Hair was removed from the skin on the hind leg of 10-week old Blab\c mice (Jackson Labs) to mark the injection site, and polyplex solutions were injected intradermally through a 29-gauge needle. Forty μg of Luciferase plasmid DNA complexed with polymers at N/P ratio of 8 was prepared as described above and was injected into each mouse in a total volume of 35 μL. Three polymers with distinctly different chemical structures were used: branched PEI, linear $PAEM_{150}$, and diblock copolymer PEG-$PAEM_{150}$. Naked plasmid DNA was diluted to the same final volume as the polyplexes with 5% glucose buffer. The same volume of the buffer solution was also administered to serve as a negative control. All the mice were housed under specific pathogen-free conditions and cared for in accordance with the University of Minnesota and NIH guidelines.

A 2.1.2 In Vivo transgene expression by immunohistochemical fluorescence staining

Mice were sacrificed with CO_2 1 day or 4 days after injection and the skin around each injection site was removed, embedded in OCT medium and snap-frozen with liquid nitrogen. The frozen skin samples were cut into 10 μm thick sections using a cryotome and placed on SuperFrost glass slides. The cryosections were dried at room temperature for 1 h then fixed in cold acetone. After equilibrating the skin specimens to room

temperature, a hydrophobic circle was drawn around the specimens with a PAP pen and the specimens were soaked in PBS for 30 min with slight agitation. The tissue sections were blocked with 5% non-fat dry milk in PBS with 0.1% Tween-20 for 30 min at room temperature in a humidity chamber, followed by staining with 1:100 diluted anti-luciferase-FITC conjugated antibody (Lifespan Biosciences) in the blocking buffer for 1 h. after washing the tissue sections 3 times with PBS, the specimens were counterstained with 1:200 diluted Hoechst 33342 (Invitrogen) and mounted with Vectashield. The tissue sections were visualized using an Olympus IX70 inverted microscope equipped with a standard FITC/TRITC/DAPI filter set and Olympus DP72 camera, and analyzed using CellSens software.

A 2.1.3 Colocalization study by immunohistochemical fluorescence staining

After the tissue sections were stained for luciferase expression as described above, the slides were probed for dendritic cell marker CD11c to study the cell type of luciferase positive cells. Tissues were blocked using Blocking Buffer (from Tyramide Signal Amplification (TSA) Biotin System, Perkin Elmer) for 30 min, followed by streptavidin and biotin solutions (Vector Laboratories) for 15 min each in the humidity chamber. Slides were then stained with biotin-labeled anti-CD11c (Biolegend) for 30 min followed by biotin-labeled anti-rabbit IgG (Invitrogen) for 1 h. signal was developed using TSA Biotin System (Perkin Elmer) and a streptavidin labeled with Alexa Fluor 350 (Invitrogen). Tissue sections were mounted with Vectashield and using an Olympus IX70 inverted microscope equipped with a standard FITC/TRITC/DAPI filter set and Olympus DP72 camera, and analyzed using CellSens software.

A 2.2 Results

Naked luciferase plasmid and different polyplexes containing PEI, $PAEM_{150}$, and PEG-$PAEM_{150}$, were injected intradermally into the hind quadriceps region of mice. After day 1 and 4, animals were sacrificed. The dermal tissue of the injection sites was harvested, cryosectioned, stained with Hoechst for cell nuclei (blue) and with a fluorescein-labeled polyclonal antibody against luciferase (green), and imaged under a fluorescence microscope. The skin sections included the epidermal and dermal tissue as shown in Fig. 25. We can see that mice received naked plasmid and the polyplexes all contained skin cells positively transfected with luciferase gene. On the other hand, mice receiving buffer only injections did not show any detectable luciferase signal. The number of luciferase expressing cells in mice with naked plasmid and polyplexes were qualitatively comparable on day 1(Fig. 25A), but polyplexes appeared to have transfected more skin cells in mice than the naked plasmid on day 4 (Fig. 25B). Polyplexes may be able to provide protection for the plasmid from enzymatic degradation, providing sustained presence of plasmid in the local tissue and leading to the prolonged local gene transfection in vivo. Results from our previously published work strongly suggested the depot effect created by polyplex gene delivery in vivo [117].

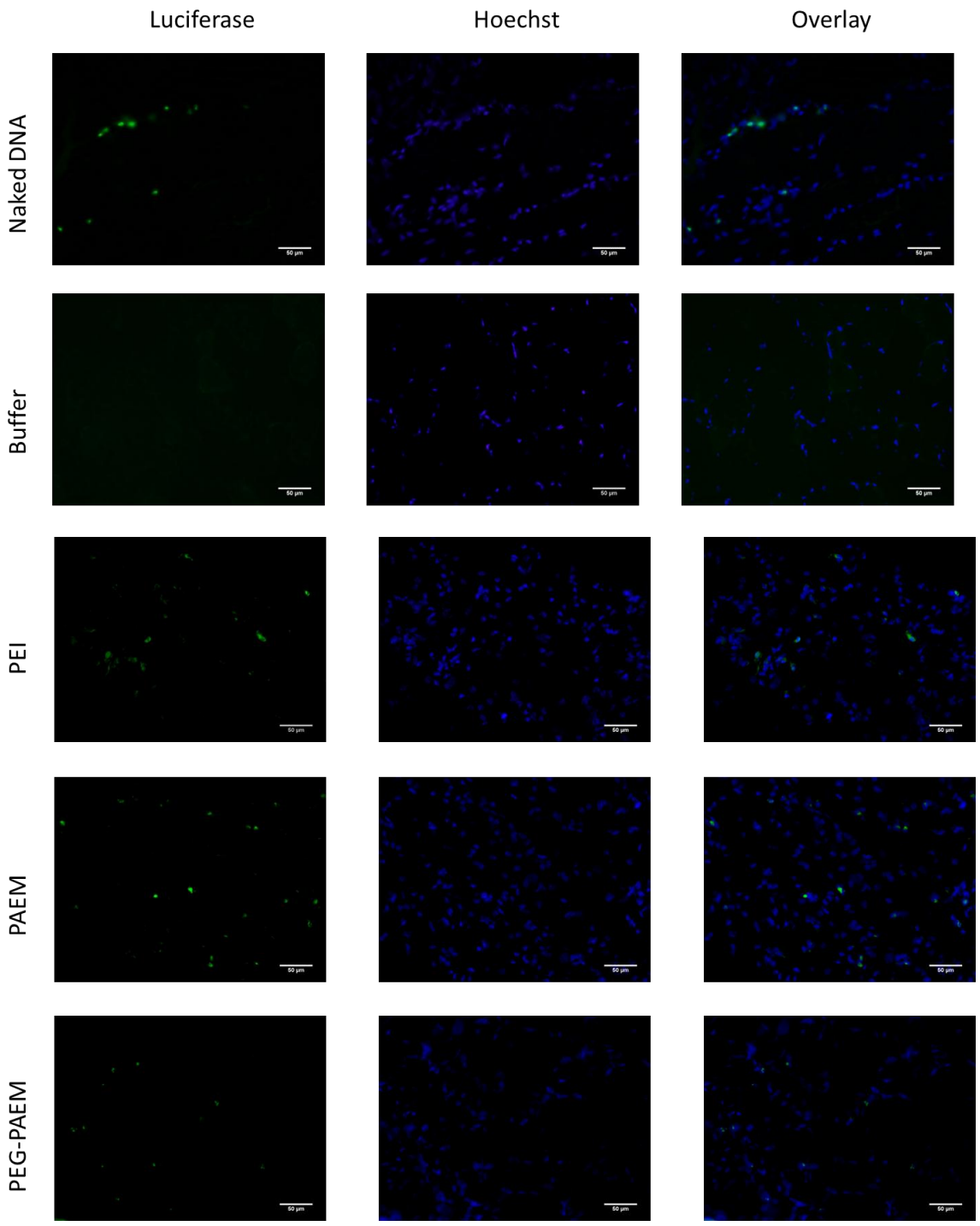
Luciferase
Hoechst
Overlay
Naked DNA
Buffer
PEI
PAEM
PEG-PAEM

A

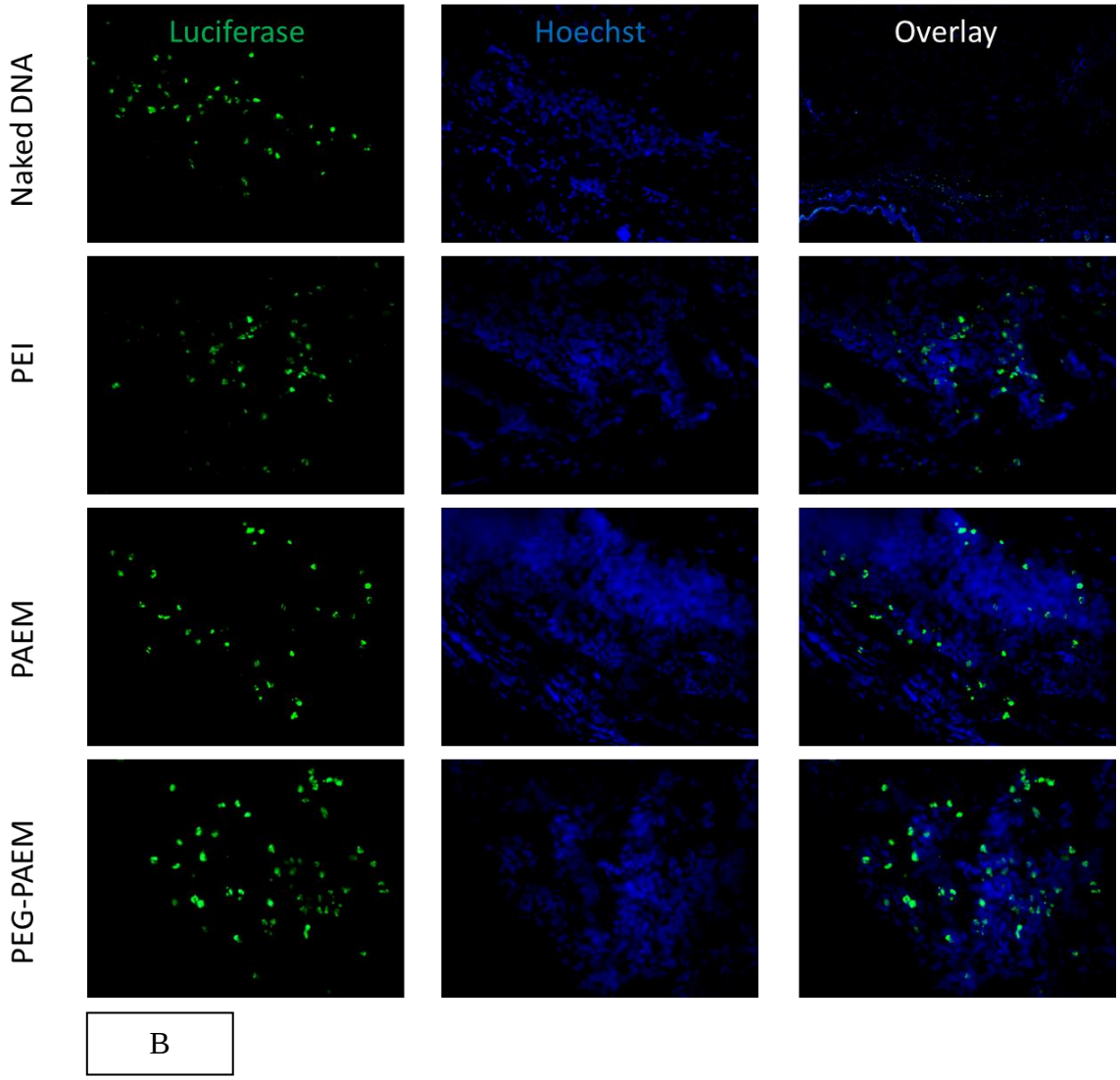

Fig. 25. Transgene expression in the skin of mice after intradermal injection in the right hind quadriceps region. A representative set of fluorescence microscopy images of mouse skin cross-sections. Luciferase expressing cells (green) were detected by a polyclonal antibody against luciferase. Cell nuclei were stained blue (Hoechst). Scale Bar: 50 μm. (A) One day after injection, and (B) four days after injection.